THERMAL AND PHASE-CHANGE WAVE PROPAGATION AND VELOCITIES SUBJECT TO SHRINKING CORE PHENOMENA FOR MELTING AND FREEZING PACKED-BEDS OF ENCAPSULATED PHASE-CHANGE MATERIALS

by

Glen Orval West

A dissertation submitted to the faculty of
The University of Utah
in partial fulfillment of the requirements for the degree of

Doctor of Philosophy

Department of Mechanical Engineering

The University of Utah

December 2017

The University of Utah Graduate School

STATEMENT OF DISSERTATION APPROVAL

The dissertation of **Glen Orval West**

has been approved by the following supervisory committee members:

Kent S. Udell	, Chair	**Oct. 26, 2017** Date Approved
Kuan Chen	, Member	**Oct. 26, 2017** Date Approved
John McLennan	, Member	**Oct. 26, 2017** Date Approved
Eric R. Pardyjak	, Member	**Oct. 26, 2017** Date Approved
Amanda D. Smith	, Member	Date Approved

and by **Tim Ameel**, Chair/Dean of

the Department/College/School of **Mechanical Engineering**

and by David B. Kieda, Dean of The Graduate School.

ABSTRACT

This research focuses on heat transfer between a fluid and a packed-bed comprised of encapsulated phase-change materials (PCMs). The objective of this work is to develop and validate models that can be used to predict the propagation of melting and freezing fronts and sensible heat fronts as a heated or cooled fluid is injected into the packed-bed. To achieve this objective, an analytical model was developed to study sensible and phase-change thermal wave propagation with respect to time and spatial variation along a 0.356 m axial bed length, with a 0.023 m^2 cross-sectional area, under low temperature test conditions between 15 to 50 °C, for time intervals ranging from 5 to 18 hours. Model results exhibit classical thermal waveforms in the sensible heat transfer regime, exponential variations in temperature near the phase-change front, and lagging thermal wave velocities for partially frozen or melted conditions. Time-scales for complete melting or freezing were identified for both a range of low Biot numbers (0.001 to 1), and high Biot numbers (1 to 1000) conditions through the development of a shrinking core model applicable to phase-change within the capsules.

To validate this model and to further investigate the thermal characteristics of the system, a bench-scale fluidized packed-bed test system was developed with air used as the heat transfer fluid. Charging operations required preheating the bed supply air, while discharging operations required cooling the air prior to delivery at the bed. Temperature data support the mathematical models used to predict the behavior of thermal and phase-

change fronts advancing through the bed during melting and freezing processes. Test data allowed an accurate assessment of the time of arrival for the phase-change wave front at each known temperature transducer location and thus quantify the velocity of both the melting and freezing fronts. Velocities of isotherms in the partial phase-change region were also identified.

The temperatures and measured velocities were used to determine some unknown properties of the commercial encapsulated PCM product such as phase-change temperature, specific heats, and fraction of capsule mass comprising the PCM material. Thus, the analytical predictions represented the data very well. Temperature profiles under sensible heat transfer conditions were well represented by the classic diffusion-dispersion equation. Temperature data near the phase-change fronts show an exponential temperature profile, but significant air-to-capsule heat transfer limitations are apparent very near the front. The estimated timescale for complete melting obtained from the shrinking core model was in a reasonable agreement with what was observed in the experiments.

In addition to the exploration and validation of models for thermal and phase-change wave behaviors and temperature distributions across the bed, exergy of the bed was evaluated based on direction of flow and exergy efficiencies were estimated for two different flow arrangements, namely parallel and counter flow. Exergy efficiencies were uniform for both arrangements under test conditions in which sensible heat transfer occurred. Test results reveal that for parallel flow through the bed, where both charging and discharging occur from the bottom or the top inlet, as opposed to counter flow, in which the bed is charged and discharged through opposite inlets, longer charging times and more uniform discharge temperatures are characteristic of parallel flow arrangements.

Praise be to God, who gives us life and sustains it, for blessing me with the gifts and talents to accomplish all things worth pursuing.

TABLE OF CONTENTS

LIST OF TABLES

Tables

NOMENCLATURE

A	dimensionless temperature coefficient
Bi	Biot number
C	constant of integration
c_b	specific heat of bed, J/kg K
c_{p_g}	specific heat of air, J/kg K
c_{pc}	specific heat of PCM, J/kg K
D_p	particle diameter, m
h	convection heat transfer coefficient, W/m^2 K
h_g	enthalpy of air, J/kg
k_b	bed thermal conductivity, W/m K
k_g	air thermal conductivity, W/m K
k_{pc}	PCM thermal conductivity, W/m K
$\dot{m}$	mass flow, kg/s
$\dot{m}_{cs}$	mass flux per unit area across the frontal cross-section, kg/s m^2
q	total heat transfer, W
q_r''	heat flux per unit area in the radial direction, W/m^2
R	capsule radius, m
r	radial coordinate, m
r_{pc}	phase-change boundary radius, m
T	temperature, K
T_∞	bulk fluid temperature, K
T_e	exit temperature of air, K

T_f	front temperature, K; final temperature, K
T_i	injection temperature of air, K
T_o	initial temperature of air, K
T_{pc}	phase-change temperature, K
T_s	capsule surface temperature, K
t	time, s
t'	scaled time
t^*	scaled time
Δt	time step, s
u_{pc}	PCM internal energy, J/kg
Δu_{pc}	phase-change energy requirement, J/kg
v_g	Darcy velocity, m/s
v_{pc}	thermal wave front velocity under phase-change conditions, m/s
v_T	isothermal wave front velocity, m/s
v_{th}	thermal wave front velocity, m/s
v_{model}	theoretical wave front velocity, m/s
X_{st}	storage fluid stream exergy, J
X_{rec}	retrieval fluid stream exergy, J
x	axial coordinate, m
x_f	front location, m

Greek

α	thermal diffusivity, m^2/s
β	time constant, s^{-1}; energy of phase-change, J/m^3K
γ	transformation variable, m
δ	dimensionless distance
ε	mass fraction of PCM
ζ	dimensionless time

η_{Carnot}	Carnot efficiency
η_{II}	exergy efficiency
θ	dimensionless temperature
λ	degree of solidification
λ_o	initial degree of solidification
ρ_b	bed density, kg/m^3
ρ_g	air density, kg/m^3
ρ_{pc}	PCM density, kg/m^3
ϕ	porosity
χ	distance constant, m^{-1}
ψ_e	exergy per unit time at exit of bed, J/s
ψ_i	exergy per unit time at inlet of bed, J/s
$\dot{\psi}$	exergy per unit time, J/s
$\dot{\psi}_{fi,discharge}$	exergy per unit time at inlet of bed during discharging, J/s
$\dot{\psi}_{fo,discharge}$	exergy per unit time at outlet of bed during discharging, J/s
$\dot{\psi}_{fi,charge}$	exergy per unit time at inlet of bed during charging, J/s
$\dot{\psi}_{fo,charge}$	exergy per unit time at outlet of bed during charging, J/s
ω	ratio of phase-change boundary radius to capsule radius

ACKNOWLEDGEMENTS

Many thanks to the faculty at the University of Utah, specifically Dr. Kent Udell for his direction during this undertaking, and for allowing me to work independently and make my own decisions as much as possible, and then for making sure that, in the end, I made the right choices. I will always be grateful to Dr. Udell for helping me develop an interest in the area of sustainable energy, and I truly appreciate his expertise, professionalism, and friendship.

I would also like to thank Dr. Amanda Smith, Dr. Eric Pardyjak, Dr. Kuan Chen, and Dr. John McLennan for their willingness to serve as members of the committee and for their support and guidance on this project.

I wish to express my gratitude to my employer, Weber State University, for their financial contributions and facilities support, without which this work would have been much more difficult to complete.

Special thanks to Dr. Mark Fehlberg for helping me through this process and for taking the time to review my work in great detail and offer up useful comments that helped me to shape this product, and also to Dr. Donald Bloswick for threatening to hunt me down if I didn't promise him that I'd finish this degree.

CHAPTER 1

INTRODUCTION

1.1 Initiative and Purpose

Packed-bed thermal energy storage devices have the capacity to capture time-variant thermal energy resources. Such systems are designed to absorb or reject thermal energy, from sources or to their surroundings, respectively, making this energy available to perform useful work. Thermal energy storage devices in the form of packed-beds may be comprised of particles that are either solid, or in the form of encapsulated phase-change materials (PCMs). The primary advantages of latent thermal energy storage (associated with phase-change) are narrow PCM temperature ranges and the supply of isothermal streams of stored heat. The rate of heat transfer, to or from the bed, is governed by the thermal properties of the solid and the fluid, the temperature of the fluid and the surface temperature of the solid, the mass flow rate of the heat transfer fluid, and the physical characteristics of the bed.

Early analytical works by Schumann [1] resulted in the formulation of mathematical models that describe the rate of heat transfer associated with a liquid passing through a mass of crushed material treated as a packed-bed or porous media with large particle sizes. These original efforts describe the transient, temperature distribution within the confines of a right prism or cylindrical containment device. Graphical representations, generated using closed-form mathematical solutions, result in a universal model applicable

to arrangements of this nature, regardless of the physical constants associated with the system. The solution for systems involving a liquid as the heat transfer fluid may also be applied to gaseous heat transfer fluids. Analysis of one size of particle constituting the media enables the prediction of the temperature distribution, within a given prism, for other particle sizes.

Many processes are dependent upon the exchange of heat between fluids and solids. Thermal energy storage applications include, but are certainly not limited to, heating, ventilating, and air conditioning, agricultural greenhouse growing, and power generation. All of these processes benefit from waste heat recovery. Packed-beds involving encapsulated phase-change materials (PCMs) primarily experience a change in latent heat transfer as a result of melting or freezing. The effectiveness of heat transfer in packed-beds is dependent upon particle geometry and size, as well as the porosity or void fraction of the packing. Packed-beds comprised of encapsulated PCMs are expected to play an important role in the advancement of contemporary thermal energy storage solutions. Thermal energy storage devices, in the form of packed-beds, could be used in low temperature applications for building heating and cooling. A difficult challenge in sizing and matching system supply and demand, in terms of thermal energy storage, is managing frequently varying loads in terms of duration and magnitude [2].

PCMs offer distinct advantages in the form of small temperature differences between storage and retrieval processes, as well as low weight per unit storage capacity. In comparing the performance of packed-beds of solid particles undergoing sensible heat transfer [1], [2], [3], [4], and [5], to packed-beds experiencing heat transfer under latent conditions [6], [7], [8], [9], [10], [11], and [12], typically two types of models were used

to describe the transient behavior of a packed-bed thermal energy storage device. One is a single-phase conductivity model based on the assumption that the temperatures of the heat transfer fluid and the solid material are equal at any given axial location. The utilization of dimensionless parameters in this model results in a simplified set of differential equations and general solutions that are valid for multiple combinations of independent variables. Alternatively, the Schumann [1] model is used to explore the transient temperature distribution within packed-beds.

The purpose of this work is to obtain an understanding of thermal and phase-change waveforms and their respective velocities, temperature distributions, rates of heat transfer and phase-change solidification processes as a result of convection heat transfer processes, and exergy and flow characteristics and exergy efficiency, for packed-beds of encapsulated PCM during the injection of gaseous heat transfer fluids, as a function of time and location. Analysis of heat transfer modes for packed-beds containing encapsulated PCMs, when evaluated at a macroscopic level, may produce acceptable results in determining thermal energy storage capacity. Internal temperature gradients in encapsulated PCMs could be significant in terms of overall thermal energy storage performance. The direction of flow during the recovery of stored thermal energy may have a significant effect on the quality and consistency of the outlet fluid stream in terms of delivery temperature.

1.2 Packed-Bed Thermal Energy Storage

Packed-beds have the potential to effectively store and retrieve large quantities of thermal energy as a result of the ratio of heat transfer surface area-to-solid storage volume. This characteristic facilitates rapid and efficient heat storage and retrieval, by the selection of economic storage materials, while implementing simple yet inexpensive heat transfer

fluid distribution systems. For beds containing solid particles, only sensible heat transfer will occur. Packed-beds containing encapsulated PCMs undergo latent heat transfer in the form of melting and freezing, as well as superheating and subcooling outside of the phase-change heat transfer region. Figure 1.1 is representative of a typical packed-bed thermal energy storage device.

Heat storage device design is based on the appropriate selection of numerous parameters required to develop practical thermal energy storage systems. Geometry of the container, its orientation, the material used for construction, the packed-bed storage material, the heat transfer fluid, and the required charging and discharging times are all factors to be considered. For example, the amount of heat stored will depend on quantities such as the mass flow rate and the inlet temperature of the heat transfer fluid, along with the storage material and heat transfer fluid selected. The length, frontal area, and cross-sectional area of the packed-bed are also dimensions that effect the overall performance of the design [2].

The rate of heat transfer, to or from the bed, is a function of the thermal properties of the solid and the fluid, the temperature of the fluid and the surface temperature of the solid, the mass flow rate of the heat transfer fluid, and the physical characteristics of the bed. In most cases, packed-bed materials are randomly arranged in a container in which the heat transfer fluid flows.

The heat transfer mechanism between fluids and particles in packed-beds is complex due to recirculation of the fluid and inter- and intra-particle heat conduction. Heat transfer between the packed-bed and the container can also effect the performance of the thermal energy storage device.

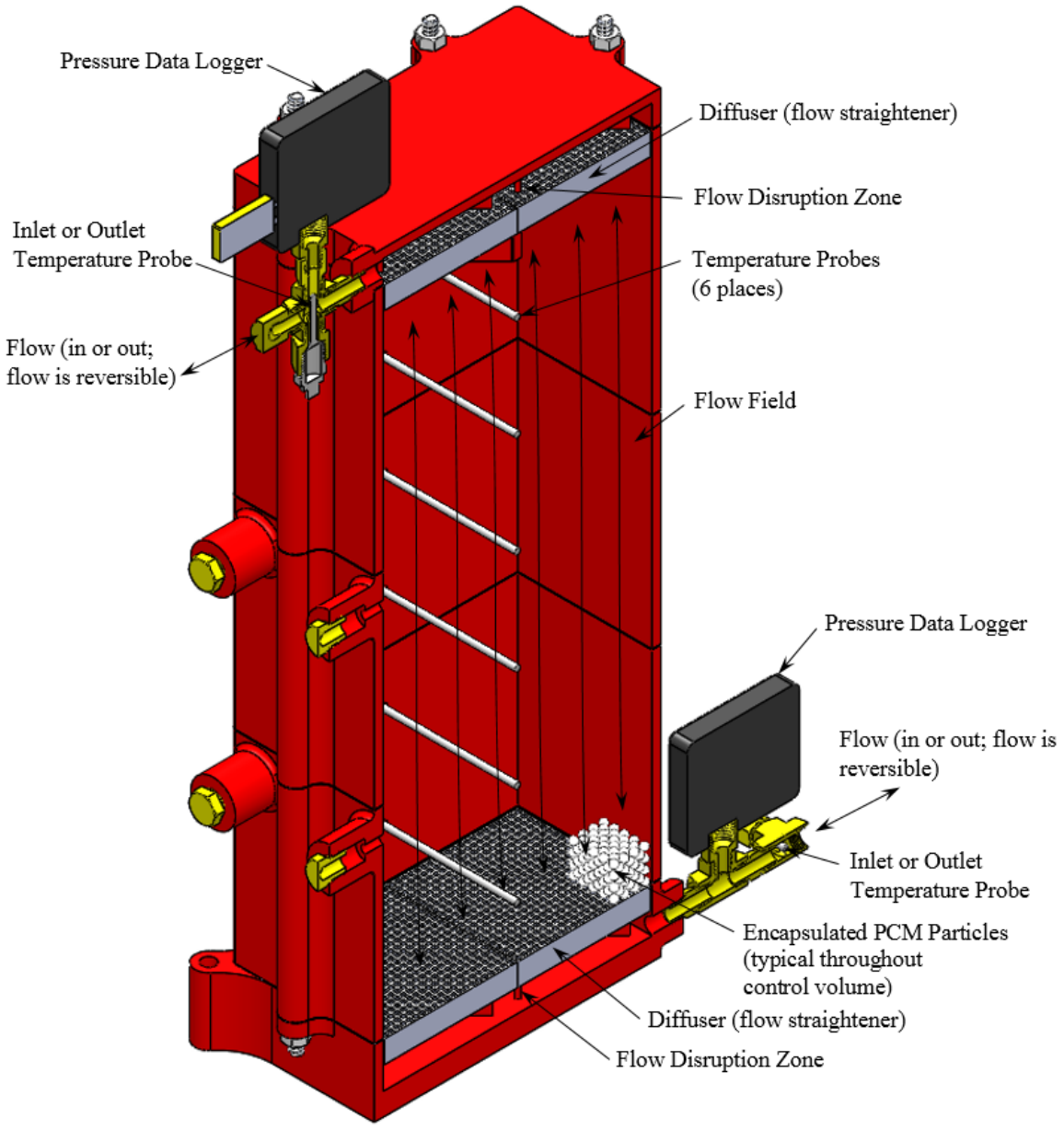

Figure 1.1 Schematic of a rectangular prism idealized packed-bed.

Packed-bed, thermal energy storage devices are advantageous in that the thermal response of such a device is relatively fast in terms of storing and retrieving thermal energy. One of the most notable disadvantages of a packed-bed used in thermal energy storage applications is the pressure drop in the fluid as it traverses the bed. The construction of very long packed-beds with small capsules would result in an extremely high pressure drop across the bed. Characteristically, packed-beds should have a large frontal area and a short length in order to reduce the pressure drop to a reasonable value [2].

1.3 Literature Review

Results of the literature review indicate the need for additional research in the area of packed-beds containing encapsulated PCMs. The literature reviewed on this subjected was the result of multiple searches using keywords such as packed-beds, phase-change materials, thermal energy storage, and air. Studies need to be conducted for thermal energy storage systems, in the form of packed-beds comprised of encapsulated PCMs, in terms of phase-change and thermal wave propagation. A contribution of new knowledge in this area will be beneficial in quantifying thermal energy storage and retrieval with respect to the time and temperature. A clear understanding of the physics of this type of system will augment the utilization of this time-variant resource, on an industrial scale, in sustainable energy applications in which thermal energy storage elements are required. A knowledge of thermal wave propagation gives credibility to temperature profiles as a function of time and location, thus improving the effectiveness of charging and discharging operations.

The geometries, materials, and heat transfer fluids vary in prior studies. A review of the literature indicates that spherical particles, contained in vertically oriented

cylindrical containers, are common for packed-bed arrangements in thermal energy storage applications.

Elements unique to this work, with the exception of Schumann's original work, are containers with rectangular cross-sections, containing encapsulated phase-change materials, in the form of spherical capsules with diameters that are one order of magnitude smaller than those used in previous studies, and that consider continuous charging and discharging operations encompassing subcooling, melting, heating, cooling, and freezing processes.

1.3.1 General Findings

Haller [13] explored different methods that characterize thermal stratification in energy storage devices from a theoretical point of view, with focus on the ability to promote and maintain stratification during charging, storing, and discharging. Existing methods for calculating stratification efficiencies were applied to the hypothetical storage processes of charging, storing, and discharging, and were compared with the rate of exergy destruction as a result of the application of these same models to data collected from experiments. Results indicate that only one method was qualitative in terms of exergy destruction due to the mixing of the heat transfer fluid and entropy changes associated with heat loss.

Dincer [14] studied thermal energy storage systems as an essential part of solar power systems. These devices were investigated with respect to heating and hot water applications, where water and phase-change materials make up the storage media. Additionally, soils, rock and other solids were used in the comparison. Packed rock beds are feasible for energy storage. The convection heat transfer coefficient between the air and the solid is high and the cost of the storage material is low. Conductivity of the bed is low

when air is not flowing. Large heat transfer surface areas can be achieved at low costs by simply reducing the size of the particles. Thermal energy storage systems were suggested for storing thermal energy at medium and high temperatures. As an example, a system comprised of oil and rock for hot water and heat recovery applications is an example of a medium temperature application. Molten nitrate salt systems may be used for steam production for process applications requiring higher temperatures. Oil-rock thermal energy storage is less expensive than molten nitrate salt systems, but is also limited to lower temperature applications. Oil-rock systems have proven successful in solar thermal applications. The selection of a thermal energy storage system depends on a number of factors such as the storage period, whether it be diurnal or seasonal, economic practicality, systems operations, as well as other parameters. In general, other factors to consider are ease of installation, maintenance, environmental impacts, safety, and sustainability.

Atul [15] used a latent heat thermal energy storage system comprised of phase-change materials to effectively store thermal energy with high-energy storage density in an isothermal storage process. Many phase-change materials melt and solidify over a wide range of temperatures, making them useful in many applications. Atul's work summarizes the investigation and analysis of available thermal energy storage systems incorporating phase-change materials for use in multiple applications.

Bédécarrats [16] studied industrial processes with thermal energy storage elements used in air conditioning or refrigeration applications, investigating a test plant configured as a tank filled with randomly dispersed commercial nodules arranged in a refrigeration loop. Spherically shaped particles with encapsulated phase-change materials were used during testing. Tests facilitated studying the behavior of the plant, particularly

in the charging mode, in order to account for subcooling during discharge. A simulation program considered aspects of surrounding heat transfer fluid and phase-change material packing effects for both charging and discharging processes.

Bédécarrats [17] also conducted experiments to investigate the performance of encapsulated phase-change energy storage devices during charging and the discharging processes. Spherical capsules, containing water with a nucleation agent as a phase-change material, filled the thermal storage tank. The heat transfer fluid circulating through the tank and around the capsules was an aqueous solution of monoethylene glycol. Experiments were conducted to investigate the effects of various parameters, including the inlet heat transfer fluid temperature and flow rate as well as the kinetics of cooling and heating effects on charging and discharging processes. Results show a significant influence of the supercooling mode of heat transfer during the charging process, specifically that the lower the inlet coolant temperature is and the larger the coolant flow rate, the faster that storage occurs. This phenomena is driven by the specification of combinations of flow rate and inlet temperature, such that total energy storage may occur over a prescribed time. When charging follows incomplete discharging, charging is the result of the solidification of some capsules that are already supercooled, while others are not. The charge mode occurs at a higher temperature over a relatively shorter duration.

Nallusamya [18] presents work that experimentally investigates the thermal behavior of a packed-bed of combined sensible and latent heat thermal energy storage units. The thermal energy storage unit contains paraffin as the phase-change material encapsulated in spherically shaped particles that are packed in an insulated cylindrical tank. Water was used as the heat transfer fluid to transfer heat from a constant temperature bath

to the tank acting as sensible heat storage system. Charging experiments were conducted at constant and varying inlet fluid temperatures to enable examination of the effects of inlet fluid temperature and flow rate on the performance of the storage tank. The variation of heat transfer fluid and phase-change material temperatures during charging and discharging operations, as well as the definition of performance characteristics such as instantaneous and total heat storage, were studied. The performance of the system was compared to conventional sensible heating systems. Results of the experiments indicate that combined storage systems employing batch-wise discharging of hot water from the tank are best suited for applications where the requirement is variable.

Mertens [19] showed that wind and photovoltaic concentrated solar power plants equipped with thermal energy storage effectively supported processes requiring on-demand intermittent energy supply. Merten's study technically evaluated the cost efficiency of thermal energy storage for solar tower power plants. The thermal energy storage element of the system consisted of a quartzite-rock bed that was charged with hot air, and discharged by cold air, in a counter flow arrangement. In principle, the system operates like a regenerator. In most cases, the discharge temperature usually decreases over time under discharge conditions. Additionally, the use of randomly packed particles in a packed-bed arrangement results in considerable pressure drop across the bed. The effects of flow and heat transfer in rock beds used for thermal energy storage were examined using a mathematical model developed using *Modelica*. Good agreement was observed between the resulting experimental data and the literature reviewed. Evaluation of the system indicates that compressor work should be considered in defining the packing geometry in order to minimize compressor work that ultimately effects the efficiency of

the overall system.

Regin [20] considered thermal energy storage systems as related to thermal applications such as space and water heating, waste heat utilization, cooling, and air-conditioning. Regin's work explored the use of phase-change materials in capsule form arranged as a packed-bed based on system effectiveness in terms of searching out methods that meet the objective of both high thermal energy storage density as well as higher efficiencies associated with thermal energy storage processes. Proper designing of thermal energy storage systems using phase-change materials requires quantitative information about heat transfer mechanisms and phase-change processes for phase-change materials. Regin investigated the development of available latent heat thermal energy storage technologies in conjunction with various aspects of thermal energy storage such as material, encapsulation methods, heat transfer effects, applications, and new phase-change materials development.

Nagano [21] analyzed a system of direct heat exchange between phase-change material granules as the solid media and air as the heat transfer fluid. The phase-change material granules consisted of a granulated porous media consisting of particle diameters on the order of about 1–3 mm. The actual phase-change material was paraffin wax. Column experiments were conducted with a packed-bed of phase-change material granules. Temperature distributions within the packed-bed were measured. Nagano's work showed the heat flux between the phase-change material granules and air may be large and uniform during phase-change. Computer models developed were based on the assumption that the temperature of the phase-change material granules is equal to that of the air passing through the packed-bed. The time for phase-change to occur proved to be in good

agreement when comparing the model and test data. Convective heat transfer coefficients during phase-change, and the time required for phase-change to occur in the system, were estimated using a numerical analysis approach.

Nithyanandam [22] analyzed the dynamic behavior of a packed-bed thermal energy storage system comprised of encapsulated phase-change materials, which were subjected to partial charging and discharging cycles, including limitations on charge and discharge temperatures as related to those akin to concentrating solar power plant operations. A transient, numerical analysis of a molten salt, single tank latent thermocline energy storage system was performed for a prescribed number of charging and discharging cycles in order to explore the dynamic response of the system. Influences of design arrangements and operating conditions on the dynamic thermal energy storage and delivery output of the system was studied to identify combinations that maximize effectiveness of thermal energy storage systems of this nature. As a result of this work, in the form of parametric studies, guidelines were developed and recommended practices established for the design of packed-bed phase-change material-based thermal energy storage systems for concentrated solar power plant operations.

Dreißigacker [23] applied thermal energy storage elements and principles to new power plant technologies such as concentrating solar power plants and adiabatic compressed air storage systems in order to establish the significance of heat storage systems as a central power plant element. Gaseous heat transfer media at elevated temperature levels were used in a regenerator-type heat storage system. Packed-bed thermal energy storage devices possess characteristically large heat transfer surface area and multiple alternatives for the use of low-cost fabrication materials. Dreißigacker noted

that packed-bed thermal energy storage device designs are prone to mechanical failures in the area of the punctiform contacts, especially during thermocyclic conditions. A simulation tool was developed to investigate the thermo-mechanical behavior during charging and discharging processes. The model was a combination of both a mechanical model of a packed-bed and a thermal model of a regenerator. The mechanical model represented the mechanical element of individual particles, based on the discrete element method. Equations were connected through the thermal expansion of particles facilitating the calculation of thermally induced forces in conjunction with resultant particle motion during the cyclic storage operations. Implementing a time-step control approach to modelling effectively increased the rate of computations. Models were validated using a test rig that was developed and fabricated. High-temperature force sensors were developed and integrated into the storage container walls to measure local mechanical particle–to-wall contact forces under static and cyclic loading conditions.

Zanganeh [24] analyzed a thermal energy storage system consisting of a packed-bed of rocks as the storage media and air as high-temperature heat transfer fluid, for application in concentrated solar power operations. A pilot-scale truncated conical shape thermal energy storage unit was fabricated buried in the ground in order to demonstrate the generation of thermoclines. A dynamic numerical heat transfer model was produced for distinct fluids and solids comprising the system, based on variable thermo-physical properties ranging from low to high operation temperatures. These models were validated via experimental results. Models were then applied to designs in order to simulate arrays of industrial-scale thermal storage units for around-the-clock concentrated solar power plant operations.

Bouadila [25] conducted an experimental study to evaluate the thermal performance of a new solar air heater collector using a packed-bed of spherical encapsulated phase-change materials in a latent heat storage system. Application of the first- and second-law of thermodynamics facilitated computation of energy and exergy efficiencies for daily operation of the system in both closed and opened configurations and in open cycle modes. Solar energy harvested was stored in packed-beds during the day and was extracted at night. Experimentally obtained results were used to evaluate system performance, based on noted temperature distributions in different locations of the collectors. Daily energy efficiencies varied and were approximately twice of those for variable exergy efficiencies.

Singh [26] studied the intermittent nature of solar energy as connected to the uninterrupted supply of thermal energy storage as required to match the varying thermal load requirements. A packed-bed control volume occupied by media similar to porous media in the form of, and created by, randomly packing particles of specific materials into a container was used to capture thermal energy rejected by solar air heaters. Studies were conducted on packed-beds in order to analyze and evaluate their performance in this application. Studies included design options for packed-beds and materials used for thermal energy storage, heat transfer enhancement, flow phenomena, and pressure drop through the bed. Conclusions indicate that several studies have been conducted on systems containing rocks and pebbles as packing material or storage media; however, very few studies have been conducted on large-sized packing materials, or even on medium-sized storage elements in packed-beds to date.

Torab [27] studied the optimization of randomly packed-beds of spheres containing

phase-change materials. A one-dimensional, transient, separate-phase model was used to simulate the performance of this type of packed-bed. Governing equations for the time-dependent temperature distributions for both the storage material and the fluid were solved using finite difference methods. Models proved to be accurate when compared to the experimental results obtained in previous studies. Objectives of optimization schemes for these types of systems were to achieve maximum utilization of the thermal energy storage and recovery capacities for the overall storage system for a given set of operating conditions and constraints. The results of this study provided optimum combinations of bed length, size of particles, and the relative size of the cross-section to the particle diameter. Significant constraints used in the optimization process were maximum and minimum pressure drop, minimum ratio of tank diameter to particle diameter, and minimum size of particles. Exergy was used as a measure of storage utilization and capacity, and provides a measure of the quality of the recoverable energy.

Sanderson [28] developed a simple model that represents and provides a qualitative understanding of axial dispersion in packed-beds. Sanderson's model was verified by comparison with current models under development. Temperature wave front velocities, storage tank geometry, the significance of natural convection, and convection heat transfer coefficient instabilities were explored and analyzed with regard to the application and performance of efficiently designed packed-bed thermal storage systems.

Bouguettaia [29] proved that packed-beds are a relatively economical way of recovering waste heat from low-grade energy sources, particularly hot air streams, and are also a means of providing energy storage from heat stores, by transferring heat to cooler air streams at later stages in various processes. Bouguettaia performed work on packed-

beds that used gravel beds as the storage medium. Volumetric convection heat transfer coefficients were determined from airstreams passing upwards through a vertical circular-section test column. The column was filled with glass balls and hollow plastic spheres filled with air, water, and palm oil, which were randomly packed in such a way that normal voidage was obtained. Air was passed through the bed materials at various inlet temperatures, and the air mass velocities and bed heights were varied. The volumetric convection coefficients of heat transfer were correlated in terms of dimensionless groups for both heating and cooling processes. Findings indicated that when the beds are cooled, the convection heat transfer rates are significantly higher. Data on the efficiency of systems containing thermal energy storage devices and on pressure drops across these types of beds show that equations used to predict outlet temperatures from the beds are effective. The application of these types of packed-beds can be utilized in both space heating and air conditioning systems with respect to measurable economic terms and resulting outcomes, where equations were developed for sizing a bed for specific time delays and attenuations of temperature profile amplitudes.

1.3.2 Thermal Characteristics

Schumann's [1] model describes the time-dependent temperature distribution for a packed-bed with a liquid heat transfer fluid. Schumann's model is applicable to packed-bed arrangements, in which the heat transfer fluid is a liquid, regardless of related independent variables. Schumann experimented with one size of particle and concluded that temperature distributions could be predicted for other particle sizes. Schumann also developed a closed-form solution to model gas flowing through a packed-bed. This model was based on the liquid model and is identical to the complimentary error function model.

Ananthanarayanan [6] and Schmidt [2] applied Schumann's model to packed-bed arrangements for both solid particles and encapsulated PCMs. Results indicated that intra-particle conduction and axial dispersion were dependent upon four dimensionless parameters, namely the Biot number, the heat capacity ratio, the thermal capacity ratio, and the Peclet number. Figures 1.2 and 1.3 show the application of Schumann's model to both sensible heating and cooling processes.

Ismail [30] produced a comparative numerical study for packed-bed thermal energy storage models for phase-change materials under sensible and latent heat transfer conditions. Four different models were used in the investigation including a continuous solid phase model, Schumann's model, a single phase model, and a thermal diffusion model that considered thermal gradients within the particles.

Yang [7] created a numerical model for packed-beds containing layers of encapsulated PCMs, each with distinct melt point temperatures. Yang applied Schumann's one-dimensional model assuming laminar, incompressible, steady state, fully-developed flow while neglecting heat transfer in the radial direction, heat transfer to the surroundings, and natural convection effects during the melting process of the PCM. Further, the thermal resistance of the capsule wall was taken as zero, and the thermo-physical properties of both the PCM, and the heat transfer fluid, were assumed to be independent of temperature. Chen [31] investigated the performance of a cold storage system using water-porous capsules as a form of PCM. A lumped model was used to develop the characteristics of the system. A solution to the model was obtained using Laplace transformation methods. Experimental temperature data were collected and examined for various porosities, fluid flow rates, and inlet temperatures, but the wave velocities were not defined.

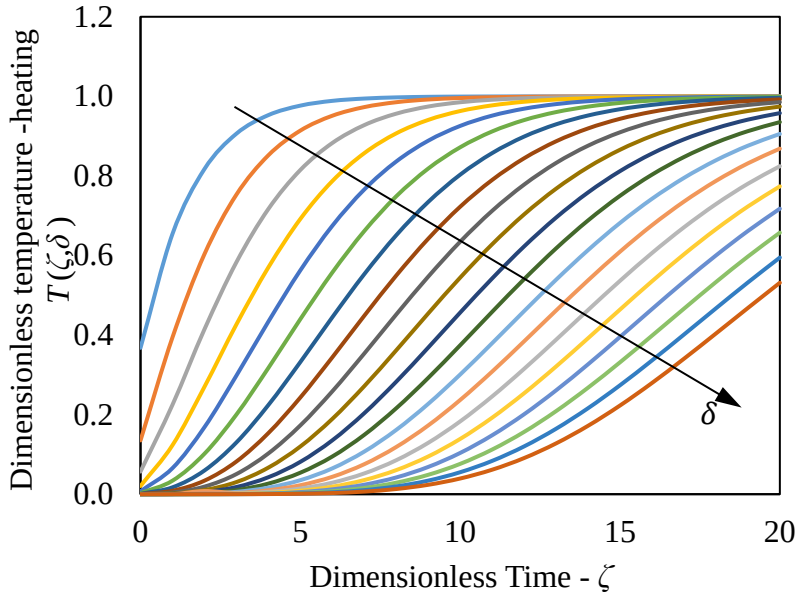

Figure 1.2 Dimensionless temperature model for sensible heating. The figure shows temperature versus time profiles with respect to of axial position along the length of the bed in the direction of flow. [2]

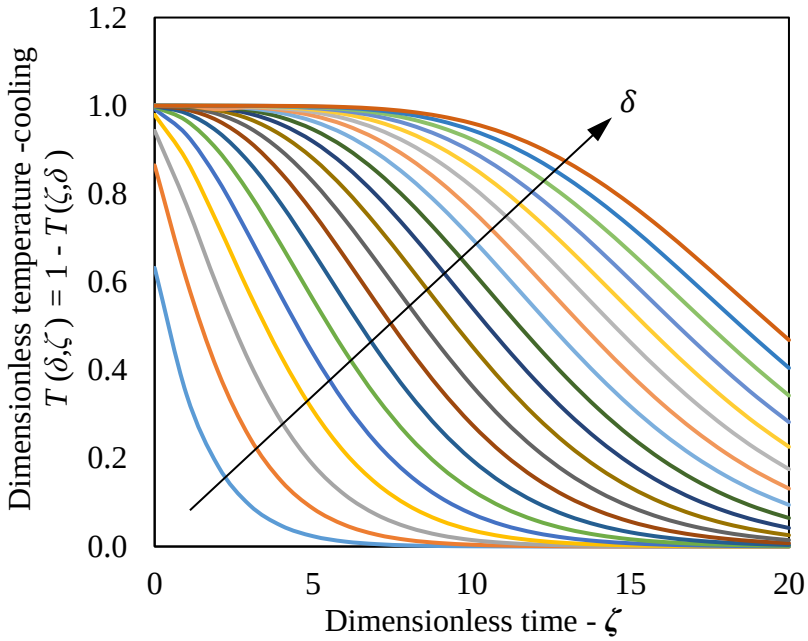

Figure 1.3 Dimensionless temperature model for sensible cooling. The figure shows temperature versus time profiles with respect to axial position along the length of the bed in the direction of flow. [2]

1.3.3 Energy and Mass Transport

Convection heat transfer coefficients in packed-bed, thermal energy storage devices are primarily dependent upon heat transfer fluid flow characteristics through the bed as well as the thermal properties of the bed storage material. Considerable resistance to heat transfer is encountered at the surface-to-fluid interface between the particles and the fluid. This resistance to heat flux is inversely proportional to the convection heat transfer coefficient. Resistance to conductive heat transfer also occurs within the particles that form the bed. Heat transfer within the particles is referred to as intra-particle heat transfer. Heat transfer may also occur from particle to particle as a result of the particles being in direct, physical contact. This mode of heat transfer is referred to as inter-particle heat transfer [2].

Incropera [32] developed a correlation for the convection heat transfer coefficient, for a packed-bed of solid particles, with a gas as the heat transfer fluid. The correlation is based on the Colburn *j* factor, defined by the Prandtl and Stanton numbers. The Stanton number, a modified form of the Nusselt number, is proportional to the convection heat transfer coefficient, and inversely proportional to the heat transfer fluid density, velocity, and specific heat. The Nusselt number, a dimensionless temperature gradient at the surface, is proportional to the convection heat transfer coefficient and the characteristic length (diameter of a sphere), and is inversely proportional to the thermal conductivity of the heat transfer fluid. The Stanton number is proportional to the Nusselt number and inversely proportional to the Reynolds and Prandtl numbers. As a result, the convection heat transfer coefficient is intrinsic to these dimensionless parameters.

Incropera [32] provides exact and approximate solutions for thermal characteristics of a sphere, initially at a uniform temperature, that experiences a change in convection

conditions. Exact solutions have been developed for the transient, one-dimensional, heat equation for a sphere. Single term approximate solutions, for this same transient response in spheres, are available in graphical form (Heisler charts) [33]. Transition and separation effects play an important part in terms of boundary layer development for flow around a sphere, particularly with respect to steady-state flow conditions.

Regin [8] proposed a model to determine the Nusselt number associated with the thermal resistance between the wall of a spherical, encapsulated PCM, and the heat transfer fluid flowing around the capsule. In this case, the Nusselt number is governed by the porosity of the packing, the heat transfer fluid properties, and the Reynolds and Prandtl numbers.

Benmansour [3] also suggested a correlation for the Nusselt number as applied to packed-beds comprised of encapsulated PCM. The relationship is a function of the Reynolds and Prandtl numbers.

Two independent studies conducted by Karthikeyan [11, 34] cited a model used to estimate the Nusselt number for a packed-bed of encapsulated PCMs. The model for the Nusselt number was based on the particle diameter, the heat transfer fluid velocity and viscosity, and the void fraction.

Ismail [9] cited a correlation for the Nusselt number applicable to a packed-bed containing spherical shells filled with PCM. The expression is dependent upon both the Reynolds and Prandtl numbers. A mathematical model was developed to determine the rate of heat transfer to or from the spherical shell containing the PCM. The model was also used to calculate the temperature at any given radius within the capsule, and to compute the amount of heat transferred to or from the capsule, during charging and discharging

processes.

Bédécarrats [35] developed a model for the Nusselt number for a vertically oriented, cylindrical right prism, filled with encapsulated phase-change materials. The correlation is a function of the Reynolds and Prandtl numbers, in addition to an empirical storage coefficient.

Hernandez-Guerrero [36] analyzed charging and discharging processes for latent thermal energy storage cells. Cells were analyzed to better understand the behavior of overall thermal energy storage system performance. Two cases were investigated; one in which PCMs were melted and frozen when a constant, uniform temperature was imposed at the lower surface of the cell, and two, a process in which the PCM melts and freezes under conditions in which a fluid flows under the cell. Direct heating and cooling from a fluid was not considered.

Aceves-Saborio [37] analyzed latent heat storage systems using a lumped model allowing the specification of PCMs using two thermodynamic parameters in combination with a specific range of operation temperatures. The model was modified by first considering the latent heat storage system as being formed by multiple, independent PCM capsules, second, that the PCMs that fill the capsules have different phase-change temperatures, and third, that the PCM melts over a finite range of temperatures. Results show that the efficiency of the model represents a higher bound for efficient operation of the system under negligible sensible heat transfer conditions using a single PCM. Multiple PCMs resulted in higher efficiencies under sensible heat transfer conditions. These efficiencies establish upper boundaries for the efficiencies of latent heat storage systems and give a measure of the potential for reversible operation.

A comprehensive review of previous studies resulted in multiple approaches to estimating the Nusselt number or the convection heat transfer coefficient.

1.3.4 Configurations and Effectiveness

Schmidt [2] indicated that the most efficient thermal energy storage device should be configured such that a large convection heat transfer surface area-to-storage volume ratio exists. Packed-beds are one type of thermal energy storage device that maximizes this ratio. This characteristic facilitates rapid and efficient heat storage and retrieval, by the selection of economic storage materials, while implementing simple, yet inexpensive, heat transfer fluid distribution systems. Schmidt optimized two quantities for packed-beds comprised of solid particles, namely the ratio of the amount of heat stored in the bed to the amount of incoming thermal energy, and the ratio of the heat stored in the bed to the maximum amount of heat that would be stored if the bed were to reach a temperature equal to the temperature of the inlet fluid stream.

Torab [38] also assessed the characteristics of a packed-bed thermal energy storage device, distinguished by a stratified temperature distribution, resulting from thermally charging the bed. The magnitude of thermoclines is directly proportional to the total exergy of the bed. Second law efficiency analyses, for packed-beds comprised of solids, indicated an increase in required pumping power with decreasing particle diameter. Data indicate that the exergy for the system increases as the particle diameter decreases. Torab also observed that exergy increased as the length of the packing material increased. As a result, the second-law efficiency of a packed-bed is improved by decreasing the particle diameter, in conjunction with an increase in the axial bed length, while decreasing the frontal area with respect to fluid flow direction.

Ramana [39] defined energy efficiency as the ratio of energy added to a packed-bed, thermal energy storage device, at any instant in time, to the maximum amount of energy that can be added during the initial charging of the system. Test results indicate that, for all mass flow rates, the efficiency for both sensible and latent heat storage processes decreases over time. Data suggest that the charging efficiency is higher for latent storage systems, for all mass flow rates, directly following the charging process. During the charging process, the average temperature of the latent storage system is higher than that of the sensible system, and therefore the capability to charge the latent heat storage system decreases over time.

Barton [40] developed and tested models comparing two charging and discharging schedules for sensible heat storage systems. The 1-way schedule charged and discharged a packed-bed vertically upward; the 2-way schedule charged the bed vertically downward and discharged the bed vertically upward. In all cases, the 2-way schedule is superior to the 1-way schedule. This ranking does not take into consideration heat transfer losses through the walls of the container or losses attributed to pumping requirements. Evaluation of the model also implied that in order to obtain high storage efficiencies, the outlet temperature of the bed should be as low as possible during the charging process and as high as possible during the discharging process.

Adebiyi [41] conducted works that entailed modelling packed-bed, thermal energy storage systems comprised of PCMs. One of the main findings of this computational effort was that the use of a distinct group of PCM did not result in thermodynamically improved performance under sensible heat storage conditions. Models were constructed for high-temperature thermal energy storage systems using multiple groups of PCMs. Other factors

of interest were system performance associated with the thermal mass of the containment vessel and the variable temperature of the gas entering the packed-bed during the storage process. Results indicated that the efficiency for systems using five different groups of PCMs, as compared to one distinct group, increased efficiencies as 13 to 26%. Modelling also suggests that heat transfer to the container wall significantly effected system performance.

Kousksou [4] defined the energy efficiency of thermal energy storage systems, in the form of packed-beds comprised of encapsulated PCMs, as the ratio of transferred heat flow to the maximum transferable heat flow. Energy efficiency of the system is dependent upon the PCM melt temperature and the flow rate of the fluid through the bed. Exergy destruction, as a result of pressure drop across the bed, appears to have little effect on the irreversibility for latent thermal energy storage processes. Results indicated that energy efficiency is strongly dependent upon the melting temperature of the PCM.

Bindra [12] presented results indicating that packed-bed, sensible heat storage devices provided exergy values that were higher than those of comparable PCM storage systems. According to Bindra, the definition of exergy efficiency for a packed-bed is the ratio of exergy for charging to exergy for discharging processes. Factors influencing performance are axial dispersion and heat loss to the surroundings. In order to increase the exergy efficiency of PCM systems, the thermo-physical properties of the material should exhibit a low latent heat of transformation and low energy density. In the case of sensible heat storage, materials with high energy density typically demonstrate higher exergy recovery.

Oró [5] hypothesized that the degree of thermal stratification within a packed-bed,

thermal energy storage device affected both the energy and exergy efficiencies of the system. Stratification efficiencies, based on the first law of thermodynamics, are based on energy recovery due to charging and discharging processes occurring at specific heat transfer fluid temperatures and flow rates. Exergy efficiency for thermal energy storage devices with prominent temperature gradients, and thus more favorable stratification efficiencies, possess higher exergy values than comparable storage systems with equal energy content but with less thermal stratification. Computational modelling and experimentation indicates that the degree of stratification present within a packed-bed, thermal energy storage device is not directly related to the energy and exergy efficiency of packed-beds containing encapsulated PCMs.

Beasley [42] observed during the charging of packed-beds that fluid flowing in a vertically downward direction led to an increase in exergy of the storage medium. During periods of stagnation, when there is no flow of the heat transfer fluid, the thermocline will decay as a result of thermal diffusion. Degradation of the thermocline results in a loss of exergy. This decrease in exergy is recognized as heat loss to the surroundings, internal diffusion, and convection heat transfer driven by the mixing of the fluid within the packed-bed. The design of thermal energy storage systems in the form of packed-beds should take into consideration exergy losses occurring due to thermocline decay.

Arias [43] investigated the sensitivity of the long-term performance of solar energy systems, with respect to stratification effects within the thermal energy storage device itself. In some instances, thermal energy storage devices are designed such that the hot, charging fluid enters the top of the bed, whereas the cold, discharging fluid is introduced at the bottom of the bed. Stratification does not necessarily depend on the heat transfer

fluid density, but in some cases on the direction of the flow. In some applications, it is convenient to measure the performance of a thermal energy storage device in terms of the second-law efficiency. This efficiency is defined as the ratio of the net exergy for the discharge process to the net exergy for the charging process. Exergy is the upper limit on the amount of useful work that can be harvested from a thermal energy source. The exergy efficiency of the thermal energy storage device is a measure of the potential of the thermal energy source to do work, divided by the heat input to the system.

Kousksou [4] created theoretical models to analyze and optimize thermal energy storage systems containing PCMs. Analysis indicates that energy and exergy efficiencies are dependent upon the phase-change melting temperature. While studies have been conducted for diurnal applications, similar models could also be applied to seasonal periods of reasonable duration.

Table 1.1 summarizes the findings from the literature review regarding thermal energy storage and retrieval processes in terms of relative fluid temperature (hot or cold), fluid stream ingress (top or bottom), and particle characteristics (solid or encapsulated phase-change material). Information from previous studies, when observed with respect to flow direction for thermally charging and discharging packed-beds, is various (Table 1.1).

1.4 Motivation for Improvement

While there is some agreement among multiple, similar approaches to establishing the convection heat transfer coefficient either directly, or via the Nusselt or Stanton numbers, a considerable degree of differences exist between models. Convection heat transfer coefficients have been based on heat transfer fluid thermal conductivity, the

Table 1.1 Thermal energy storage and retrieval arrangements for packed-beds. Configurations are defined by fluid temperature (hot or cold) in combination with flow ingress (top or bottom inlet).

Reference number	Storage				Retrieval				Solid or phase-change material	
	Fluid		Ingress		Fluid		Ingress			
	Hot	Cold	Top	Bottom	Hot	Cold	Top	Bottom	Solid	PCM
[3]	x		x							x
[5]				x						x
[7]	x		x			x		x		x
[8]			x				x			x
[10]				x			x			x
[11]	x			x						x
[12]	x		x			x		x		x
[34]	x			x						x
[38]	x		x						x	
[39]	x		x							x
[40]*	x			x		x		x	x	
[40]*	x		x			x		x	x	
[42]	x		x			x		x	x	

*1-way and 2-way schedules

Nusselt number, and the particle diameter. Other models define the convection heat transfer coefficient as being proportional to the surface heat transfer coefficient and the particle surface-to-volume ratio. In some cases, the Nusselt number is only dependent upon the Reynolds and Prandtl numbers. Occasionally, the Nusselt number is based on the Reynolds and Prandtl numbers, in conjunction with an empirical storage coefficient. Other models indicate that the Nusselt number is governed by the porosity of the packing, the heat transfer fluid properties, and the Reynolds and Prandtl numbers.

The primary advantages of latent thermal energy storage with phase-change are narrow phase-change material temperature ranges and the supply of isothermal streams of stored heat. Because current approaches to quantify convection heat transfer coefficients are diverse, further research is required to identify methods that accurately predict convection heat transfer for packed-bed, thermal energy storage devices with a specific phase-change material.

Due to the variable nature of thermal energy availability, from sources such as solar thermal or industrial waste heat, reliable design criteria is vital in supporting the development of useful thermal energy storage devices. While many methods of thermal energy storage have been used, packed-beds comprised of encapsulated PCMs are a valuable thermal energy storage media due to their high energy storage densities and ability to provide stored thermal energy at a fixed temperature.

1.5 Applications

Examples of industrial applications involving packed-beds are catalytic reactors, pebble bed heaters, evaporators, absorbers, glass furnaces, and thermal energy storage units [2]. By definition, a packed-bed thermal energy storage device is comprised of closely

packed particles within the confines of a container, in which liquid or gaseous heat transfer fluids flow, thus resulting in thermal energy exchange between the fluid and the particles [1]. The primary advantages of latent thermal energy storage in a packed-bed of encapsulated PCM capsules are narrow PCM temperature ranges and the supply of isothermal streams of stored heat [2]. The supply of constant temperature thermal energy is important to the operation of systems in agricultural growing environments, direct expansion air conditioning and heat pump designs, power generation applications, and mitigation of the effects of variability associated with temperature control during heat exchange processes.

Energy storage systems with the capacity to capture and utilize waste heat will always have a place in societies that are interested in the ever-increasing quest for clean, sustainable, and renewable energy resources, and the conservation of these resources, especially when measured with respect to advancing technologies and engineering design solutions. While systems designed to harvest waste thermal energy from industrial processes are of great value, consideration should be given to systems that operate in a more passive fashion, in that they are capable of extracting thermal energy from ambient conditions and converting this energy into useful work. The economics of these types of systems must always be considered and justified on a dollar per unit of energy stored or harvested basis, in order to prove out the capital investment effectiveness of these types of ventures. In the case of this particular type of system, variables that may be assessed are the quantity and quality associated with PCMs, packed-bed design, flow distribution systems, insulation properties, and heat transfer fluid pumping power requirements.

Low, intermediate, high, and combined temperature thermal energy storage

applications are found in practice. Some of these applications are discussed below.

1.5.1 Low Temperature

Greenhouses lend themselves well to low temperature thermal energy storage [44]. The capture of thermal energy during daytime hours facilitates the use of stored thermal energy during nighttime hours, manifesting returns in the form of increased production resulting from accelerated growth rates, meaning shorter time to harvest. This method of thermal energy storage also makes the expansion of greenhouse operations into colder climates possible. Above-ground packed-beds could be used to augment these processes. Fans already in place for ventilation, and thus the release of wasted thermal energy, could be utilized to charge beds during the day, and retrieve energy at night. Additionally, improved technologies in terms of temperature control improves the ability to maintain these enclosed growing environments at a more constant temperature, thus mitigating thermal shock to the plant life during germination and growth. Figure 1.4 shows these applications.

1.5.2 Intermediate Temperature

While work has been performed in applications using thermal siphons containing refrigerants, and acting as cold-storage or as a type of icehouse storage technology to aid in supporting cooling load requirements for small commercial buildings [48], encapsulated PCMs may also be applied in supporting these types of air conditioning requirements. As an example, encapsulated PCMs could be buried underground, enclosed in an air-tight membrane impervious to ground water, that would facilitate the maximum amount of heat transfer from the packing to the surrounding soil, at a depth at which the ground

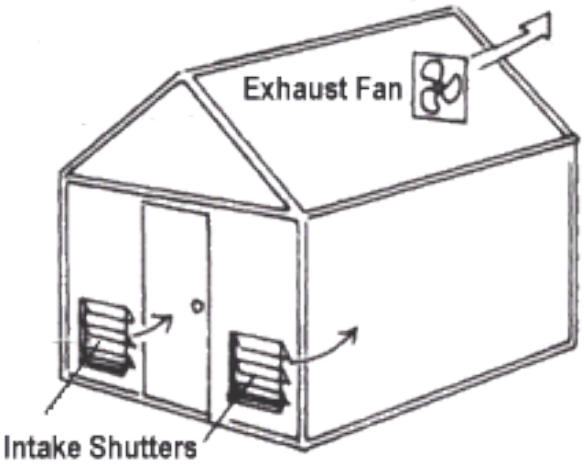

(a)

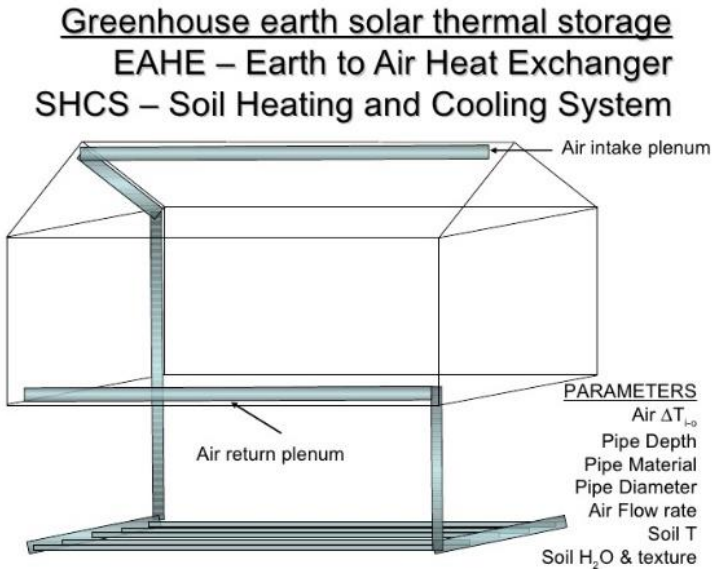

(b)

Figure 1.4 Greenhouse applications. (a) Potential for capture of thermal energy from exhaust air stream. (http://www.littlegreenhouse.com/fan-calc.shtml) [45] (b) Proposed system for heat exchange between air and soil as the storage medium. (http://www.slideshare.net/ChristopherLent1/clipboards/alternative-greenhouse-heating) [46]

temperature is nearly constant at all times of the year [47].

The configuration of the beds could be varied in terms of geometric constraints in order to optimize the size, shape, and orientation of the bed with respect to local topography, with the potential for increased coefficients of performance [49], due to the work input being strictly limited to the pump or fan work required to distribute the heat transfer fluid through the bed. The bed would be most effective during periods of higher ambient temperatures, as the fluid discharge temperatures could approach constant ground temperatures.

Direct-expansion refrigeration systems may utilize stored waste thermal energy for increased performance [50]. Depending on geographical location, underground packed-beds could be utilized to extract heat from climates with warm ambient conditions, and transfer it to the ground, at constant soil temperatures dependent upon depth. As an example, desert climates reach high daytime temperatures, with rapidly decreasing ambient temperatures past sunset hours. Matching ambient and underground bed temperatures aligns available thermal energy with optimal soil depth conditions for conduction heat transfer (Fig. 1.3 (b)), to meet air conditioning load requirements, thus improving the overall effectiveness of refrigeration and heat pump systems. Similar to the packed-bed arrangement described for greenhouse applications, underground packed-beds could be used to facilitate heat transfer between the bed and the soil in order to augment the performance of the aforementioned air conditioning and heat pump systems.

These effects would be most notable in precooling fluid streams to be introduced to environments requiring air conditioning. Cool air from the bed could be mixed with either outside air, or return air from the conditioned space, prior to delivery at the

evaporator.

This approach reduces the cooling load by decreasing the enthalpy of the conditioned air prior to additional processing. Precooling the air also improves performance by compensating for increases in conditioned air temperatures resulting from blower fan work, or thermal energy manifesting itself in the fluid stream as a result of the work input to increase the pressure of the air. Compressor work input could be reduced by decreasing the temperature of the air used during condensing. This practice effectively cools the refrigerant during the compression process, thus decreasing the specific volume of the refrigerant, and the work input to the compressor. As compressor work is reduced, the coefficient of performance for the refrigerator is increased. At lower condensing temperatures, the opportunity for subcooled, liquid refrigerant delivery to the evaporator via the expansion valve is increased, as a result of lower enthalpies for the liquid refrigerant at subcooled temperatures, making it possible for the evaporator to absorb more heat from the refrigerated space. This approach is also important in reducing the amount of air that needs to be drawn or pushed across the condenser, resulting in lower work input to condenser fans. Evaporator performance would also be enhanced by precooled air streams in that less air flow across the coil would be required as a result of lower temperature conditioned air being introduced to the climate controlled environment, thus reducing blower horsepower requirements.

This discharge fluid stream could also be delivered to the evaporator, as a precooled fluid stream at a lower temperature than that returned from the conditioned environment, thus improving the performance of the cooling system as related to the apparatus dew-point temperature [51]. These processes could be performed independently or in combination,

simultaneously, in order to optimize refrigeration system performance. This design could be modeled as an internal convection to conduction heat transfer problem. The system would take advantage of the apparent availability of energy at the dead-state with respect to the atmosphere, and transform it such that useful work requirements in terms of refrigeration compressor work could be decreased. These methods may also be enhanced by exploring the opportunities available through packed-bed stratification, in the form of encapsulated PCMs with different phase-change temperatures, with the materials being stored in an underground, stratified arrangement coincident with ground temperatures that are congruent with the PCM melting point temperature.

Heat pump operation (Fig. 1.5) would also be effected by applying these thermal energy storage principles. One of the most common energy sources for heat pumps is atmospheric air. One problem with air source systems is frosting, which occurs in humid climates when temperatures drop to around 2 to 5°C. In some cases, coils can be defrosted by reversing the cycle, at the cost of decreased efficiency [49]. Above-ground, well-insulated packed-beds, containing warm air harvested during the daytime hours, could be used to abate frosting that occurs at air temperatures near freezing. Thermal energy storage devices would also allow the expansion of heat pump applications to colder climates as a result of utilizing thermal energy stored during the day and retrieved at night. Figure 1.5 shows the refrigeration and heat pump systems and operations previously described.

Power generation operations benefit from thermal energy storage [48]. The Brayton cycle with intercooling, reheating, and regeneration is commonly used in power generation. Intercooling and reheating decrease the thermal efficiency of the Brayton cycle, and are always accompanied by regeneration [49]. Thermal energy storage has

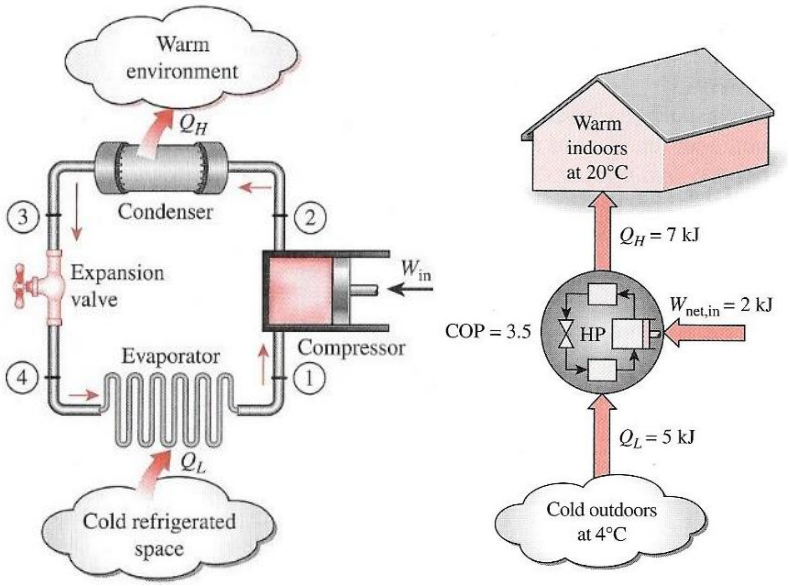

(a) (b)

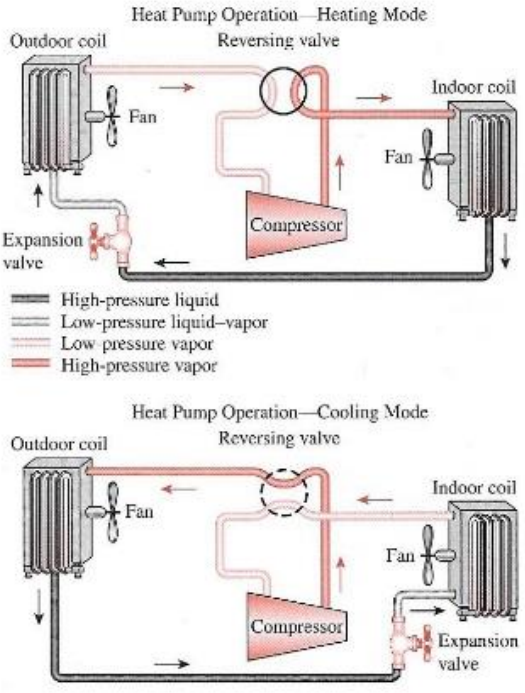

(c)

Figure 1.5 Air conditioning and heat pump applications. (a) Refrigeration system. (b) Heat pump layout. (c) Heat pump operation modes. Packed-beds of PCM utilized in improving coefficient of performance of direct expansion refrigeration systems. (© Cengel and Boles) [49]

application in advanced-adiabatic, compressed air energy storage systems (AA-CAES) used for power generation. Figure 1.6 shows this system schematically.

1.5.3 High Temperature

The net work of a gas turbine cycle is increased by decreasing the compressor work, increasing the turbine work, or both. On the compression side, a reduction in compression work is accomplished by compressing the air in multiple stages, and intercooling the air between stages. Intercooling [49, 52, and 53] between each stage of compression is accomplished via air-to-air heat exchangers. Heat rejection rates at the intercoolers increase as the number of stages of compression increases. Heat rejection per intercooler is higher in lower multiples of stages of compression; however, higher multiples of stages of compression have an increased number of intercoolers, thus resulting in overall higher heat rejection rates. Turbine work is increased by employing multistage expansion techniques coupled with reheating. Steady-flow compression or expansion work is proportional to the specific volume of the gas. As a result, the specific volume of the working fluid should be as low as possible during compression, and as high as possible during expansion. Because intercooling and reheating decrease the thermal efficiency of the cycle, they are always accompanied by regeneration [49]. These principles find application in the AA-CAES shown in Figure 1.6. During multistage compression, thermal energy rejected at each intercooler is simply lost to the surroundings. Packed-bed thermal energy storage devices would capture this heat and return it to the compression fluid stream prior to combustion. Storing and using the heat rejected to the atmosphere during intercooling mitigates exergy destruction. Additionally, after-cooling the compressed air to the temperature of the air in the cavern would also capture waste thermal

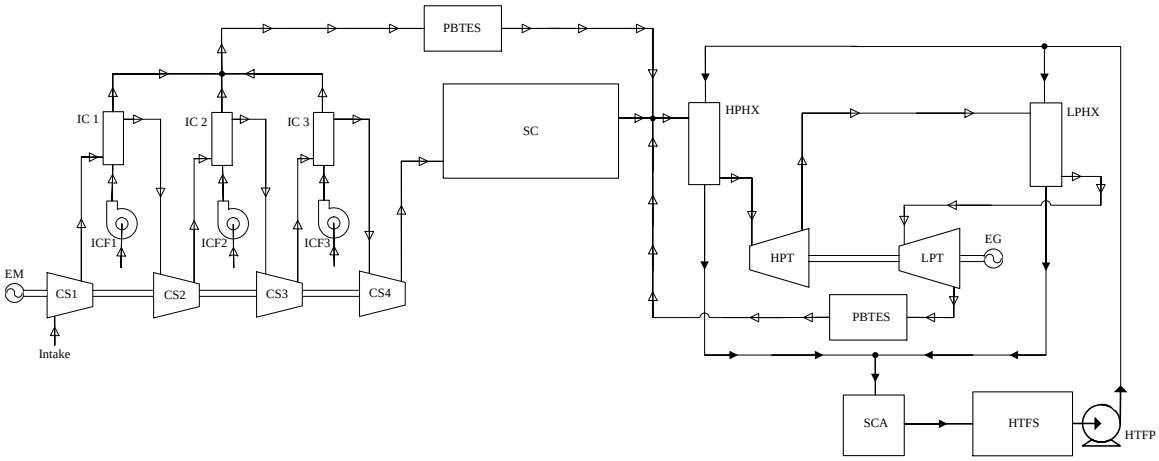

Figure 1.6 Compressed air energy storage schematic. Component legend: CS–Compressor stage, EG–Electric generator, EM–Electric motor, HPHX–High pressure heat exchanger, HPT–High pressure turbine, HTFP–Heat transfer fluid pump, HTFS–Heat transfer fluid storage, IC–Intercooler, ICF–Intercooler fan, LPHX–Low pressure heat exchanger, LPT–Low pressure turbine, PBTES–Packed-bed thermal energy storage, SC–Storage cavern, SCA–Solar connector assembly. The packed-bed thermal energy storage (PBTES) component supports the capture and reuse of thermal energy used to improve overall power plant thermal efficiency.

energy that otherwise might be lost to the ground comprising the cavern. This waste thermal energy would facilitate additional preheating of the air prior to delivery at the combustion chamber. Purged exhaust gases at the outlet of the turbine at the final stage of expansion could also be stored and used for this same purpose. Potential also exists in capturing waste heat at the outlet of the regenerator for use in similar processes. In short, significant amounts of waste heat could be captured, stored, and reintroduced at prescribed temperatures, at multiple points in the AA-CAES power production process. The temperature and pressure of the air entering the high pressure turbine decreases over time as a result of isentropic expansion as mass is transferred from the cavern. In the case of preheating the air prior to introduction at the turbine, the air released from the cavern is heated, at a constant pressure, using energy harvested from waste thermal energy sources such as inter- or after-cooling, in an air-to-air heat exchange process. Thermal energy stored in packed-beds could be used for this purpose. Expansion through turbines without prior heating is extremely inefficient and results in air temperatures that are considerably lower than ambient temperatures. As a result of excessive air temperatures at the exit of both the high and low pressure turbines, employing a time varying heat input prior to expansion of the air in the turbines would optimize thermal energy expenditures [54]. A knowledge of thermal wave propagation in packed-beds would produce optimization parameters directly.

Improved power plant designs preheat the air prior to delivery at the turbine in an air-to-air heat exchange process. Thermal energy stored in packed-beds would be used for this purpose. Expansion through turbines without prior heating is inefficient and results in air temperatures that are lower than ambient. Employing a time varying heat input prior to

expansion of the air in turbines optimizes thermal energy utilization [54]. A knowledge of thermal wave propagation in packed-beds would produce optimization parameters directly.

1.5.4 Combined Temperature Ranges

The performance of combined heat and power systems may be enhanced by the implementation of a thermal energy storage element in the design of the system [55]. Thermal energy storage systems have the potential to reduce energy consumption and carbon dioxide emissions. Typically, the thermal capacitance of the thermal energy storage device is considered, as opposed to the material that constitutes the device, in order to establish the overall capacity of the thermal energy storage system. The size of the storage system is a function of the thermal energy storage material and the materials required for fabrication of the vessel. The efficiency of heat exchangers must be taken into consideration when losses result from thermal dissipation. Different types of thermal energy storage devices may display unique thermal loss characteristics. In some applications, multiple thermal energy storage devices may be required in order to maximize the thermal energy benefit [55]. Figure 1.7 depicts a combined heat and power system (CHP) that incorporates a thermal energy storage tank.

When a CHP system produces excess heat, it may be stored in a thermal energy storage device, such as a packed-bed. While packed-beds of encapsulated PCMs have a wide applicability across a range of temperatures, their proper design requires an understanding of time-temperature response to various operating conditions as well as heating and cooling rates. While detailed modeling of all heat transfer processes is possible, the approach taken in this work is to capture the dominant processes through the examination of the thermal waves that propagate through the packed-bed during charging

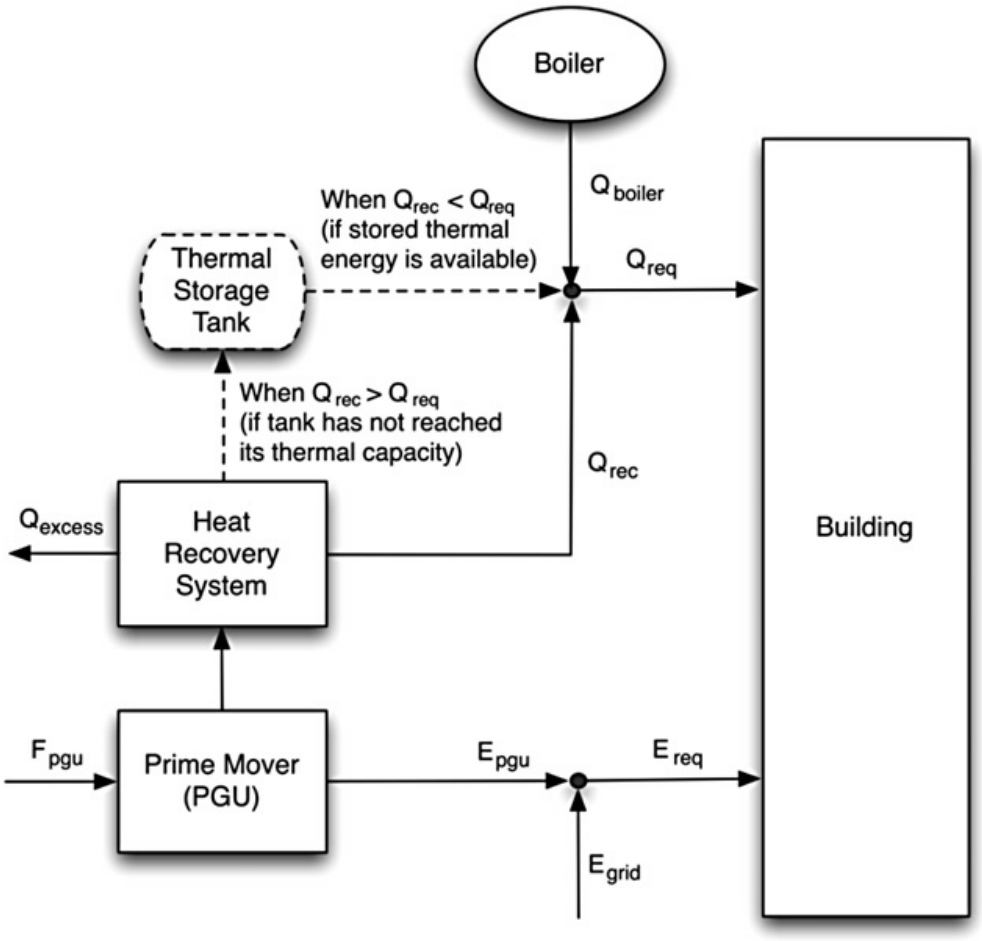

Figure 1.7 CHP-TS system schematic with thermal storage tank. (© Amanda D. Smith) [55]

and discharging operations. The idea of velocities of isotherms reaching axial locations at a given time facilitates thermal energy storage and retrieval with improved precision in terms of temperature and quantity of thermal energy. Appropriate convection heat transfer coefficients cited in the literature may be used to estimate rates of thermal energy stored or retrieved.

1.6 Objectives

One objective of this research is to develop models that predict the temperature distributions with respect to time, as well as thermal and phase-change wave propagation and velocities under sensible and latent heat transfer conditions, respectively, for thermal energy storage systems in the form of packed-beds comprised of encapsulated PCMs. While the experimental configuration employed in this study is similar to those cited in the literature, the literature does not reflect any work regarding the propagation of thermal or phase-change waves, and the velocity of these waves, in packed-beds of encapsulated PCMs. Temperature distributions expressed in terms of a dimensionless distance across the bed will also be explored in order to confirm the applicability of axially exponential temperature distributions along the length of the bed. Additionally, while an extensive review of the literature and previous works for heat transfer in packed-beds and thermal energy storage devices containing PCMs gives insight into fundamental heat transfer processes, primarily in the form of convection heat transfer coefficients during the charging and discharging processes for thermal energy storage in packed-beds consisting of encapsulated PCMs, none provide a clear description of how these convective heat transfer processes control the propagation of the thermal waves to be expected during the melting, heating, cooling, and freezing of a packed-bed of encapsulated PCMs. The rate at which

melting and freezing occur in the encapsulated PCM will be addressed in order to establish a more robust method for estimating convection heat transfer coefficients, which will require an alternative approach to estimating these coefficients using the temperature and time data collected during experimentation, with the intent of this effort being to define the dominant heat transfer mechanisms that control the performance of packed-beds of encapsulated PCMs. This work tests the theory that the propagation of temperature and phase-change waves predict the melting and freezing processes of encapsulated PCMs when a gaseous heat transfer fluid flows through the packing. Finally, energy storage will be quantified in order to prove that the hypothesis for the most efficient operation of energy storage and retrieval processes in a packed-bed of encapsulated PCM, in terms of energy and exergy management, occurs under conditions when the bed is charged, with hot fluid in a vertically downward direction, and is discharged with cold fluid in a vertically upward direction, under forced convection heat transfer conditions.

CHAPTER 2

THEORY AND MODELS

2.1 Sensible Temperature Distributions in Packed-Beds

Schumann [1] developed a closed-form solution to model gas flowing through a packed-bed. This model is based on a model for liquid heat transfer fluids, and is identical to the complimentary error function model. The model shown in Figure 2.1 shows the temperature-time curve for any axial location in a packed-bed of particles undergoing sensible heat transfer.

Chen [31] investigated the performance of a cold storage system using water-porous capsules as a form of a PCM. A lumped model was used to develop the characteristics of the system. A solution to the model was obtained using Laplace transformation methods. Experimental temperature data were collected and examined for various porosities, fluid flow rates, and inlet temperatures, but the wave velocities were not defined.

In general, the waveform profiles shown in Figure 2.1 can be derived using Laplace transforms with the boundary conditions of $T \rightarrow T_i$ as $\gamma \rightarrow -\infty$ and $T \rightarrow T_o$ as $\gamma \rightarrow +\infty$. The distribution is governed by γ

$$\frac{T - T_i}{T_i - T_o} = 1 - \frac{1}{2}\operatorname{erfc}\left(\frac{\gamma}{2\sqrt{\alpha t}}\right) \tag{2-1}$$

where T is the temperature as a function of time, t , T_i is the injection temperature of the

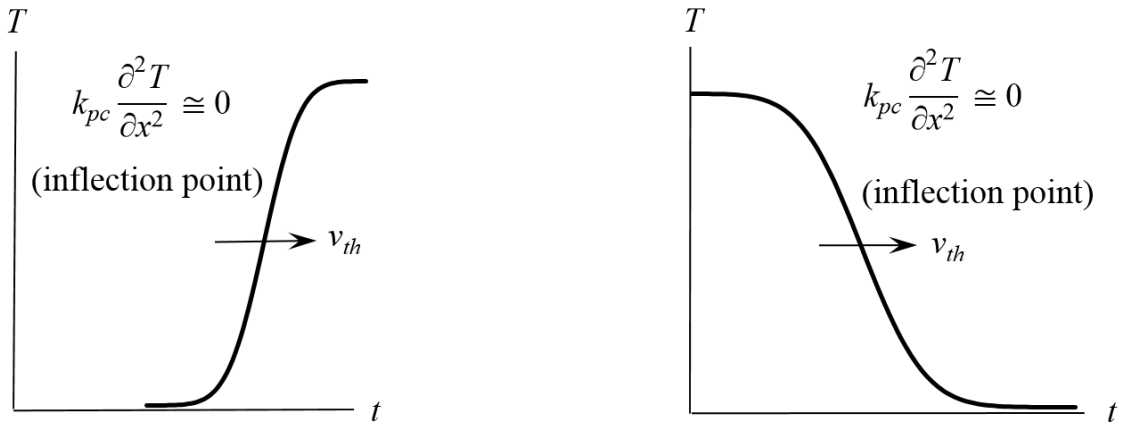

(a) (b)

Figure 2.1 Temperature-time curves for thermal waveforms in packed-beds. (a) Sensible heating. (b) Sensible cooling. The model is based on the complimentary error function (Equation 2-3). The thermal wave velocity is defined by the propagation of the mean-temperature isotherm (where the second derivative is zero).

air, T_o is the initial temperature of the air, α is the thermal diffusivity, and the transformation variable, γ, is defined as

$$\gamma = x - v_{th}t \tag{2-2}$$

with x as the axial coordinate with respect to the inlet of the bed, and v_{th} is the thermal wave front velocity. The complimentary Gaussian error function [32] is defined as

$$\text{erfc } w \equiv 1 - \text{erf } w \tag{2-3}$$

where the error function is

$$\text{erf } w \equiv \frac{2}{\sqrt{\pi}} \int_0^w e^{-\nu^2} \, d\nu \tag{2-4}$$

The thermal diffusivity, α, is defined as the ratio of thermal conductivity to the product of the density and the specific heat for the bed, where k_b is the bed thermal conductivity, ρ_b is the bed density, and c_b is the specific heat of the bed.

$$\alpha = \frac{k_b}{\rho_b c_b} \tag{2-5}$$

The density and specific heat of the bed are defined as

$$\rho_b = \phi\rho_g + (1 - \phi)\rho_{pc} \tag{2-6}$$

and

$$c_b = \phi c_{p_g} + (1 - \phi)c_{pc} \tag{2-7}$$

where ϕ is the porosity of the packing, ρ_g is the density of the air, ρ_{pc} is the PCM density, c_{p_g} is the specific heat of air, and c_{pc} is the specific heat of the PCM, or heat capacity of the phase-change material itself.

2.2 Phase-Change and Thermal Wave Fronts

The same model proposed by Schumann [1] for waveforms, and the propagation of waves experiencing sensible heat transfer, may be applied to a cascading arrangement of both thermal and phase-change waveforms and wave propagation as shown in Figure 2.2.

Considering a packed-bed of encapsulated PCM with a phase-change temperature T_{pc}, initially at a temperature T_o, subjected to heating through the injection of a hot fluid, $T_i > T_{pc}$, the propagation of thermal waves in terms of temperature versus position may be described as shown in Figure 2.2.

The application of an energy balance to the system to calculate the thermal wave front velocity, v_{th}, or the phase-change melt front velocity, v_{pc}, is governed by [54]

$$-\frac{\partial(v_g \rho_g h_g)}{\partial x} = \phi \rho_g c_{p_g} \frac{\partial T}{\partial t} + (1 - \phi) \frac{\partial(\rho_{pc} u_{pc})}{\partial t} \tag{2-8}$$

where v_g is the Darcy velocity defined as the flow per unit cross-sectional area of the porous media, h_g is the enthalpy of the air, and u_{pc} is the PCM internal energy.

$$-\frac{\partial(v_g \rho_g h_g)}{\partial x} = \phi \rho_g c_{p_g} \frac{\partial T}{\partial t} + (1 - \phi) \frac{\partial(\rho_{pc} u_{pc})}{\partial t} \tag{2-8}$$

Transforming Equation 2-8 to a coordinate system that travels with the phase-change requires that

$$\gamma = x - v_{pc} t \tag{2-9}$$

with v_{pc} representing the thermal wave front velocity under phase-change conditions.

Applying the transformation gives

$$\frac{\partial \gamma}{\partial x} = 1 \tag{2-10}$$

$$\frac{\partial}{\partial x} = \frac{\partial}{\partial \gamma} \frac{\partial \gamma}{\partial x} = \frac{\partial}{\partial \gamma} \tag{2-11}$$

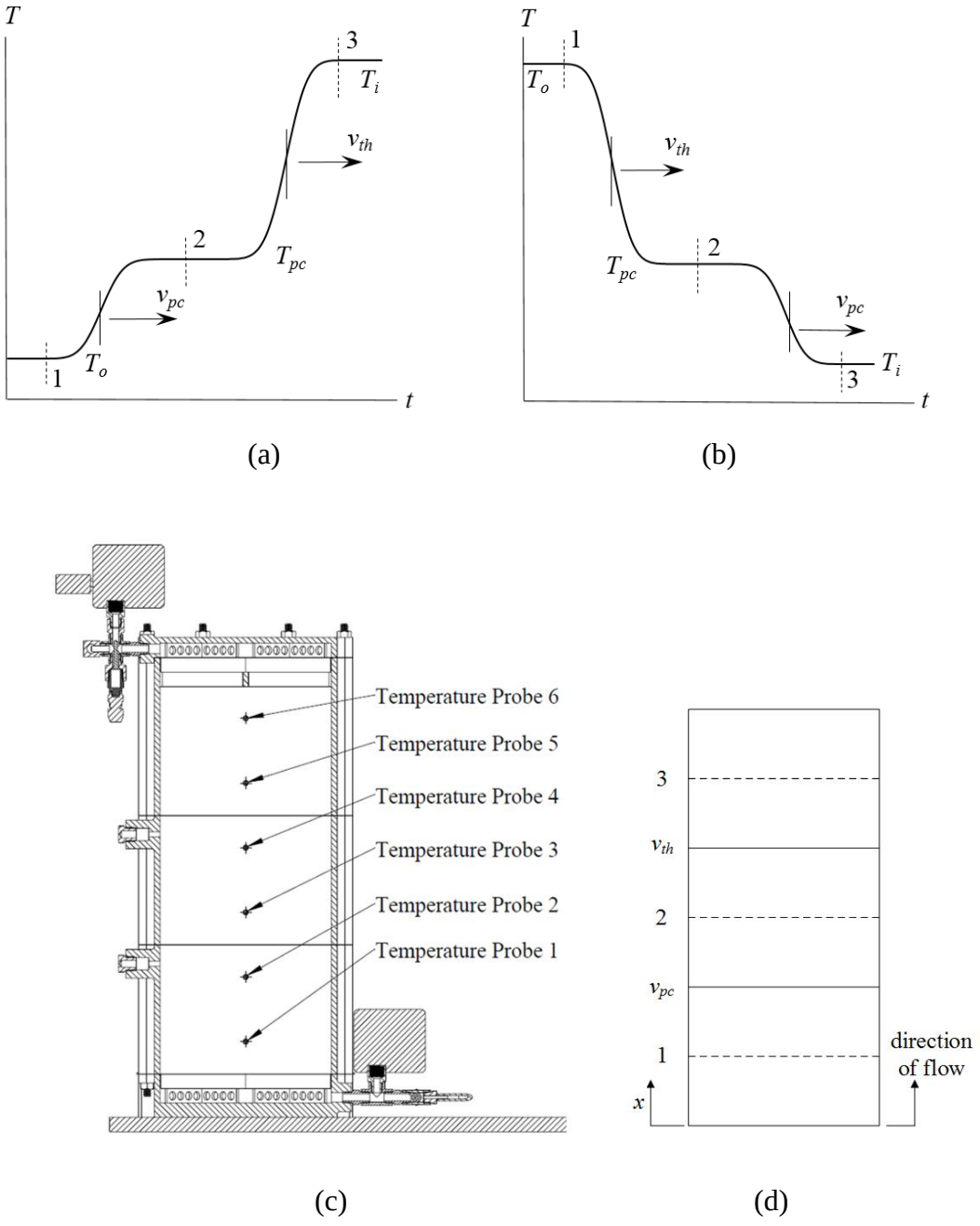

Figure 2.2 Waveform propagation model for packed-beds. The figure shows advancement of thermal wave fronts, v_{th}, and phase-change wave fronts, v_{pc}, with respect to the time, t, the injection temperature of the air, T_i, and the initial temperature of the air in the bed, T_o. (a) Melting and heating. (b) Cooling and freezing. (c) Section view of the experimental apparatus with temperature probes arranged along the central axis of the bed. (d) Schematic diagram of the packed-bed showing the propagation of isotherms across the packing in a direction that is normal to the direction of flow of the heat transfer fluid. The figure shows isotherm travel for the melting and heating processes.

$$\frac{\partial \gamma}{\partial t} = -v_{pc} \tag{2-12}$$

As a result, Equation 2-8 may be written as

$$-\frac{d\left(v_g \rho_g h_g\right)}{d\gamma} = -v_{th}\frac{d[\phi T \rho_g c_{p_g} + (1-\phi)\rho_{pc} u_{pc}]}{d\gamma} \tag{2-13}$$

where the thermal wave front velocity, v_{th} , or the phase-change melt front velocity, v_{pc} , is constant.

Rearranging Equation 2-13 gives

$$\frac{d\left\{-v_g \rho_g h_g + v_{th}[\phi T \rho_g c_{p_g} + (1-\phi)\rho_{pc} u_{pc}]\right\}}{d\gamma} = 0 \tag{2-14}$$

Integrating Equation 2-14 with respect to γ yields

$$v_{pc}\left[\phi T \rho_g c_{p_g} + (1-\phi)\rho_{pc} u_{pc}\right] - v_g \rho_g h_g = C \tag{2-15}$$

Applying this relationship at points 1 and 2 in Figure 2.2 produces

$$v_{pc}\left[\phi T_i \rho_g c_{p_g} + (1-\phi)\rho_{pc} u_{pc_1}\right] - v_g \rho_g c_{p_g} T_i = v_{pc}\left[\phi T_{pc} \rho_g c_{p_g} + (1-\phi)\rho_{pc} u_{pc_2}\right] - v_g \rho_g c_{p_g} T_{pc} \tag{2-16}$$

or

$$v_{th}\left[\phi \rho_g c_{p_g}(T_i - T_{pc}) + (1-\phi)\rho_{pc}(u_{pc_1} - u_{pc_2})\right] = v_g \rho_g c_{p_g}(T_i - T_{pc}) \tag{2-17}$$

with T_{pc} defined as the phase-change temperature of the PCM.

The ratio of the thermal wave front velocity to the Darcy velocity is written as

$$\frac{v_{th}}{v_g} = \frac{\rho_g c_{p_g}(T_i - T_{pc})}{\phi \rho_g c_{p_g}(T_i - T_{pc}) + (1-\phi)\rho_{pc}(u_{pc_1} - u_{pc_2})} \tag{2-18}$$

with the phase-change media internal temperature defined as

$$u_{pc} = c_{pc} T + \varepsilon \Delta u_{pc} \tag{2-19}$$

where ε is the mass fraction of the PCM in the capsule, and Δu_{pc} is the phase-change energy

requirement.

Rearranging Equation 2-16 results in the ratio of the phase-change front velocity to the Darcy velocity.

$$\frac{v_{pc}}{v_g} = \frac{1}{\phi + \frac{(1 - \phi)\rho_{pc}c_{pc}}{\rho_g c_{p_g}} + \frac{(1 - \phi)\rho_{pc}\varepsilon\Delta u_{pc}}{\rho_g c_{p_g}(T_i - T_{pc})}} \tag{2-20}$$

2.3 Degree of Solidification

The potential also exists for the velocity of an isotherm resulting from fluid flow through porous media, comprised of encapsulated PCM, to be effected by a partial phase-change of the material within the capsules of a particular region. The model [56] shown in Figure 2.3 and 2.4 is used to explain this phenomena.

In this case, the energy equation for steady, one-dimensional uniform flow of air with a prescribed velocity, density, specific heat, and temperature may be written as

$$k_{pc}\frac{\partial^2 T}{\partial x^2} - v_g\rho_g c_{p_g}\frac{\partial T}{\partial x} = [\phi \rho_g c_{p_g} + (1 - \phi)\rho_{pc}c_{pc}]\frac{\partial T}{\partial t} + \beta\frac{\partial T}{\partial t} \tag{2-21}$$

where k_{pc} is the PCM bed thermal conductivity and β is the energy of phase-change in a partially frozen, or solidified media, and is defined as

$$\beta = (1 - \phi)\rho_{pc}\Delta u_{pc}\varepsilon\frac{d\lambda}{dT} \tag{2-22}$$

where ΔT is the temperature range over which the full transition occurs and λ is the degree of solidification. For a value of $\lambda = 1$, the PCM is completely melted, where a value of $\lambda_o = 0.5$ indicates a state in which 50% of the volume of the material is frozen. For a freezing or melting front in which there is complete phase-change at a specified temperature, λ is equal to 1, and, as a result, $\beta = 0$. Figures 2.3 and 2.4 show the relationship between λ and

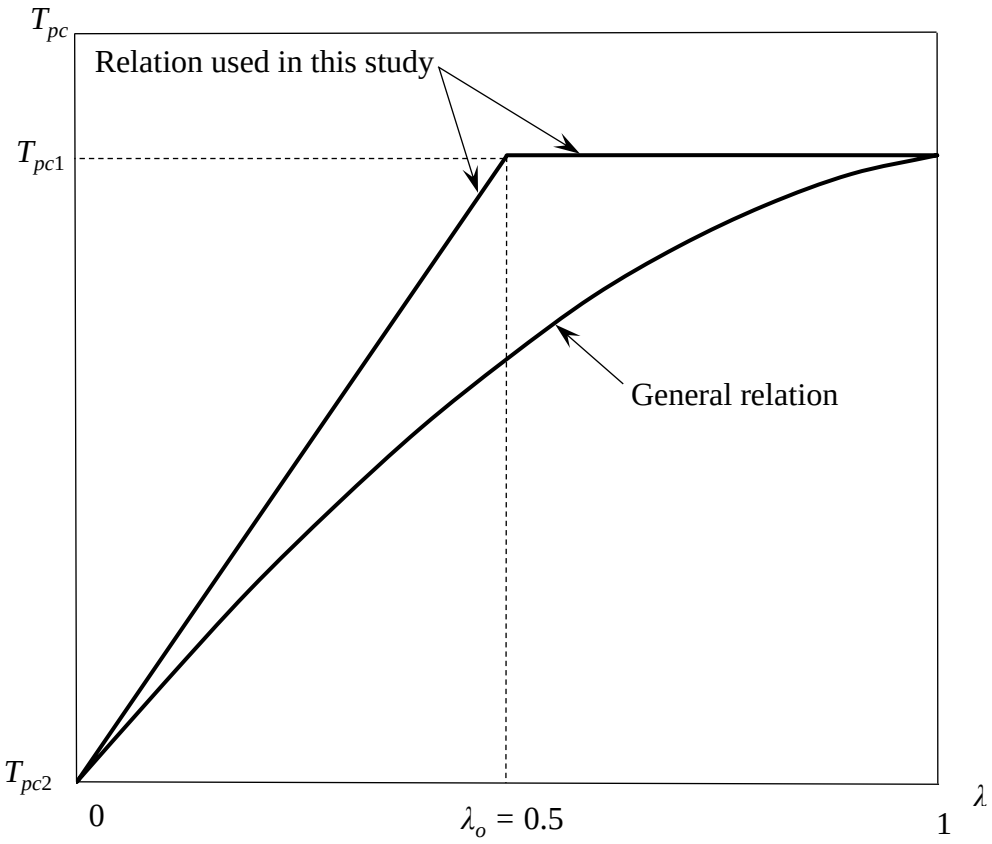

Figure 2.3 Percent solidification during the melting process. The figure shows the axial location in the packed-bed due to shrinking core phenomena for capsules during melting [56].

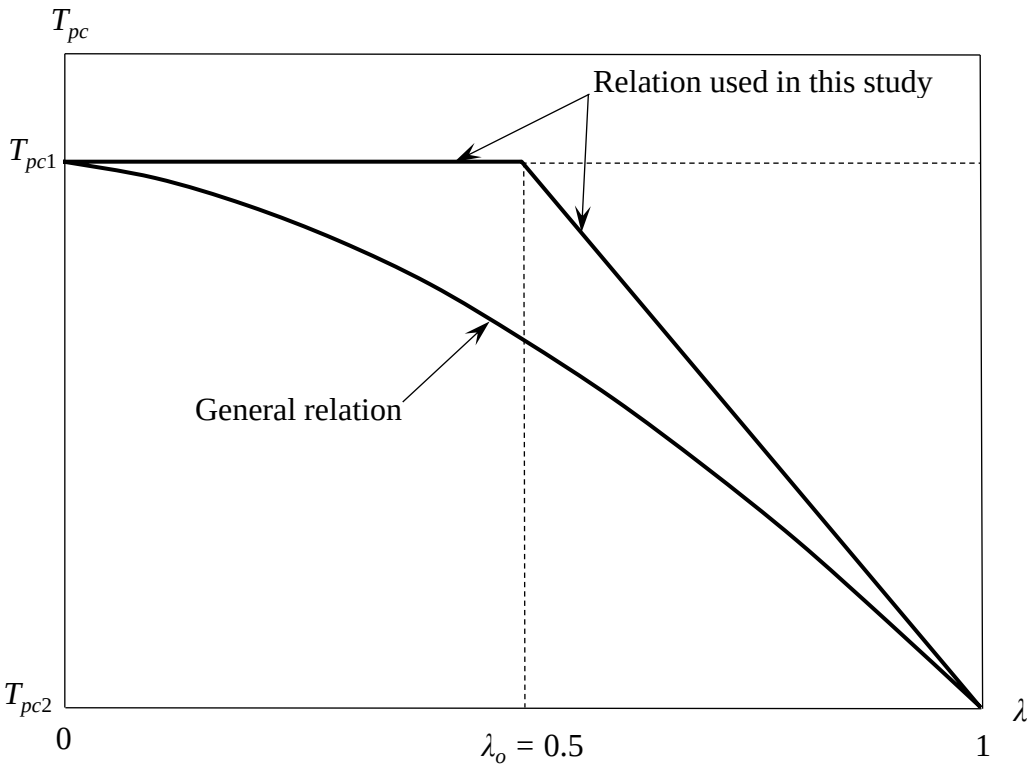

Figure 2.4 Percent solidification during the freezing process. The figure shows the axial location in the packed-bed due to shrinking core phenomena for capsules during freezing [56].

the range of phase-change temperatures.

2.4 Isotherm Velocity Under Partial Phase-Change Conditions

Schuman's [1] model also serves as the basis for the derivation of the velocity of an isotherm by defining the temperature derivative and setting it equal to zero.

$$dT = \frac{dT}{dx}dx + \frac{\partial T}{\partial t}dt = 0 \tag{2-23}$$

$$\left[\frac{dx}{dt}\right]_T = -\frac{\dfrac{\partial T}{\partial t}}{\dfrac{\partial T}{\partial x}} \tag{2-24}$$

$$\frac{\partial T}{\partial t} = \frac{-\left(k_{pc}\dfrac{\partial^2 T}{\partial x^2} - v_g\rho_g c_{p_g}\dfrac{\partial T}{\partial x}\right)}{[\phi\rho_g c_{p_g} + (1-\phi)\rho_{pc}c_{pc}] + \beta)} \tag{2-25}$$

Diffusion, representative of an inflection point where the second derivative is equal to zero, may be neglected when tracking the propagation of mean-temperature isotherms. In the case of partial melting or freezing, the temperature gradient is nearly linear, resulting in the first derivative outweighing the second in terms of computational impact. Setting the diffusion term $k_{pc}\frac{\partial^2 T}{\partial x^2} \cong 0$, and substituting Equation 2-25 into Equation 2-24, results in

$$\left[\frac{dx}{dt}\right]_T = \frac{v_g\rho_g c_{p_g}}{[\phi\rho_g c_{p_g} + (1-\phi)\rho_{pc}c_{pc}] + \beta} \tag{2-26}$$

or the ratio of the isothermal wave front velocity, v_T, to the Darcy velocity.

$$\frac{v_T}{v_g} = \frac{1}{\dfrac{[\phi\rho_g c_{p_g} + (1-\phi)\rho_{pc}c_{pc}]}{\rho_g c_{p_g}} + \dfrac{\beta}{\rho_g c_{p_g}}} \tag{2-27}$$

For the form of $\lambda = f(T)$, the derivative of λ with respect to temperature is

$$\frac{d\lambda}{dT} = \frac{(1 - \lambda_o)}{(T_{pc2} - T_{pc1})} \tag{2-28}$$

where λ_o is the initial degree of solidification. Equation 2-27 then becomes

$$\frac{v_T}{v_g} = \frac{1}{\frac{[\phi\rho_g c_{p_g} + (1-\phi)\rho_{pc} c_{pc}]}{\rho_g c_{p_g}} + \frac{(1 - \lambda_o)(1-\phi)\rho_{pc}\Delta u_{pc}\varepsilon}{\rho_g c_{p_g}(T_{pc2} - T_{pc1})}} \tag{2-29}$$

If the phase-change does not proceed to completion upon passage of the phase-change wave, the effect of partial phase-change needs to be considered in defining the phase-change wave velocity, thus the final form of Equation 2-20 for the ratio is

$$\frac{v_{th}}{v_g} = \frac{1}{\frac{\phi + (1 - \phi)\rho_{pc} c_{pc}}{\rho_g c_{p_g}} + \frac{(1 - \phi)\rho_{pc}\varepsilon\lambda_o \Delta u_{pc}}{\rho_g c_{p_g}(T_i - T_{pc2})}} \tag{2-30}$$

2.5 Axial Temperature Profiles

For a thermal energy storage system in which hot air is injected into a packed-bed of encapsulated PCM in a frozen state, the temperature distribution near the phase-change fronts in the bed may be predicted according to the model [57] developed and shown in Figure 2.5.

The thermal front velocity, defined as the velocity of an isothermal front undergoing a phase-change, v_{pc} , is given by Equation 2-31.

$$\frac{v_{pc}}{v_g} = \frac{1}{\phi + \frac{(1 - \phi)\rho_{pc} c_{pc}}{\rho_g c_{p_g}} + \frac{(1 - \phi)\rho_{pc}\varepsilon\Delta u_{pc}}{\rho_g c_{p_g}(T_i - T_{pc})}} \tag{2-31}$$

The energy equation for the region $x \le x_f$ is written as

$$\frac{\partial k_b \frac{\partial T}{\partial x}}{\partial x} - \frac{\phi \dot{m}_{cs} c_{p_g} \partial T}{\partial x} = \rho_b c_b \frac{dT}{dt} \tag{2-32}$$

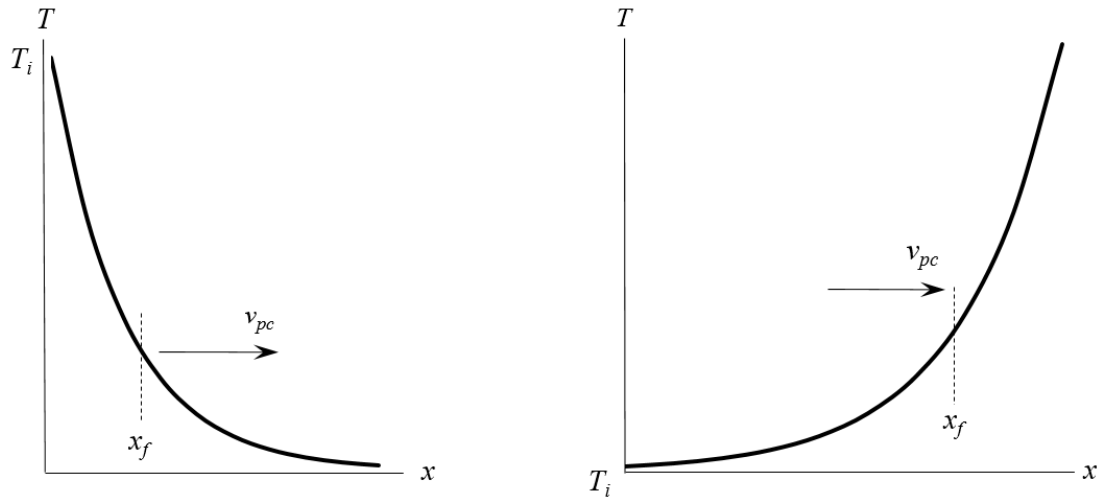

(a) (b)

Figure 2.5 Axial temperature distribution model. The model shows the temperature distribution as a function of axial location in the bed during phase-change. (a) Melting. (b) Freezing. Theory indicates that the temperature profile over the bed in the axial direction during the melting process decreases exponentially while the temperature distribution over the bed in the axial direction increases exponentially until the point at which the injection temperature is reached [57].

The density and specific heat of the bed are defined as

$$\rho_b = \phi\rho_g + (1-\phi)\rho_{pc} \tag{2-33}$$

and

$$c_b = \phi c_{p_g} + (1-\phi)c_{pc} \tag{2-34}$$

where the mass flux, $\dot{m}_{cs}$, is per unit area across the frontal cross-section of the packing and c_{pc} is the specific heat of the PCM, or heat capacity of the phase-change material itself.

Transforming Equation 2-32 onto a coordinate system that travels with the thermal front gives

$$\gamma = x - v_{pc}t \tag{2-35}$$

$$\frac{d\left(k_b \frac{\partial T}{\partial \gamma}\right)}{d\gamma} - \frac{\phi\dot{m}_{cs}c_{p_g}dT}{d\gamma} = -v_{th}\rho_b c_b \frac{dT}{d\gamma} \tag{2-36}$$

or

$$\frac{d[k_b \frac{dT}{d\gamma} - \phi\dot{m}_{cs}c_{p_g}T + v_{th}\rho_b c_b T]}{d\gamma} = 0 \tag{2-37}$$

Integrating Equation 2-37 with respect to γ yields

$$k_b \frac{dT}{d\gamma} + [v_{th}\rho_b c_b - \phi\dot{m}_{cs}c_{p_g}]T = C \tag{2-38}$$

The relation for the constant of integration, *C*, is derived from the boundary condition at

$$\gamma = -\infty$$

where, $\frac{dT}{d\gamma} = 0$ and $T = T_i$

As a result

$$C = [v_{pc}\rho_b c_b - \phi\dot{m}_{cs}c_{p_g}]T_i \tag{2-39}$$

Defining the dimensionless temperature as

$$\theta = \frac{T_i - T}{T_i - T_f} \tag{2-40}$$

results in

$$\frac{d\theta}{d\gamma} + \frac{[v_{pc}\rho_b c_b - \phi \dot{m}_{cs} c_{p_g}]}{k_b}\theta = 0 \tag{2-41}$$

Equation 2-41 is governed by the coefficient

$$\frac{v_{pc}\rho_b c_b}{k_b} - \frac{\phi \dot{m}_{cs} c_{p_g}}{k_b} \tag{2-42}$$

specifically if the coefficient is either positive or negative (non-zero). By substituting Equation 2-31 into Equation 2-42, it can be shown that

$$\frac{v_{pc}\rho_b c_b}{k_b} - \frac{\phi \dot{m}_{cs} c_{p_g}}{k_b} = \chi \tag{2-43}$$

where

$$\chi = -\frac{v_g \rho_{pc} c_{pc}}{k_b} \frac{1}{\left[\frac{\rho_{pc} c_{pc} (T_i - T_{pc})}{\rho_{pc} \Delta u_{pc}} + 1\right]} \tag{2-44}$$

The solution to Equation 2-38 is of the form

$$\theta = Ae^{\chi \gamma} \tag{2-45}$$

since $\theta = 1$ at $\gamma = 0$, then $A = 1$.

The temperature distribution for the bed may be predicted according to Equation 2-45, which is applicable to both melting and freezing processes.

2.6 Shrinking Core Model

Shrinking core phenomena may be described as the condition under which an encapsulated PCM undergoes either melting or solidification, in which a fraction of the

spherically encased material within the confines of the shell is liquid with the remainder being solid, over the course of the phase-change process. As heat is transferred to the phase-change material, melting occurs and the capsule liquefies from the outside of the shell inward. During the solidification process, in which heat is transferred from the phase-change material to the heat transfer fluid, the phase-change material solidifies from the outside toward the center of the shell.

Ismail [9] developed a mathematical model to determine the rate of heat transfer to or from a spherical shell containing PCM. The model was also used to calculate the temperature at any given radius within the capsule, and to compute the amount of heat transferred to or from the capsule, during melting and freezing processes.

The rate of phase-change in a spherical domain subjected to convective heating or cooling can be represented by the movement of a phase-change boundary with respect to time.

Considering the system shown in Figure 2.6 and assuming that the core is at the phase-change temperature, T_{pc} , heating the capsule to the phase-change boundary drives the shrinking of the core as defined by the energy balance

$$4\pi r_{pc}^2 \rho_{pc} \varepsilon \Delta u_{pc} \frac{dr_{pc}}{dt} = 4\pi r_{pc}^2 k_{pc} \left.\frac{\partial T}{\partial r}\right|_{r=r_{pc}} \tag{2-46}$$

or

$$\frac{dr_{pc}}{dt} = -\frac{k_{pc}}{\rho_{pc} \varepsilon \Delta u_{pc}} \left.\frac{\partial T}{\partial r}\right|_{r=r_{pc}} \tag{2-47}$$

The heat flux, q'', at the phase-change boundary, r_{pc} , may be quantified as

$$-k_{pc} \left.\frac{\partial T}{\partial r}\right|_{r=r_{pc}} = q''_{r=r_{pc}} \tag{2-48}$$

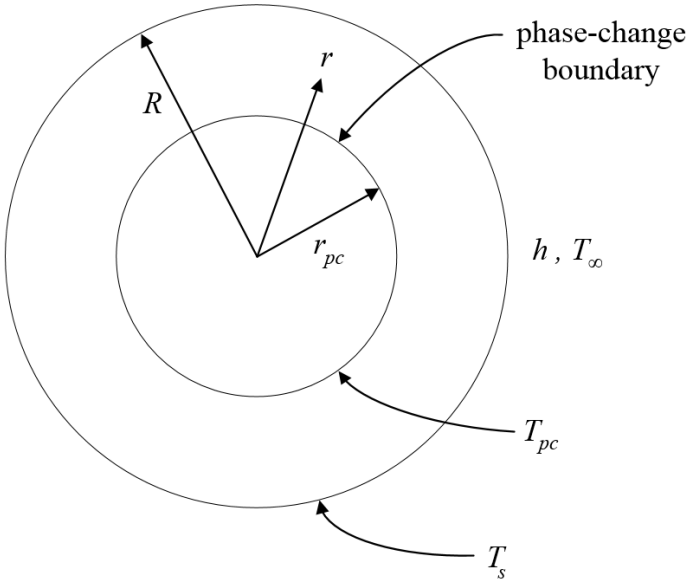

Figure 2.6 Shrinking core model for spherical domain. This model shows the change in the position of the phase-change boundary, for a spherical shell encapsulating a phase-change material, under both melting and solidification processes occurring at a constant temperature.

Assuming that the heat capacity of the PCM is much smaller than the change of internal energy due to phase-change implies that the temperature distribution in the outer region that lies between the capsule surface and the phase-change boundary becomes a series of steady-state profiles that change only as r_{pc} changes. As a result, the energy equation may be approximated as

$$\frac{1}{r^2}\frac{d\left(r^2\frac{dT}{dr}\right)}{dr} = 0 \tag{2-49}$$

Integrating once gives

$$r^2\frac{dT}{dr} = C_1 \tag{2-50}$$

and twice produces

$$T = -\frac{C_1}{r} + C_2 \tag{2-51}$$

Applying boundary conditions

$$T = T_s \text{ at } r = R \tag{2-52}$$

and

$$T = T_{pc} \text{ at } r = r_{pc} \tag{2-53}$$

where R is the capsule radius.

As a result

$$C_1 = -\frac{\left(T_s - T_{pc}\right)}{\left(\frac{1}{r_{pc}} - \frac{1}{R}\right)} \tag{2-54}$$

and

$$C_2 = T_{pc} + \frac{(T_s - T_{pc})}{\left(\frac{1}{r_{pc}} - \frac{1}{R}\right)} \tag{2-55}$$

or

$$T = T_{pc} + \frac{T_s - T_{pc}}{\left(\frac{1}{r_{pc}} - \frac{1}{R}\right)}\left[\frac{1}{r_{pc}} - \frac{1}{r}\right] \tag{2-56}$$

where T_s is the capsule surface temperature.

The total heat transfer through the shell [58] is obtained from Equation 2-48 and 2-56 and is defined as

$$4\pi R^2 k_{pc} \left.\frac{dT}{dr}\right|_{r=R} = 4\pi k_{pc} \frac{(T_s - T_{pc})}{\frac{1}{r_{pc}} - \frac{1}{R}} = q \tag{2-57}$$

The heat transfer through the shell is also equal to the heat transfer from the gas.

$$4\pi R^2 h(T_\infty - T_s) = q \tag{2-58}$$

where T_∞ is the bulk fluid temperature and h is the convection heat transfer coefficient. Solving for the following temperature differences

$$T_s - T_{pc} = \frac{q\left[\frac{1}{r_{pc}} - \frac{1}{R}\right]}{4\pi k_{pc}} \tag{2-59}$$

and

$$T_\infty - T_s = \frac{q}{4\pi R^2 h} \tag{2-60}$$

followed by adding and rearrangement gives

$$q = \frac{4\pi R^2 (T_\infty - T_{pc})}{R^2\left(\frac{1}{r_{pc}} - \frac{1}{R}\right)k_{pc} + \frac{1}{h}} \tag{2-61}$$

This is equivalent to the heat flow at the phase-change boundary

$$q = 4\pi r_{pc}^2 k_{pc} \left.\frac{\partial T}{\partial r}\right|_{r=r_{pc}} \tag{2-62}$$

or

$$k_{pc}\left.\frac{\partial T}{\partial r}\right|_{r=r_{pc}} = \frac{1}{4r_{pc}^2}\frac{(T_\infty - T_{pc})R^2}{\left[\left(\frac{1}{r_{pc}} - \frac{1}{R}\right)\frac{R^2}{k_{pc}} + \frac{1}{h}\right]} \tag{2-63}$$

Substituting Equation 2-63 into Equation 2-47 and simplifying results in

$$\frac{dr_{pc}}{dt} = \frac{-(T_\infty - T_{pc})k_{pc}}{\left(\frac{r_{pc}}{R}\right)^2 R\left[\left(\frac{R}{r_{pc}} - 1\right) + \frac{k_{pc}}{Rh}\right]\rho_{pc}\Delta u_{pc}\varepsilon} \tag{2-64}$$

Equation 2-64 may be written as

$$\frac{d\,\omega}{dt} = -\beta f(\omega) \tag{2-65}$$

where ω is the ratio of phase-change boundary radius to capsule radius defined as

$$\omega = \frac{r_{pc}}{R} \tag{2-66}$$

and

$$\beta = \frac{(T_\infty - T_{pc})k_{pc}}{R^2\rho_{pc}\varepsilon\Delta u_{pc}} \tag{2-67}$$

with the Biot number defined as

$$Bi = \frac{hR}{k_{pc}} \tag{2-68}$$

and

$$f(\omega) = \frac{1}{\omega^2\left[\left(\frac{1}{\omega} - 1\right) + \frac{1}{Bi}\right]} \tag{2-69}$$

Beginning with the initial ratio of phase-change boundary radius to capsule radius equal to 1

$$\omega_o = 1 \tag{2-70}$$

and

$$f(\omega_o) = Bi \tag{2-71}$$

Equations 2-72 and 2-73 imply two different time scales, one for large *Bi* where time scales with β, and a second one for small *Bi* that scales with $\beta\, Bi$. For large *Bi*, a scaled time, *t'*, is defined as

$$t' \equiv \beta t \tag{2-72}$$

For small, *Bi*, a scaled time, *t**, is defined as

$$t^* \equiv Bi\beta t \tag{2-73}$$

Quantitative descriptions of the movement of the change in the phase-change radius with time are obtained by numerically integrating Equation 2-65 using the backward Euler method.

$$\omega_1(\Delta t) = -\beta f(\omega_o)\Delta t + \omega_o \tag{2-74}$$

$$\omega_2(2\Delta t) = -\beta f(\omega_1)\Delta t + \omega_1 \tag{2-75}$$

…

$$\omega_n(n\Delta t) = -\beta f(\omega_{n-1})\Delta t + \omega_{n-1} \tag{2-76}$$

with Δt as the prescribed time step.

2.7 Flow and Exergy

Kousksou [4] created theoretical models to analyze and optimize thermal energy storage systems containing PCMs. Analysis indicates that energy and exergy efficiencies are dependent upon the phase-change melting temperature. While studies have been conducted for diurnal applications, similar models could also be applied to seasonal periods of reasonable duration.

The exergy of the heat transfer fluid for the energy recovery process may be written as

$$X_{st} = \int_0^t \left[\dot{m} c_{p_g} (T_i - T_o) - ln\left(\frac{T_i}{T_o}\right) \dot{m} c_{p_g} T_o \right] dt \tag{2-77}$$

Assuming that the heat transfer fluid is increasing the exergy of a packed-bed that is initially at ambient conditions, and that the fluid stream entering the bed is fixed at the limiting, operating system temperature, the ideal or Carnot efficiency is expressed as

$$\eta_{Carnot} = 1 - \frac{T_o}{T_i} \tag{2-78}$$

The exergy of the heat transfer fluid for the energy recovery process may be written as

$$X_{rec} = \int_0^t \left[\dot{m}\, c_{p_g} (T_e - T_o) - ln\left(\frac{T_e}{T_o}\right) \dot{m}\, c_{p_g} T_o \right] dt \tag{2-79}$$

where the outlet fluid temperature, T_e , is a function of time, dependent upon when the heat is recovered from the bed. The temperature of the heat transfer fluid exiting the bed may be used in calculating the recovered, fractional exergy of the storage process, in terms of a dimensionless temperature and the Carnot efficiency

$$\eta_{\mathrm{II}} = \frac{\int_0^t \left\{ \theta + \frac{1-\eta_{Carnot}}{\eta_{Carnot}} ln\left[\theta \left(\frac{\eta_{Carnot}}{1-\eta_{Carnot}} \right) + 1 \right] \right\} dt}{\int_0^t \left[1 + \frac{1-\eta_{Carnot}}{\eta_{Carnot}} ln\left(\frac{1}{1-\eta_{Carnot}} \right) \right] dt} \tag{2-80}$$

with the dimensionless temperature defined as

$$\theta = \frac{T - T_e}{T_i - T_e} \tag{2-81}$$

The fractional exergy recovered represents the exergy efficiency of the storage system. The exergy efficiency may also be described as the ratio of the exergy recovered to the exergy stored. The time-dependent exergy efficiency for the system, with respect to the charging and discharging processes, may be quantified as [4]

$$\eta_{\text{II}} = \frac{\int_0^t \left(\dot{\psi}_{e,discharge} - \dot{\psi}_{i,discharge} \right) dt}{\int_0^t \left(\dot{\psi}_{i,charge} - \dot{\psi}_{e,charge} \right) dt} \tag{2-82}$$

where the rate form of the exergy of an incompressible fluid is defined as

$$\dot{\phi} = \dot{m} \left[c_{p_g} (T - T_o) - T_o c_{p_g} ln \left(\frac{T}{T_o} \right) \right] \tag{2-83}$$

The exergy efficiency of the system, operating under steady-state conditions, may be modeled as [11]

$$\eta_{\text{II}} = \frac{\psi_e}{\psi_i} \tag{2-84}$$

CHAPTER 3

EXPERIMENTAL METHODS

3.1 Packed-Bed Design, Test Device, and Data Acquisition System

An experimental test system was fabricated and assembled that facilitated the investigation of the thermal energy storage and heat transfer characteristics of air flow through a packed-bed. The system is shown in Figures 3.1 through 3.5. A packed-bed particle container 0.152 m wide x 0.152 m deep x 0.356 m high was fabricated from ABS*plus* – P340 production grade thermoplastic. The container was filled with 3 to 5 mm encapsulated PCM capsules. The container was filled by pouring the capsules into the container, thus resulting in a random packing arrangement.

3.1.1 Temperature Probes

All temperature measurements were made with Omega Engineering PT100 RTD sensors. The sensors are constructed of a 0.125 inch in diameter Type 316L stainless steel case that houses class A, Pt 100 Ohm 4-wire platinum RTD elements with a temperature range of -50 to 250°C and a fast response time of 3.5 seconds or less 63% response in water. Temperature probes 1 through 6 were 4.5 inches long while the probes at the inlet and the outlet of the bed were 2 inches in length (www.omega.com).

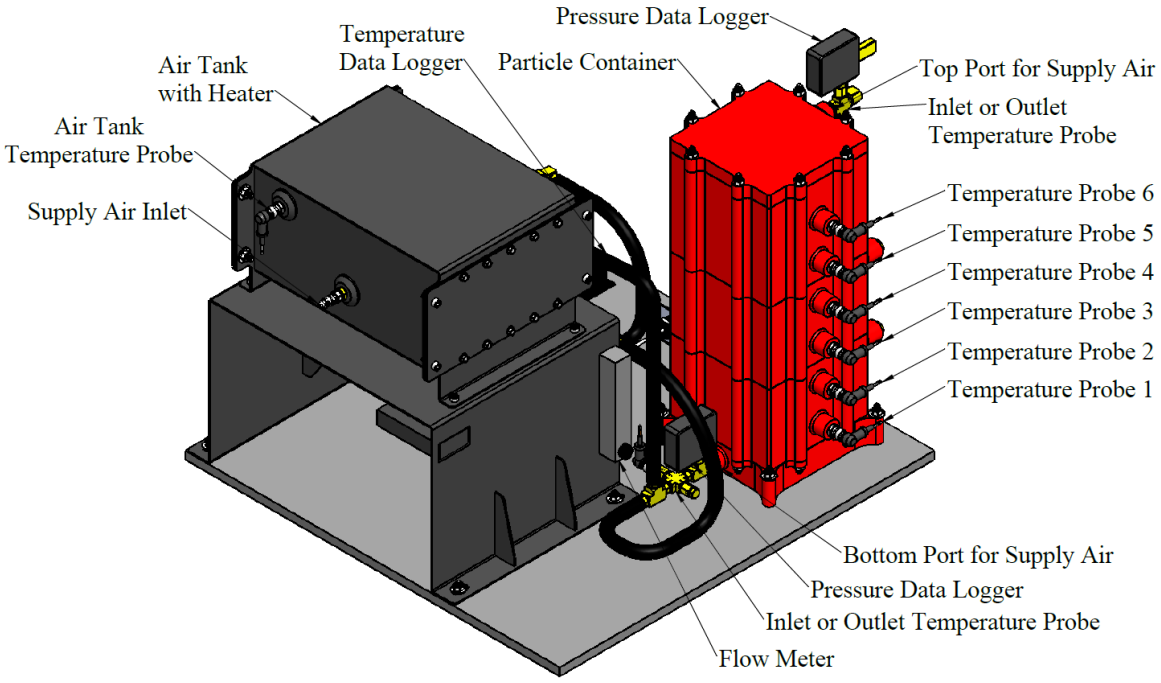

Figure 3.1 Experimental apparatus. The temperature probes are arranged along the central axis of the bed.

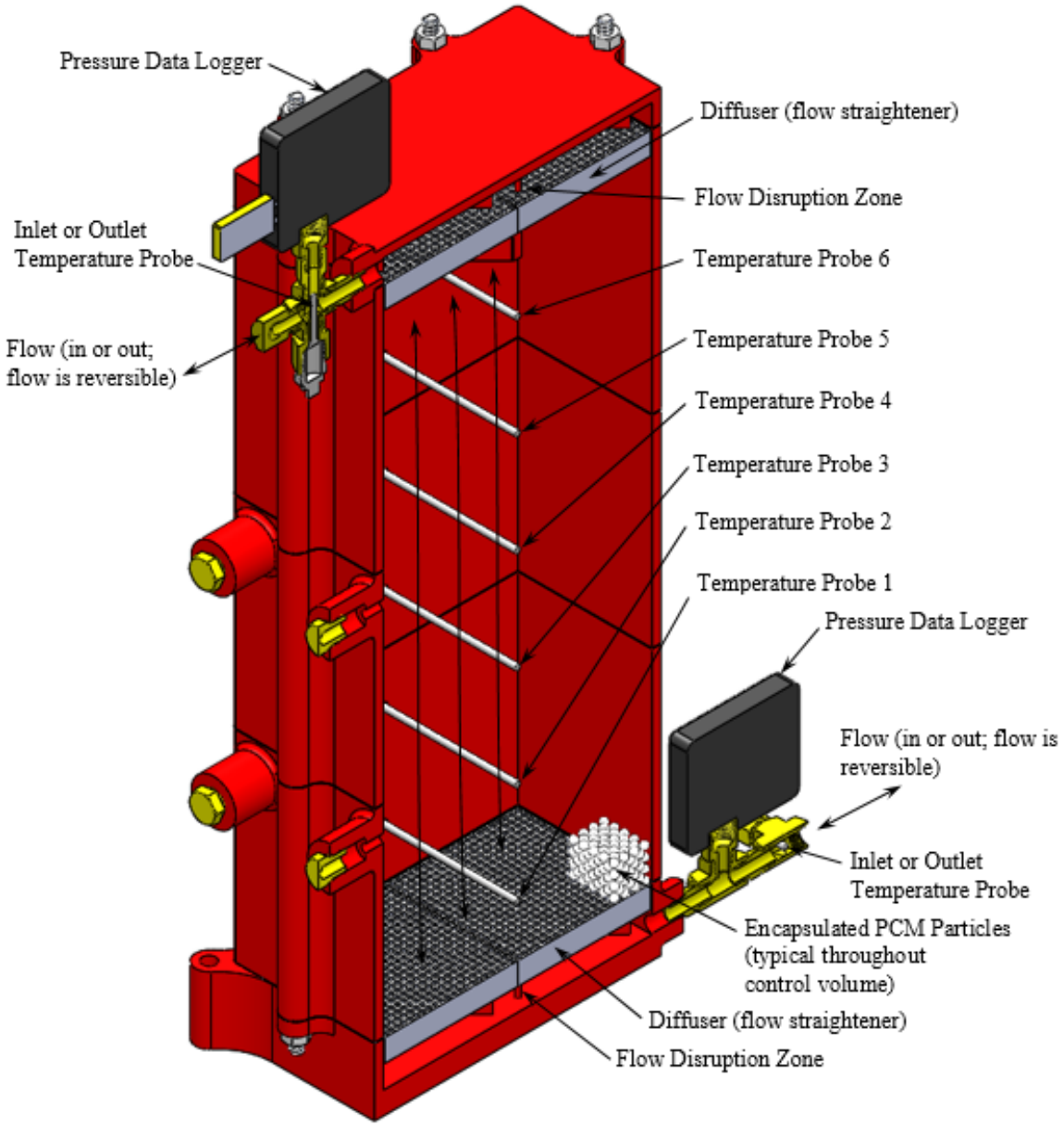

Figure 3.2 Packed-bed design. Isometric section view showing the inner workings of the packed-bed thermal energy storage device.

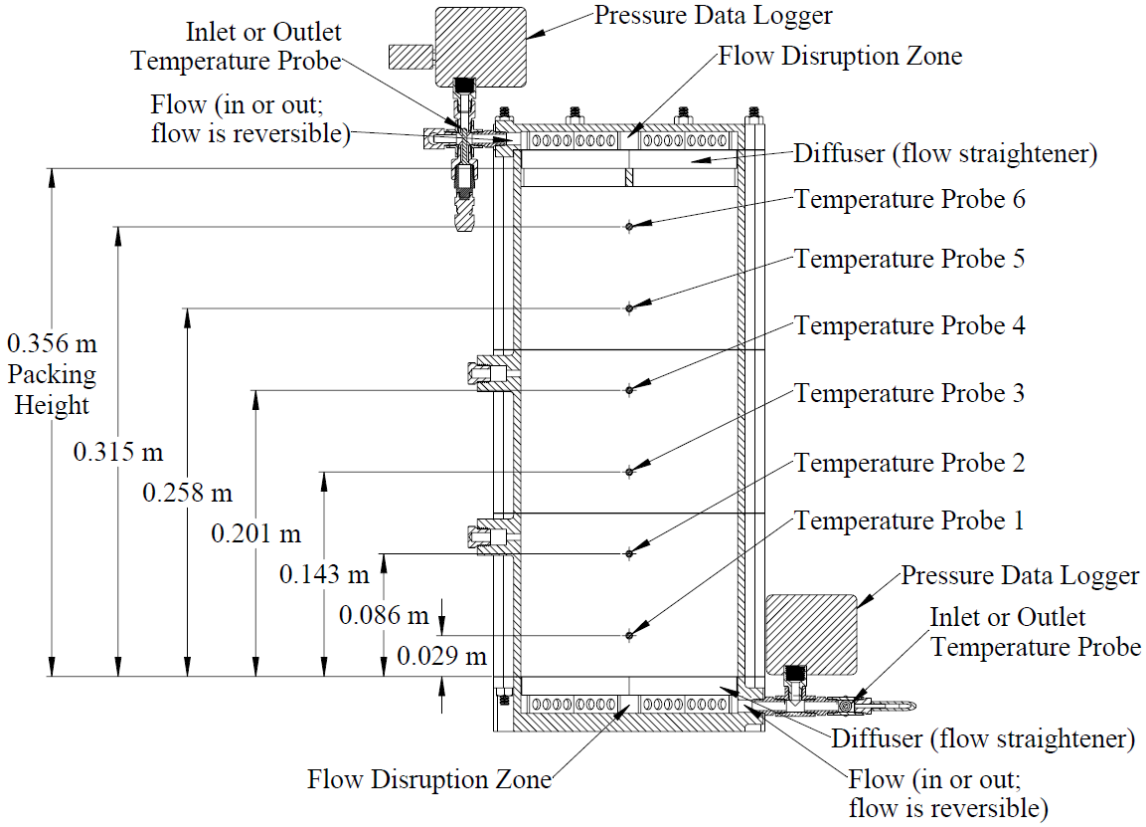

Figure 3.3 Section view of packed-bed. The figure shows dimensional location of the six temperature probes embedded in the packing and arranged along the central axis of the bed.

Figure 3.4 Experimental test apparatus and data acquisition system.

(a)

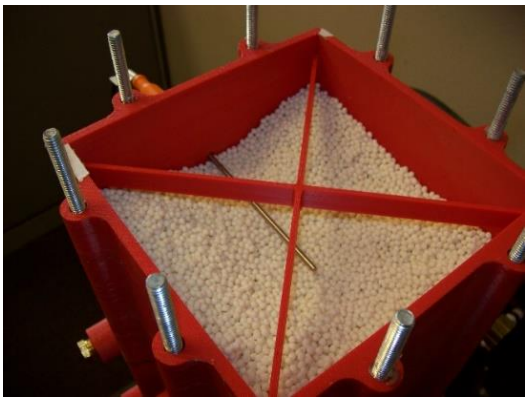

(b)

(c)

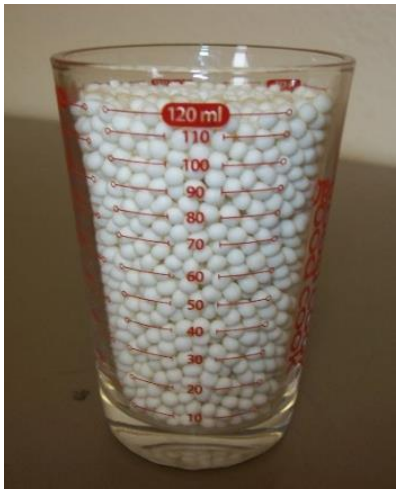

(d)

Figure 3.5 Packed-bed arrangement and encapsulated phase-change material. (a) Open-topped view of the packed-bed with all of the air diffusers removed. (b) Open-topped view of the packed-bed with some of the capsules removed to show one of six temperature probes inserted along the longitudinal axis of the bed. (c) Relative capsule size. (d) Relative porosity.

3.1.2 Temperature Data Logger

Temperatures were recorded using an Omega Engineering OM-CP-OCTRTD 8 channel temperature logger with a 100 Ohm Pt RTD input, a 0.01 °C resolution, and a calibrated accuracy of +/- 0.1 °C, capable of measuring up to 10,992 measurements per channel with a temperature measurement range from -200 to 850°C. Data acquisition rates range from 2 seconds to 12 hours. The data acquisition rates for the experiments conducted in this work are discussed later in section 4.1 (www.omega.com).

3.1.3 Pressure Data Loggers

Pressures were measured using Omega Engineering OM-CP-PRTC210 pressure data loggers with semiconductor strain gauge sensors for pressures ranging from 0 to 30 psig. The device is capable of recording 10,992 readings per channel (www.omega.com).

3.1.4 Heater

A moisture-resistant, seamless Type 304 stainless steel ceramic insulated heater was used to heat the air. The heater is capable of generating 350W of heat at 120VAC with an amperage draw of 2.9A (www.mcmaster.com).

3.1.5 Flowmeter

Volumetric flow rates of the air were controlled using a Key Instruments part number 61010_R3 65 mm glass ball and tube panel-mounted flow meter rated for air. The ball diameter was ¼" with a mass of 0.3372 g. The tube identification number is 6G10 R3. Flow rates were adjustable from 0 to 23.6 liters per minute. Maximum operating pressure is 200 psig at 70°F. The accuracy of the meter was +/- 5 % over the full range of the measuring scale (www.mcmaster.com).

3.2 Design of Experiment

Packed-beds are thermal energy storage devices comprised of either solid particles or encapsulated PCMs with high specific heat, high thermal diffusivity, reversible heating and cooling capability, and a large heat of fusion [1]. Thermal energy storage devices utilizing PCMs are desirable in that they exhibit smaller temperature swings during the storage-to-retrieval cycle, and have higher energy capacities per unit weight or volume, compared to conventional storage systems. Thermal energy storage systems, incorporating PCMs as the storage media, require injection of a fluid with a heating temperature that is above, and a cooling temperature that is below, the phase-change temperature of the material [1].

In this study, experiments are designed to obtain temperature distributions in packed-bed thermal energy storage devices, as a function of both time and position, in order to validate theoretical models for thermal waveforms and wave speeds across the packing. Wave propagation for both sensible and phase-change heat transfer regimes will be explored.

The temperature of the capsule surface is dependent upon the transient heat conduction from the surface to the interior of the particle, where the phase-change occurs. Inter-particle conduction effects, resulting from capsules being in direct physical contact, are assumed negligible. Thermal dispersion resulting from the mixing action that occurs as the heat transfer fluid is forced through the bed, is dependent upon eddy flow fields in the bed, and thermal diffusivity of the fluid [1]. In order to minimize the fluid pressure drop across the bed, frontal cross-sectional areas may be increased, and bed lengths decreased.

Flowing gaseous heat transfer fluid around the particles in the bed in sensible and latent heat transfer conditions produces data indicating rates of heat exchange from the fluid to the particles during charging and discharging operations. A knowledge of the relationship between time, temperature, and position related to storing and retrieving thermal energy aids in the understanding of the connectivity between the Biot and Nusselt numbers and lends improved insight to the applicability of lumped capacitance methods or shrinking core models, that take into consideration spatial effects, in estimating convection heat transfer coefficients for these processes.

One of the main objectives associated with thermal energy storage systems is the successful harvest and re-use of thermal energy that is rejected from processes involving thermal energy that is stored in a passive manner, such as via solar collection methods or other techniques, or that is the result of other work-producing processes that transfer heat energy to the surroundings.

Obtaining information with respect to heat energy storage over time facilitates the evaluation of packed-bed thermal energy storage devices' potential for capturing various temperature grades of thermal energy, and provides a way for assessing the exergy efficiency of such devices and the opportunity to produce useful work from otherwise wasted thermal energy.

3.3 Phase-Change Material Selection for Packed-beds

An experiment was designed to study the temperature versus time phenomena intrinsic to packed-beds of encapsulated PCMs as a result of injecting hot or cold air into the bed. The encapsulated PCM used in this study was selected to ensure that the capsules were an order of magnitude smaller in diameter than spherical shells filled with different

PCM compounds used in previous studies. The porosity of the bed was estimated by filling a 120 ml container with PCM capsules and water. The water was then transferred to another 120 ml container, and the volume of the water was measured. The void fraction, or porosity, was estimated as the ratio of the volume of water to the total volume of the capsules and the water combined.

Selection of the form and composition of the encapsulated PCM used in this study is primarily due to its serviceability in the low and intermediate temperature applications previously described. This form of storage media is available in phase-change temperatures ranging from -30 to 65°C. A PCM with a nominal phase-change temperature of 32°C was procured in order to design the experiment around temperatures in close proximity to those related to the applications of interest. The manufacturer of the encapsulated PCM provided information indicating that the capsules were spherical in shape, on the order of 3 to 5 mm in diameter, and were a combination of octadecane and eicosane with a latent heat of 150 J/g, a thermal conductivity of 0.090 W/m K, and a density of 1 g/ml. Table 3.1 provides additional information on the PCM used in the experiments.

3.4 Charging and Discharging Procedures

Low pressure air was either cooled (using an ice bath) or heated, depending upon testing requirements in terms of melting, heating, cooling, or freezing processes, and then delivered to the bed at a prescribed volumetric flow rate and temperature. Air exiting the bed was exhausted to the atmosphere.

Charging refers to adding thermal energy to the bed; discharging specifies removing thermal energy from the bed. Experiments designed under forced convective heat transfer conditions include charging and discharging from the bottom of the bed,

Table 3.1 Physical properties and values used in the analysis of data.

Quantity	Description	Source	Nominal	Applied	Units
c_{pg}	specific heat of air	[32]	1,007	1,007	J/kgK
c_{pc}	specific heat of PCM	Estimated	720	720	J/kgK
D_p	particle diameter	Manufacturer	0.004	0.004	m
k_{pc}	PCM thermal conductivity	Manufacturer	0.09	0.09	W/mK
k_g	air thermal conductivity	[32]	0.0263	0.0263	W/mK
T_{pc}	phase-change temperature	Manufacturer	32	28	°C
u_{pc}	PCM internal energy	Manufacturer	146,000	240,000	J/kg
v_g	Darcy velocity	Prescribed	0.013	0.013	m/s
ε	mass fraction of PCM	Estimated	0.8	0.17	-
λ_o	initial degree of solidification	Estimated	0.17	0.17	-
ρ_g	air density	[32]	1.1614	1.1614	kg/m^3
ρ_{pc}	PCM density	Estimated	800	750	kg/m^3
ϕ	porosity	Estimated	0.65	0.65	-

charging from the bottom of the bed and discharging from the top of the bed, charging and discharging from the top of the bed, and charging from the top of the bed and discharging from the bottom of the bed. Flow arrangements for the preceding configurations are referred to as either parallel or counter flow, with parallel flow indicating charging and discharging from a common port (bottom of the bed for charging and discharging or top of the bed for charging and discharging). Counter flow conditions are such that the bed is charged and discharged from opposite ends. Test configurations were such that the temperature probes were aligned with the longitudinal axis of the bed, and uniformly spaced in the direction of air flow.

An experiment was also designed to sub-cool the bed, ensuring complete solidification of the PCM, prior to melting, heating, cooling, and freezing the bed, in a continuous data collection process. Figure 3.6 shows schematic diagrams of experimental arrangements.

The temperature of the bed was measured with respect to time at six discrete locations (Fig. 3.3) using Omega temperature probes. Temperatures were recorded using an Omega 8 channel temperature logger.

The temperature of the heat transfer fluid was continuously monitored at the inlet and outlet of the container. Temperatures at these locations were measured using Omega temperature probes and recorded using an Omega 8 channel temperature logger. Pressures at these locations were recorded using Omega pressure data loggers. The volumetric flow rate of the air was controlled and monitored using a panel mounted flow meter rated for air.

Temperature measurements were recorded over time during the initial cooling,

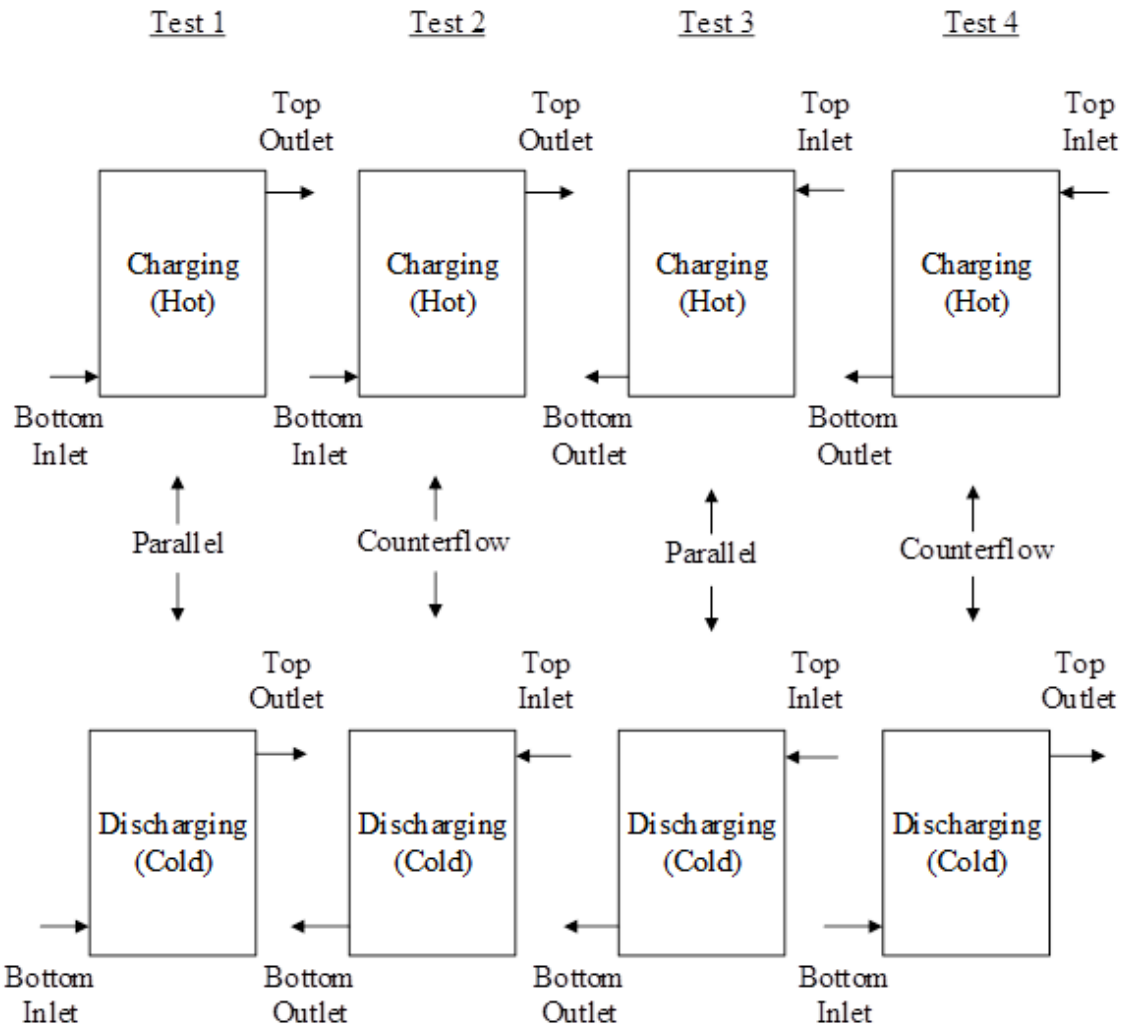

Figure 3.6 Various flow arrangements for testing.

melting, heating, cooling, and freezing of the PCM particles. Temperature data were continuously collected from the onset of initial cooling, through the melting process, and until termination of the freezing process.

3.5 Experimental Procedure for Sensible Heat Transfer

The supply air pressure was initially set to zero, and then increased to the working pressure prescribed for the experiment. Flow to the system was regulated via three, quarter-turn ball valves, one acting as supply to the system and the other two as exhaust ventilators. The volumetric flow rate to the system was controlled using the flow meter. Once the volumetric flow to the system was established, the controller monitoring the temperature of the air in the tank was energized. At this point, power was supplied to the heater to begin the heating process. Upon completion of the heating process, the cooling process was initiated by disconnecting power to the heater, and injecting air at ambient temperature into the bed. The temperature at the inlet and the outlet of the packed-bed was monitored and recorded, as was the temperature at six vertically oriented, axial locations for the process. Figure 3.6 indicates the flow configurations for Tests 1 through 4.

3.6 Experimental Procedure for Latent and Sensible Heat Transfer

The supply air pressure was initially set to zero, and then increased to the working pressure prescribed for the experiment. Flow to the system was regulated via three, quarter-turn ball valves, one acting as supply to the system and the other two as exhaust ventilators. The volumetric flow rate to the system was controlled using the flow meter. Once the volumetric flow to the system was established, the controller monitoring the temperature of the air in the tank was energized.

At this point, cold air was injected into the bed in order to ensure solidification of the PCM, prior to the melting and heating process. Once the bed was cooled to a uniform temperature, power was supplied to the heater to begin the melting process. Upon completion of the melting process, the cooling and subsequent freezing process was initiated by disconnecting power to the heater, and again injecting cold air into the bed. Air was injected at the bottom of the bed for all phases of the process. The temperature at the inlet and the outlet of the packed-bed was monitored and recorded, as was the temperature at six vertically oriented, axial locations for all phases of the cycle.

CHAPTER 4

EXPERIMENTAL RESULTS

4.1 Thermal Waves Under Sensible Heat Transfer Conditions

A summary of the tests conducted is found in Table 4.1. The data shown in Figures 4.1 and 4.2 are typical temperature-time histories for sensible heating and cooling processes. A nearly linearly decreasing outlet temperature during cooling may be observed in Figure 4.1, while a more constant, uniform outlet temperature is evident in Figure 4.2. The data for Test 2 (Fig. 4.1) were collected under forced convection conditions, in a counter flow arrangement (Fig. 3.1), while the data for Test 3 (Fig. 4.2) were obtained under forced convection conditions, but in a parallel flow arrangement. Similarly, the data for Test 4 (Fig. 4.3) were collected under forced convection conditions, in a counter flow arrangement (Fig. 3.1), while the data for Test 1 (re-test) (Fig. 4.4) were obtained under forced convection conditions, but in a parallel flow arrangement.

4.2 Thermal Waves Under Latent and Sensible Heat Transfer Conditions

Test results in terms of temperature measurement and thermal wave propagation, with respect to the bed during melting and freezing processes for the cycle, are depicted in Figures 4.5 and 4.6, respectively. The temperature profiles and waves are reflective of the six temperature probes being vertically oriented, or longitudinally arranged (Fig. 3.3).

Table 4.1 Test conditions summary. Test numbers correspond with the configurations shown in the preceding figure showing parallel and counter flow arrangements (Fig. 3.1). Test 12 was conducted under parallel flow conditions.

Test	Processes	Date	Start	End	Sampling rate [Hz]	Ambient temperature [°C]
2	Charging / Discharging *	7/6/2016	11:45 a.m.	6:16 p.m.	0.2	27
3	Charging / Discharging *	7/7/2016	11:13 a.m.	6:48 p.m.	0.2	24
4	Charging / Discharging *	7/8/2016	7:30 a.m.	2:15 p.m.	0.2	26
1 (Re-test)	Charging / Discharging *	7/12/2016	10:23 a.m.	6:33 p.m.	0.2	22
12	Charging / Discharging *	9/24/2016	8:00 a.m.	1:35 a.m.	0.2	20

* Charging indicates heating and discharging indicates cooling

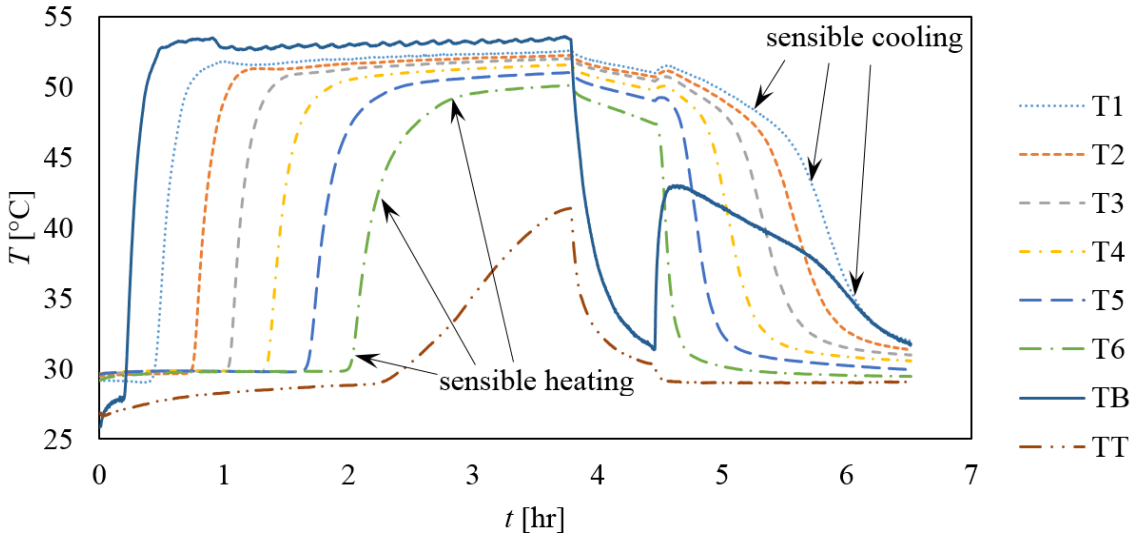

Figure 4.1 Data for Test 2 in a counter-flow arrangement. Hot air injected at the bottom of the bed for heating and cold air injected at the top of the bed for cooling. TB is the temperature probe at the bottom of the bed and measures the inlet temperature during heating and the outlet temperature during cooling; conversely, TT is the temperature probe at the top of the bed and measures the outlet temperature during heating and the inlet temperature during cooling. T1 through T6 are the temperature probes arranged along the longitudinal axis of the bed. In this case, T1 is closest to the bottom inlet (TB) during heating, while T6 is nearest the top inlet (TT) during cooling.

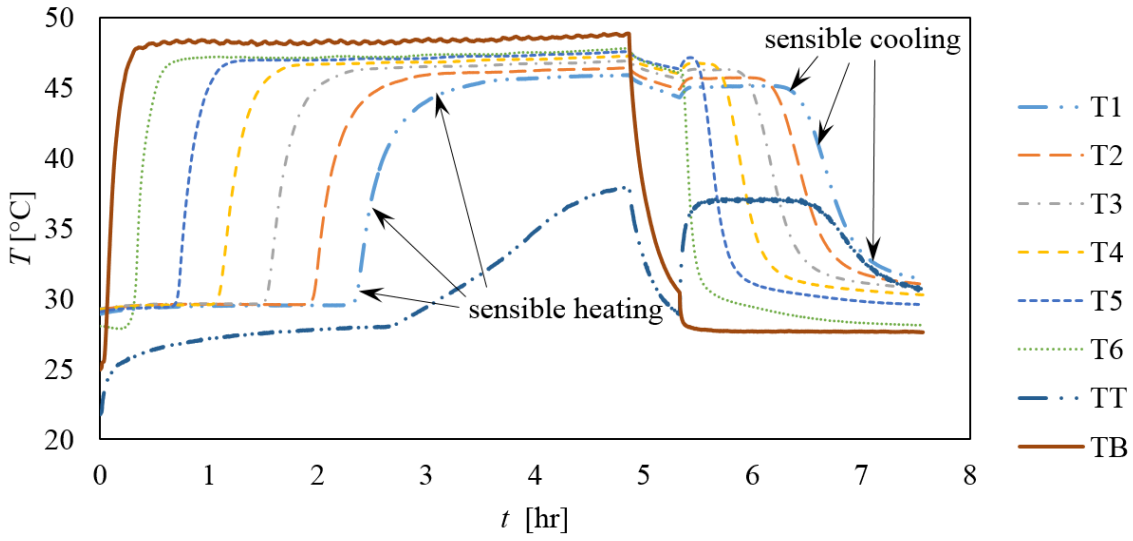

Figure 4.2 Data for Test 3 in a parallel flow arrangement. Hot air injected at the top of the bed for heating and cold air injected at the top of the bed for cooling. TB is the temperature probe at the bottom of the bed and measures the outlet temperature during heating and cooling; conversely, TT is the temperature probe at the top of the bed and measures the inlet temperature during heating and cooling. T1 through T6 are the temperature probes arranged along the longitudinal axis of the bed. In this case, T6 is closest to the top inlet (TT) during heating and cooling.

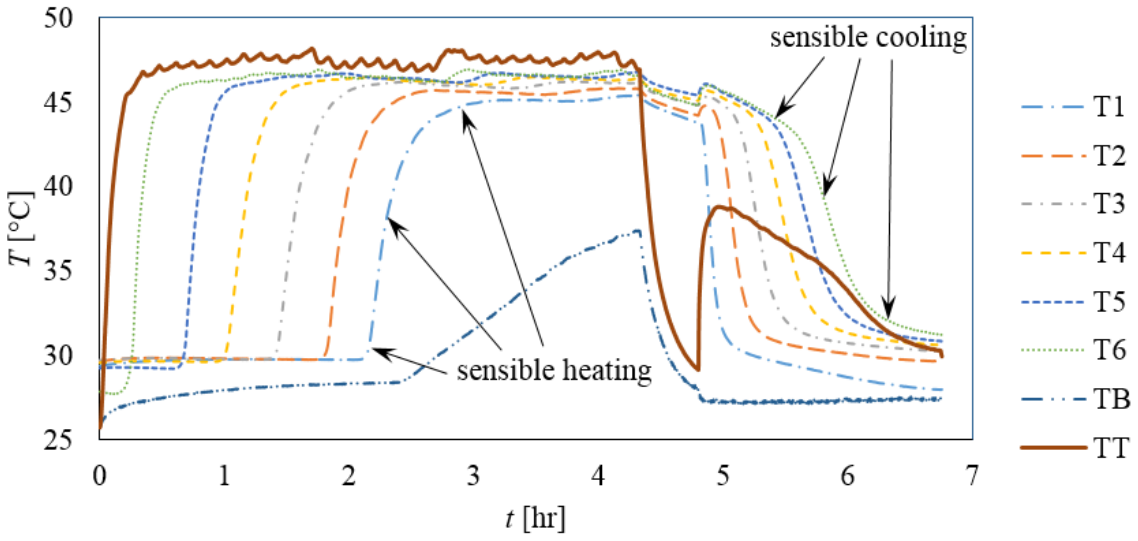

Figure 4.3 Data for Test 4 in a counter-flow arrangement. Hot air injected at the top of the bed for heating and cold air injected at the bottom of the bed for cooling. TB is the temperature probe at the bottom of the bed and measures the inlet temperature during cooling and the outlet temperature during heating; conversely, TT is the temperature probe at the top of the bed and measures the inlet temperature during heating and the outlet temperature during cooling. T1 through T6 are the temperature probes arranged along the longitudinal axis of the bed. In this case, T6 is closest to the top inlet (TT) during heating, while T1 is nearest the bottom inlet (TB) during cooling.

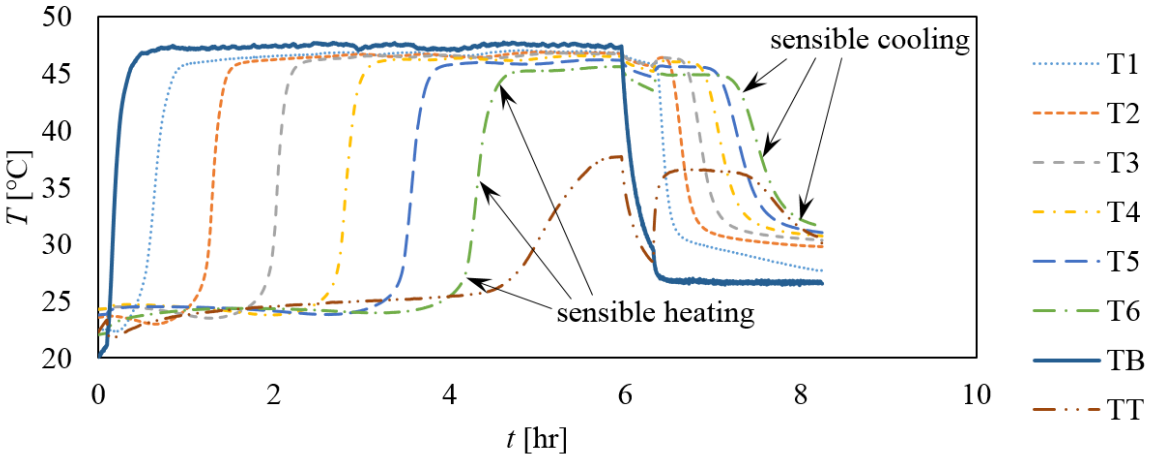

Figure 4.4 Data for Test 1 (re-test) in a parallel flow arrangement. Hot air injected at the bottom of the bed for heating and cold air injected at the bottom of the bed for cooling. TB is the temperature probe at the bottom of the bed and measures the inlet temperature during heating and cooling; conversely, TT is the temperature probe at the top of the bed and measures the outlet temperature during heating and cooling. T1 through T6 are the temperature probes arranged along the longitudinal axis of the bed. In this case, T1 is closest to the bottom inlet (TB) during heating and cooling.

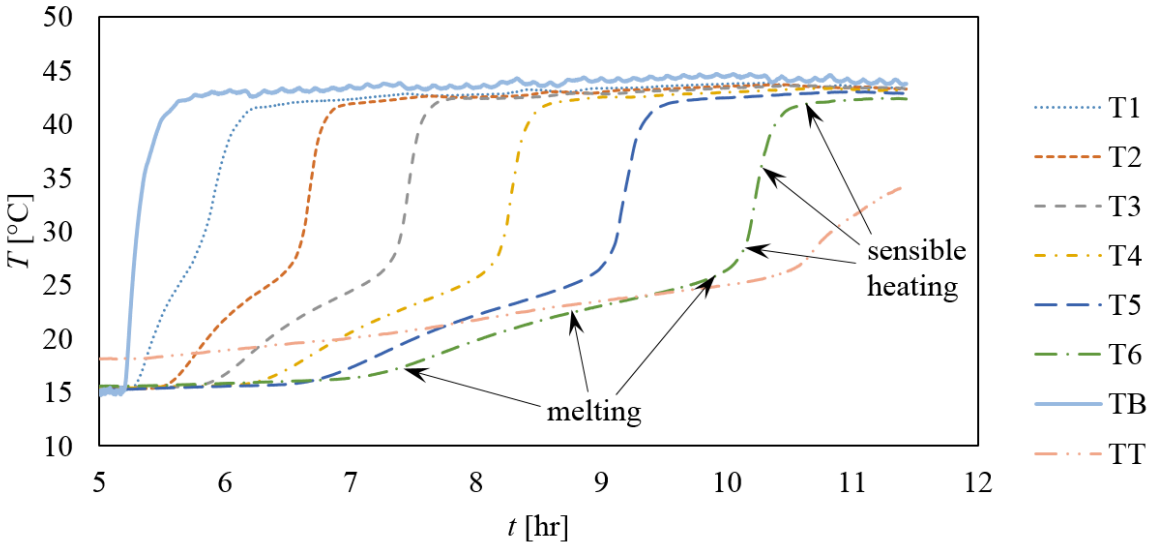

Figure 4.5 Data for Test 12 in a parallel flow arrangement. Hot air injected at the bottom of the bed for melting and heating. TB is the temperature probe at the bottom of the bed with TT identified as the temperature probe at the top of the bed. T1 through T6 are the temperature probes arranged along the longitudinal axis of the bed. In this case, T1 is closest to the bottom inlet (TB) during melting and heating.

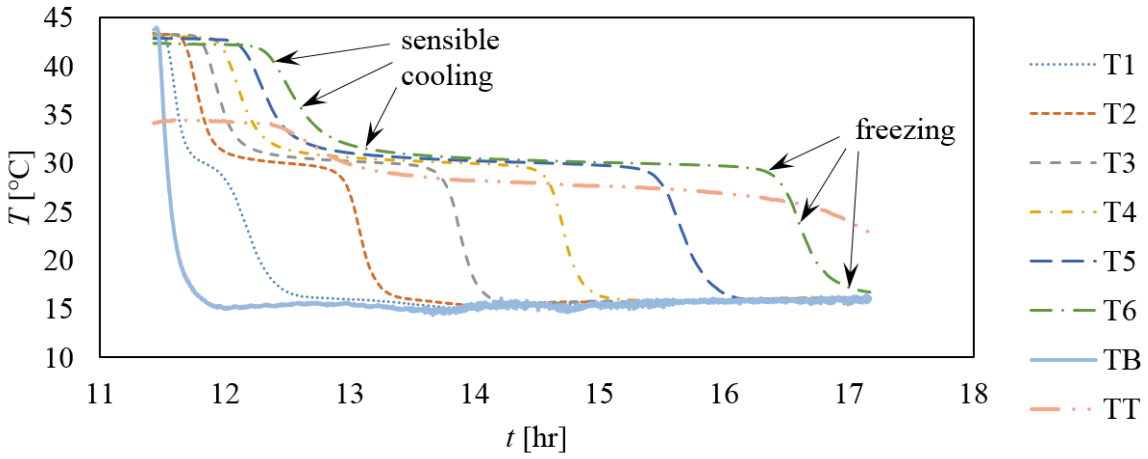

Figure 4.6 Data for Test 12 in a parallel flow arrangement. Cold air injected at the bottom of the bed for cooling and freezing. TB is the temperature probe at the bottom of the bed with TT identified as the temperature probe at the top of the bed. T1 through T6 are the temperature probes arranged along the longitudinal axis of the bed. In this case, T1 is closest to the bottom inlet (TB) during cooling and freezing.

CHAPTER 5

ANALYSIS AND EVALUATION OF EXPERIMENTAL DATA

5.1 Thermal Waveforms Under Sensible Heat Transfer Conditions

Examination of Figures 5.1 through 5.3 shows that analysis of the data collected during testing under sensible heat transfer conditions (Figures 4.1, 4.2, 4.3, and 4.4) results in an acceptable fit to the model developed by Schumann [1] that yields a closed-form solution for a gas flowing through a packed-bed, that is identical to the complimentary error function model, a solution for which was obtained using Laplace transformation methods. Equation 5-1 shows this relationship in the form of a dimensionless temperature as the output, with the complimentary error function waveform profile shape governed by the transformation variable for distance, γ, and the thermal diffusivity, α

$$\frac{T - T_i}{T_i - T_o} = 1 - \frac{1}{2}\operatorname{erfc}\left(\frac{\gamma}{2\sqrt{\alpha t}}\right) \tag{5-1}$$

5.2 Phase-Change and Thermal Wave Fronts

The model developed by Schumann [1] adapted to a system in which both latent and sensible heat transfer occurs, as shown in Figure 4.2, adequately serves in application with regard to describing and predicting thermal waveform shapes and profiles, as well as the propagation of waves undergoing both sensible and latent heat transfer processes in a cascading wave arrangement. The effect of this adaptation with respect to experimental data is shown in Figures 5.4, 5.5, and 5.6.

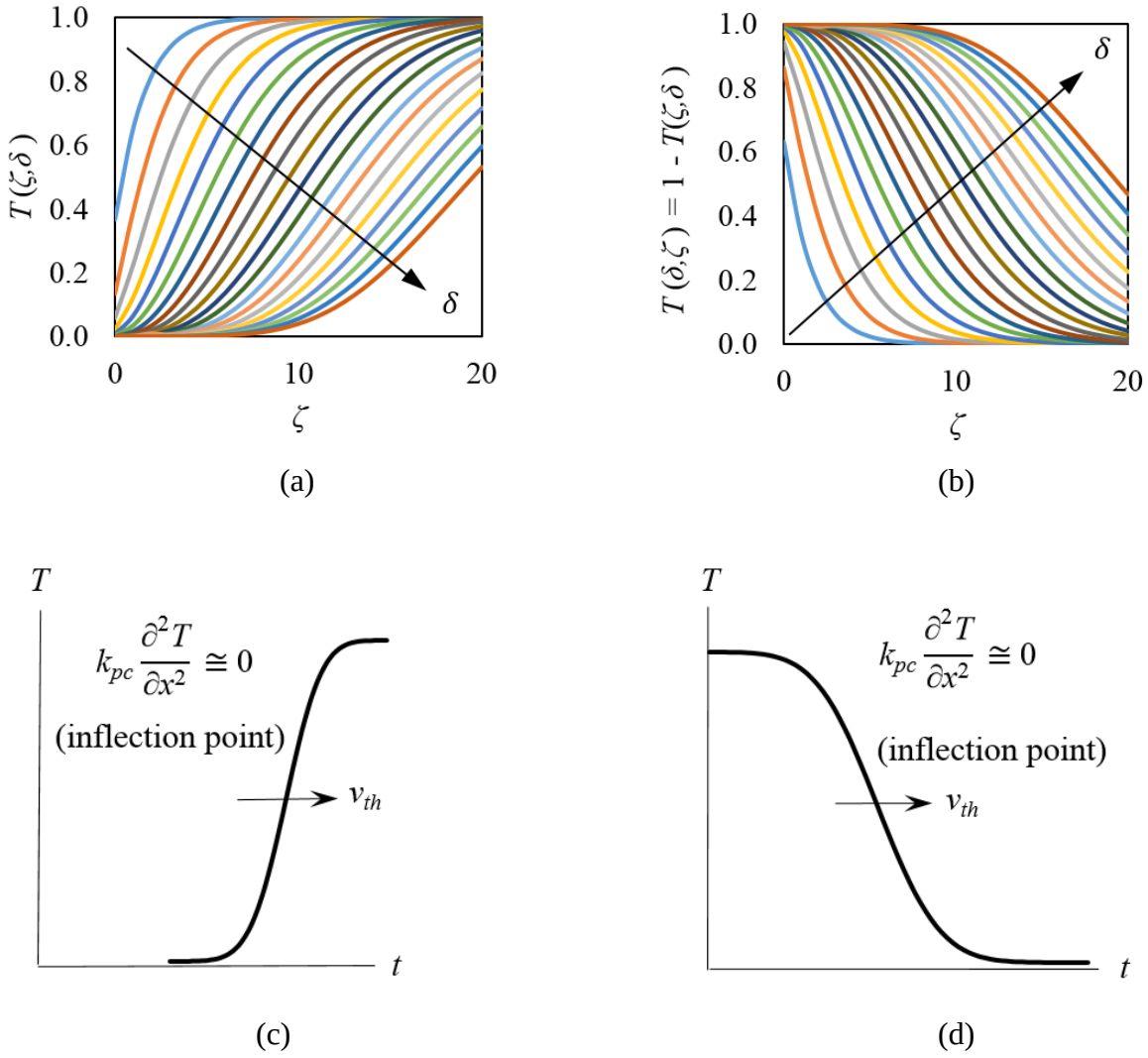

Figure 5.1 Waveform models for sensible heating and cooling. (a) Schumann's [29] model for heating. (b) Schumann's [29] model for cooling. (c) Error function model (Equation 5-1) for heating. (d) Error function model (Equation 5-1) for cooling.

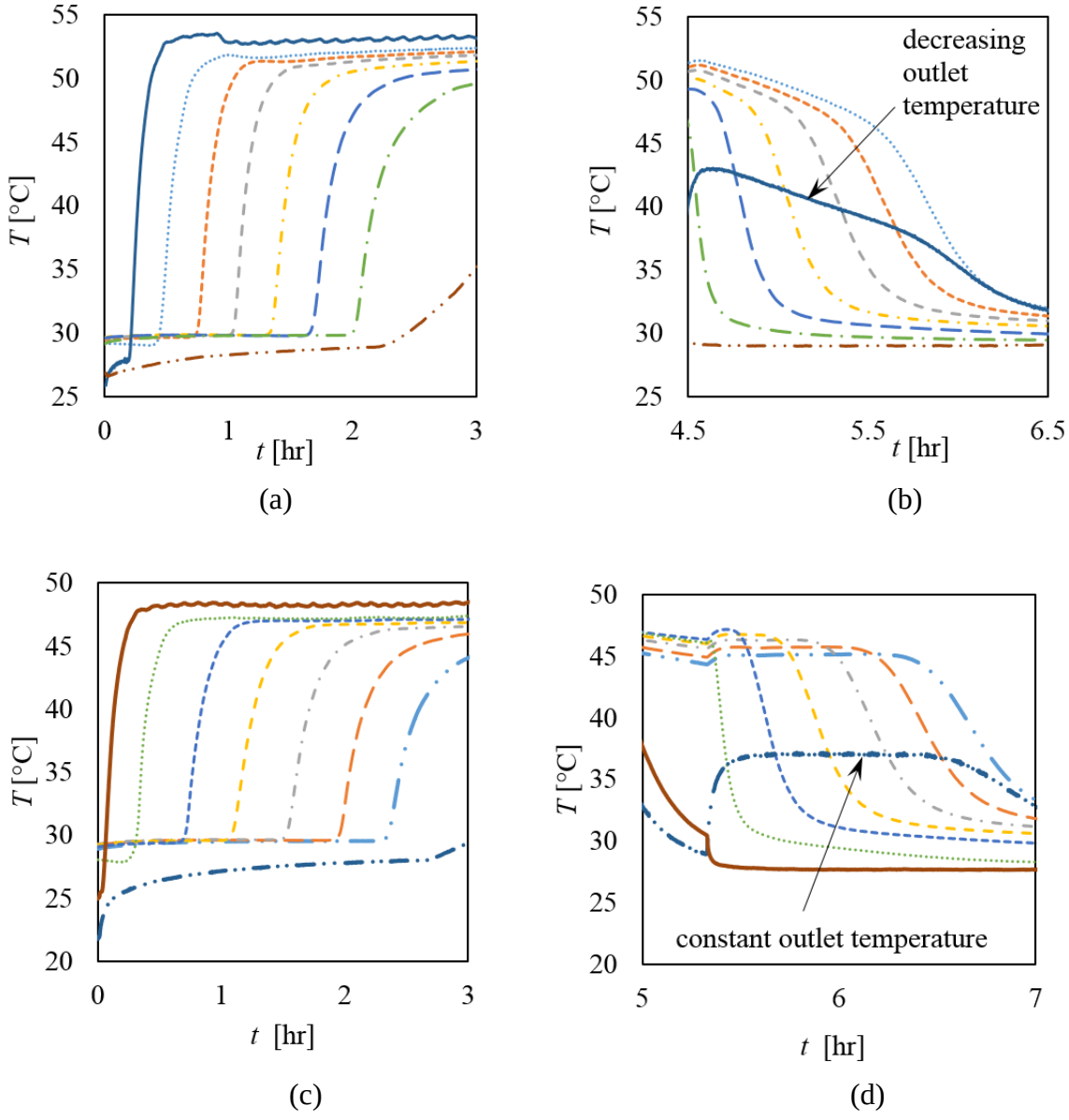

Figure 5.2 Waveform test data for sensible heating and cooling. (a) Sensible heating for Test 2. (b) Sensible cooling for Test 2 indicating decreasing outlet temperature. (c) Sensible heating for Test 3. (d) Sensible cooling for Test 3 indicating constant outlet temperature.

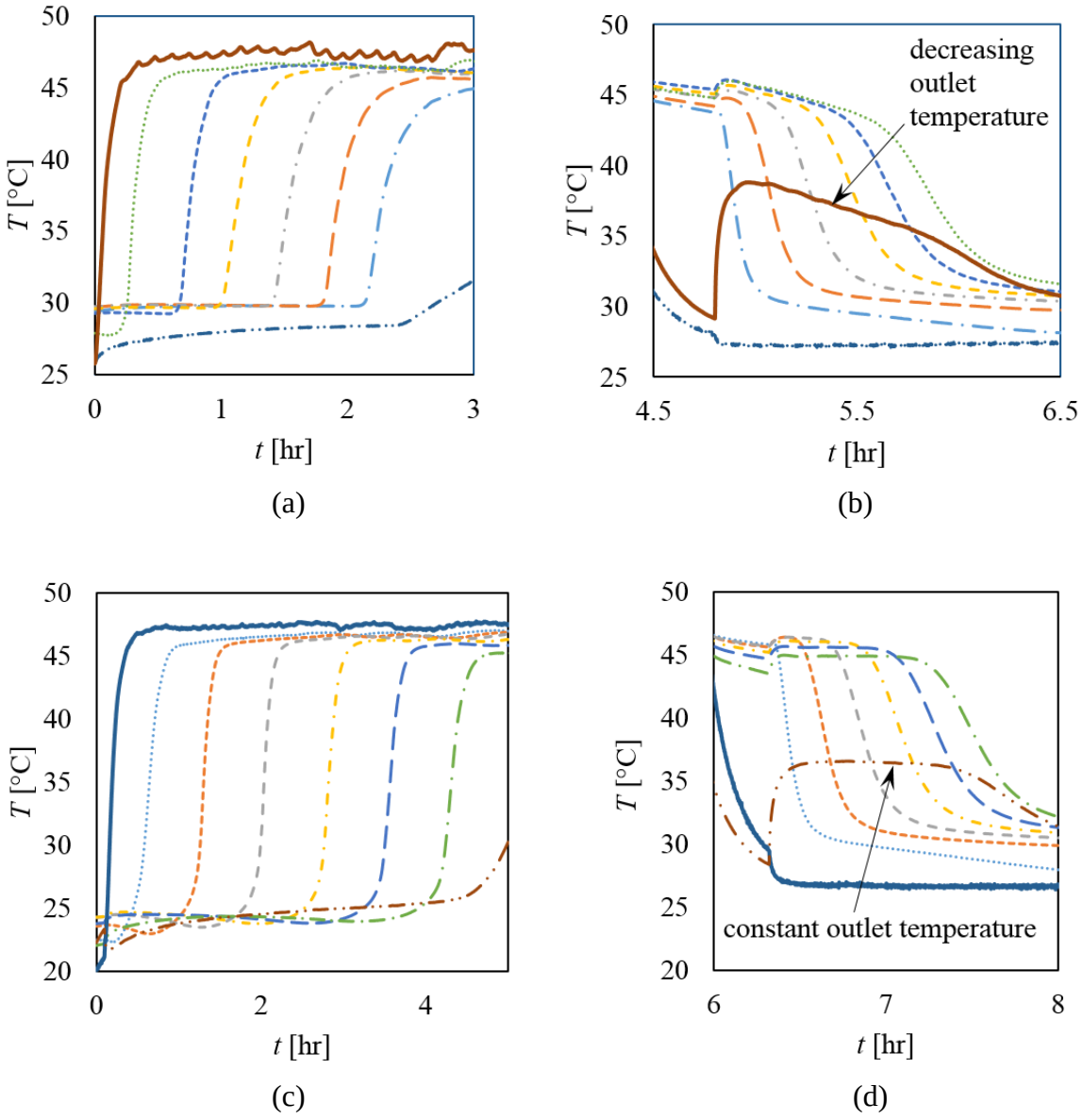

Figure 5.3 Waveform test data for sensible heating and cooling. (a) Sensible heating for Test 4. (b) Sensible cooling for Test 4 indicating decreasing outlet temperature. (c) Sensible heating for Test 1 (re-test). (d) Sensible cooling for Test 1 (re-test) indicating constant outlet temperature.

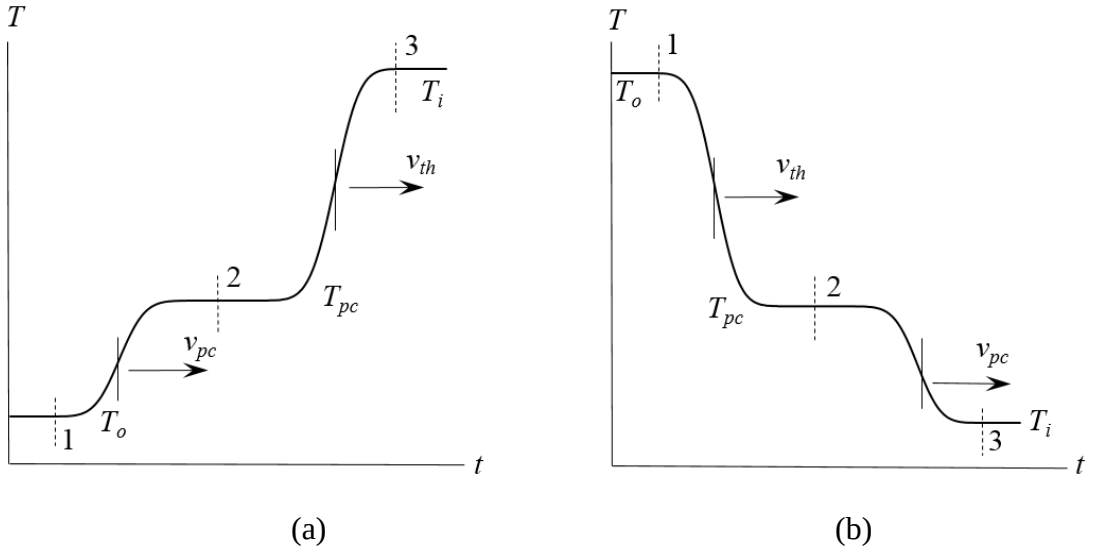

Figure 5.4 Waveform propagation model for packed-beds. The figure shows advancement of thermal wave fronts, v_{th}, and phase-change wave fronts, v_{pc}, with respect to the time, t, the injection temperature of the air, T_i, and the initial temperature of the air in the bed, T_o. (a) Melting and heating. (b) Cooling and freezing.

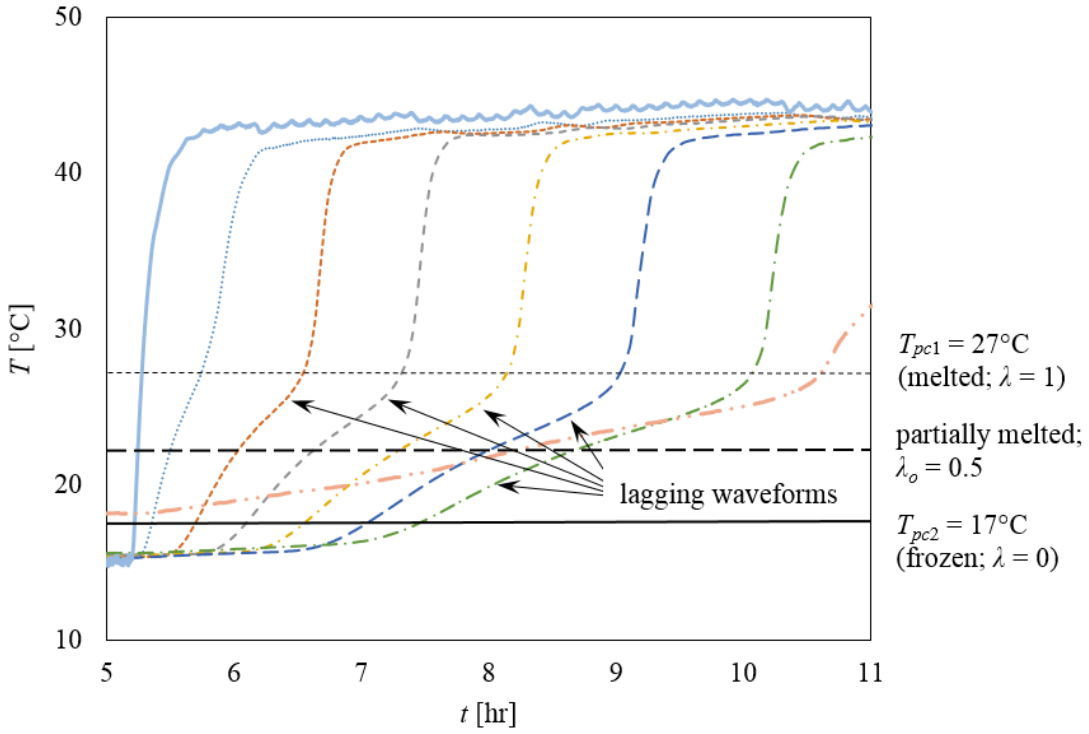

Figure 5.5 Melting and heating data for Test 12. The figure shows the phase-change temperature range and respective percent solidification of the PCM.

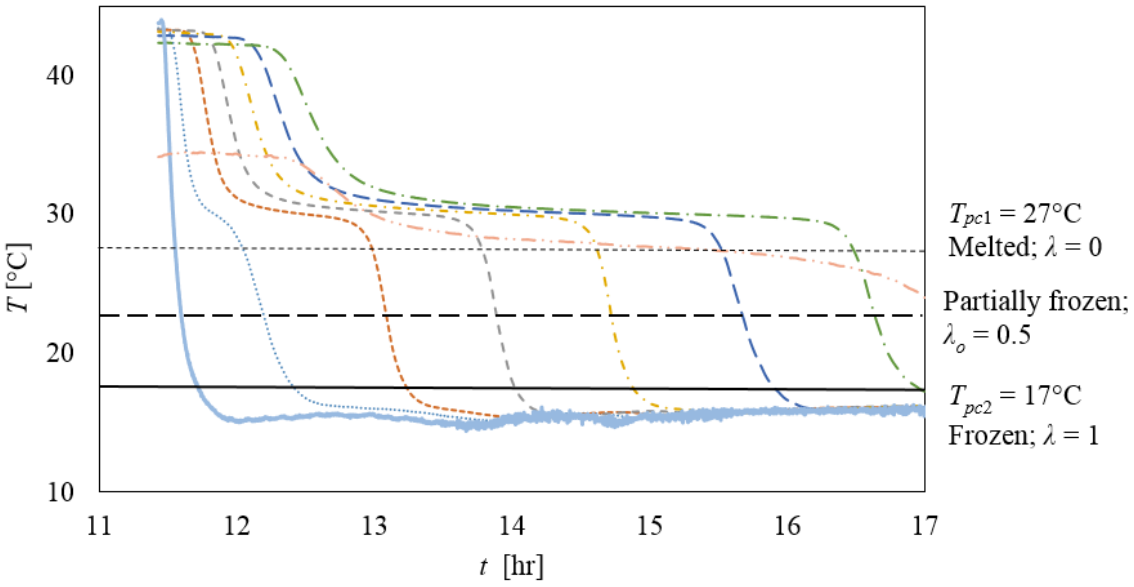

Figure 5.6 Cooling and freezing data for Test 12. The figure shows the phase-change temperature range and respective percent solidification of the PCM.

5.3 Velocity of Thermal and Phase-Change Wave Fronts

As previously stated, the ratio of the thermal wave front velocity to the Darcy velocity is given by

$$\frac{v_{th}}{v_g} = \frac{\rho_g c_{p_g}(T_i - T_{pc})}{\phi\rho_g c_{p_g}(T_i - T_{pc}) + (1-\phi)\rho_{pc}(u_{pc_1} - u_{pc_2})} \tag{5-2}$$

and the ratio of the phase-change front velocity to the Darcy velocity is expressed as

$$\frac{v_{pc}}{v_g} = \frac{1}{\phi + \dfrac{(1-\phi)\rho_{pc}c_{pc}}{\rho_g c_{p_g}} + \dfrac{(1-\phi)\rho_{pc}\varepsilon\Delta u_{pc}}{\rho_g c_{p_g}(T_i - T_{pc})}} \tag{5-3}$$

5.4 Isotherm Velocity Under Partial Phase-Change Conditions

The fundamental principles underlying Schumann's [1] model can be used to derive the velocity of an isotherm according to Equation 5-4 that gives the ratio of the isothermal wave front velocity, v_T , to the Darcy velocity, v_g, where λ_o is the initial degree of solidification.

$$\frac{v_T}{v_g} = \frac{1}{\dfrac{[\phi\rho_g c_{p_g} + (1-\phi)\rho_{pc}c_{pc}]}{\rho_g c_{p_g}} + \dfrac{(1-\lambda_o)(1-\phi)\rho_{pc}\Delta u_{pc}\varepsilon}{\rho_g c_{p_g}(T_{pc2} - T_{pc1})}} \tag{5-4}$$

Under circumstances when complete phase-change does not occur upon propagation of the phase-change wave, the effects of partial phase-change must be considered, thus defining the phase-change wave velocity as

$$\frac{v_{th}}{v_g} = \frac{1}{\dfrac{\phi + (1-\phi)\rho_{pc}c_{pc}}{\rho_g c_{p_g}} + \dfrac{(1-\phi)\rho_{pc}\varepsilon\lambda_o\Delta u_{pc}}{\rho_g c_{p_g}(T_i - T_{pc2})}} \tag{5-5}$$

Figures 5.7 through 5.11 show the wave front time of arrival for the initial cooling, melting, heating, cooling, and freezing processes.

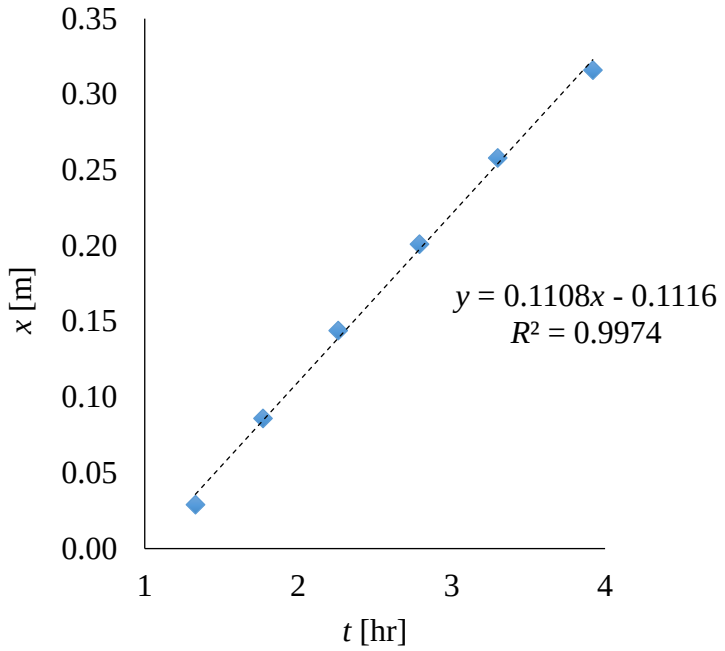

Figure 5.7 Time of arrival of thermal wave fronts at 17° C. The figure reflects test conditions with the PCM completely frozen at 17° C. Cold air was injected at the bottom of the bed (Test 12).

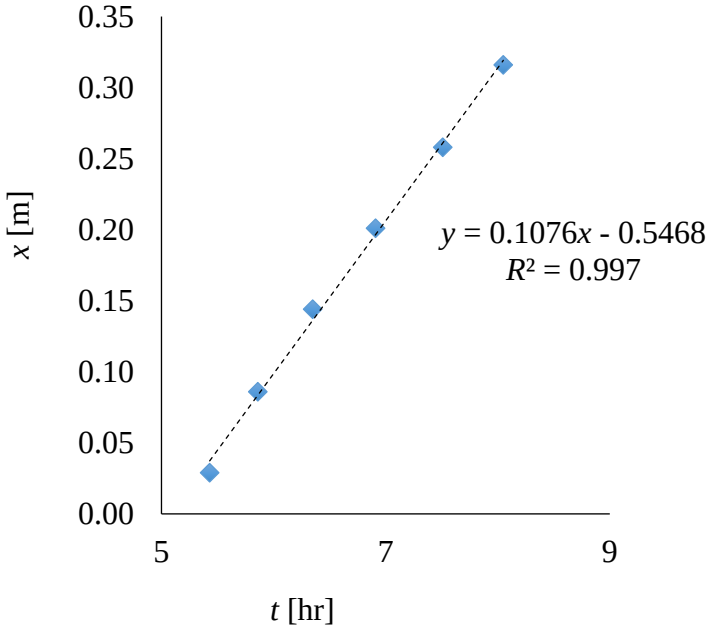

Figure 5.8 Time of arrival of thermal wave fronts at 20° C. The figure reflects test conditions for melting occurring at 20° C. Hot air was injected at the bottom of the bed (Test 12).

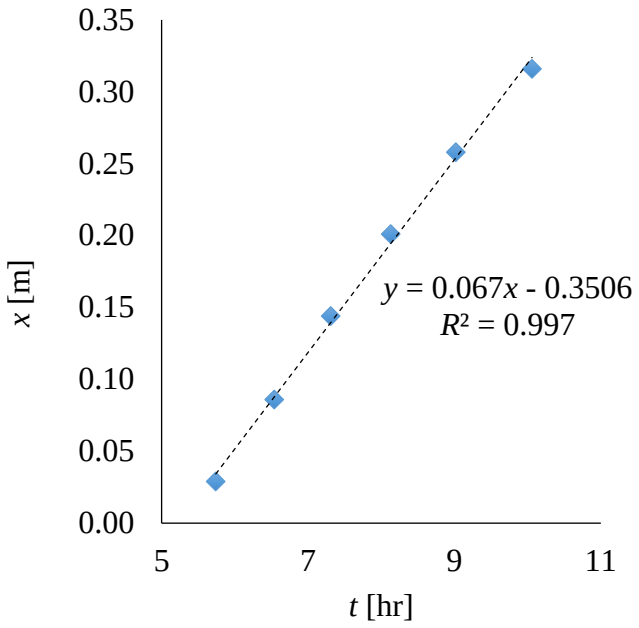

Figure 5.9 Time of arrival of thermal wave fronts at 27° C. The figure reflects test conditions for melting occurring at 27° C. Hot air was injected at the bottom of the bed (Test 12).

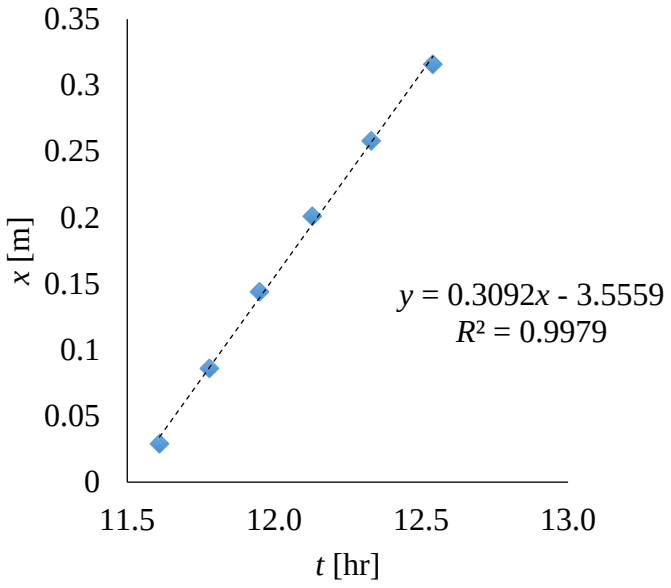

Figure 5.10 Time of arrival of thermal wave fronts at 37° C. The figure reflects test conditions with the PCM completely melted at 37° C. Hot air was injected at the bottom of the bed (Test 12).

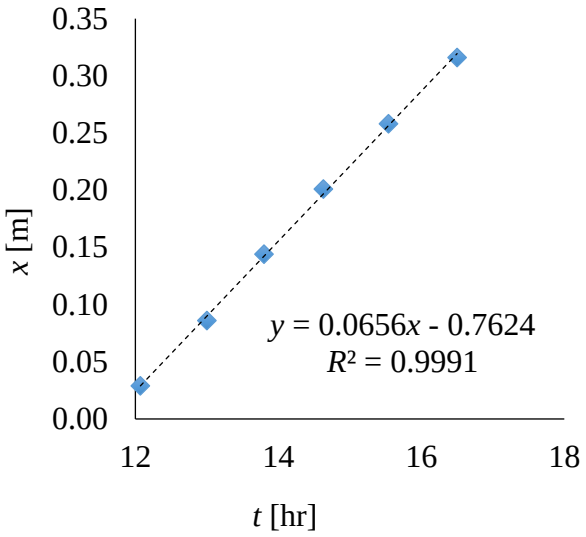

Figure 5.11 Time of arrival of thermal wave fronts at 27° C. The figure reflects test conditions for freezing at 27° C. Cold air was injected at the bottom of the bed (Test 12).

Test data indicate the time of arrival for isothermal and phase-change wave fronts. In general, plots for the time of arrival, at temperature measurement locations, fit linear relationships established in applying Equations 5-2, 5-3, 5-4, and 5-5 that may be used to estimate front velocities.

The data shown in Figure 5.5 and 5.6 describe temperatures corresponding to passing thermal waves. The velocities of the waves are measured by plotting the location of each temperature probe (Temperature Probes T1 through T6) versus the time of arrival of a particular temperature, fitting a line through the data, and then calculating the slope. The phase-change wave front, as a function of the time that phase-change begins and ends, may be used to estimate the velocity of the melt front. As an example, Figure 5.10 shows data for the melt front observed in Figure 5.5 at a phase-change temperature of 27° C.

Equation 5-2, 5-3, 5-4, and 5-5 were used to calculate the theoretical wave front velocities, v_{model}, for both partial (melting and freezing) and complete phase-change (melted and frozen) conditions. The time of arrival of thermal wave fronts was used to calculate the thermal wave front velocities, v_{th}, v_{pc}, and v_T by indicating the time that each axial temperature probe location (Temperature Probes T1 through T6) reached the temperature of the isotherm listed in Table 5.1.

Comparison of test data for the isothermal wave front velocities, v_{th} or v_{pc}, as compared to the values resulting from the theoretical model for v_{model}, results in acceptable correlations to the model (see R^2 values in Table 5.1). For the case in which no phase-change occurs (sensible heat transfer), the phase-change, thermal wave front velocity is equivalent to the isothermal wave front velocity.

The maximum deviation between the experimental and theoretical velocities is 8%,

Table 5.1 Thermal and theoretical wave front velocities. (a) Frozen; PCM in capsule completely solidified. (b) Melting; outer portion of PCM in capsule is liquid with PCM core solidified; capsule undergoing phase-change in radial direction from the outside in, exhibiting shrinking core model phenomena. (c) Melted; PCM in capsule completely liquid. (d) Freezing; outer portion of PCM in capsule is solid with PCM core liquefied; capsule undergoing phase-change in radial direction from the outside in, exhibiting shrinking core model phenomena. Equation 5-3 was used to calculate v_{pc} for melting and freezing conditions; Equation 5-2 was used to calculate v_{th} for melted and frozen conditions.

Figure	Process	Isotherm [°C]	v_{pc} or v_{th} [m/hr]	v_{model} [m/hr]	R^2
5.7	(a) Frozen	17	0.111	0.114	0.9974
5.8	(b) Melting	20	0.067	0.063	0.997
5.9	(b) Melting	27	0.107	0.114	0.997
5.10	(c) Melted	37	0.309	0.286	0.9979
5.11	(d) Freezing	27	0.066	0.069	0.9991

occurring at the completely melted phase at an isothermal temperature of 37° C.

The specific heat of the phase-change material is an average value that is used in analyzing the data to predict wave velocities. The complete phase-change process occurs over a range of temperatures, not a single phase-change temperature, due to the effects of shrinking core phenomena.

5.5 Exponential Temperature Distribution

For a thermal energy storage system in which hot air is injected into a packed-bed of encapsulated PCM in a frozen state, Equation 5-6 indicates that the dimensionless temperature distribution near phase-change fronts in packed-bed thermal energy storage devices in which a gaseous heat transfer fluid is supplied to the packing to either heat or cool the medium, is predicted according to the model [57] governed by

$$\theta = Ae^{\chi\,\gamma} \tag{5-6}$$

where χ is a distance constant and γ is the axial location in the bed.

The temperature distribution for the bed may be predicted according to Equation 5-6, which is applicable to both melting and freezing processes. This theoretical model is depicted in Figure 5.12, 5.13, and 5.14.

5.6 Shrinking Core Model

The rate of phase-change in a spherical domain subjected to convective heat transfer is given by a model that specifies the rate of change of the phase-change boundary under transient heat transfer conditions.

The shrinking core model defines the rate at which heat is transferred to the encapsulated phase-change material under partial phase-change conditions. During

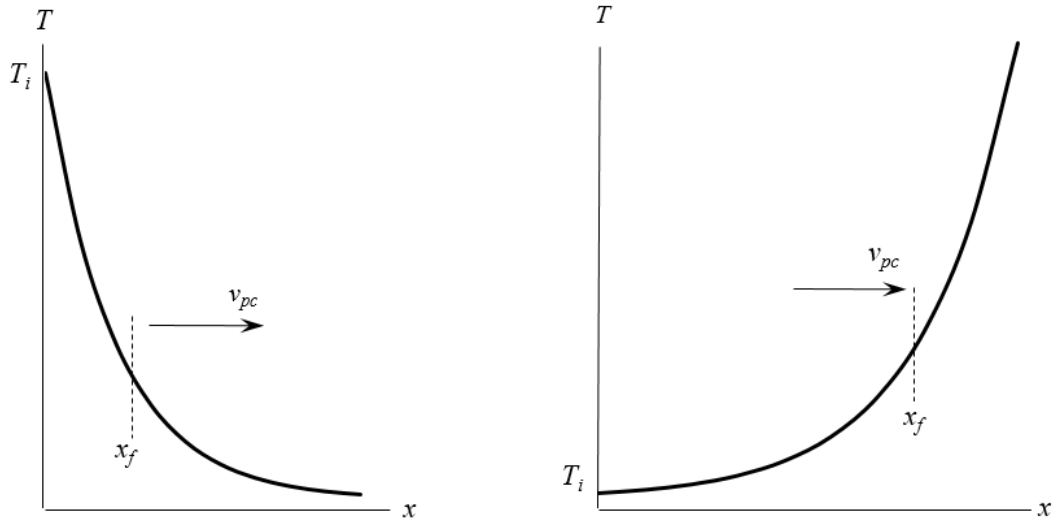

(a) (b)

Figure 5.12 Theoretical dimensionless temperature profiles across the bed. (a) Melting. (b) Freezing.

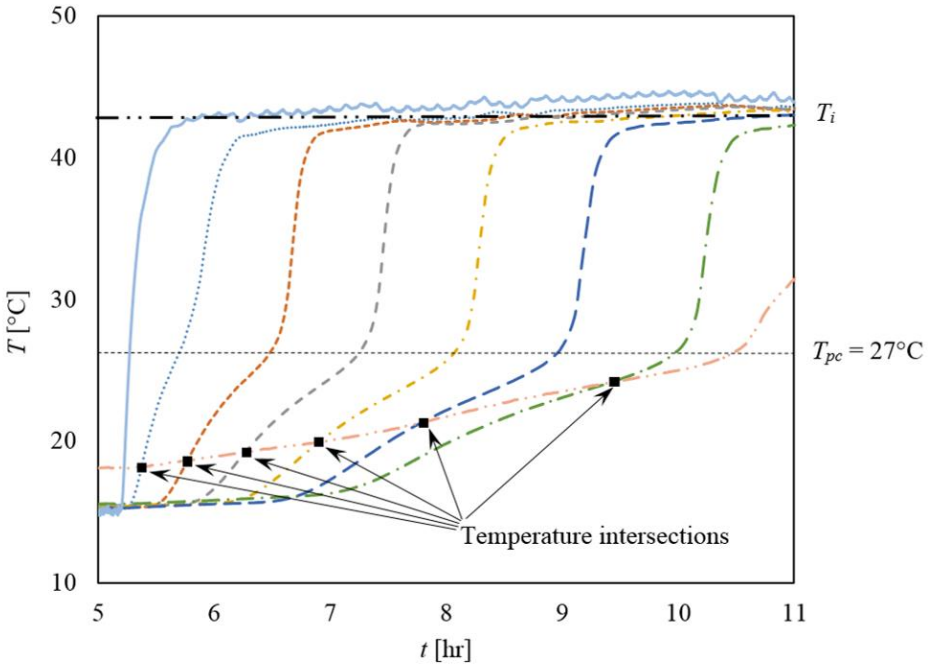

(a)

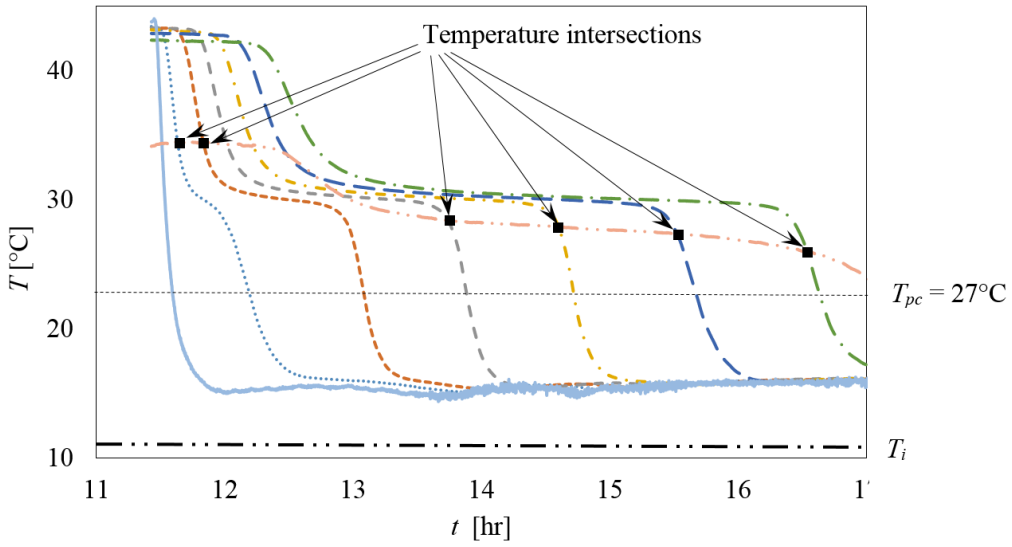

(b)

Figure 5.13 Theoretical dimensionless temperature profiles across the bed. (a) Melting and heating data for Test 12 showing outlet temperature intersections as a function of time and position. (b) Cooling and freezing data for Test 12 showing outlet temperature intersections as a function of time and position.

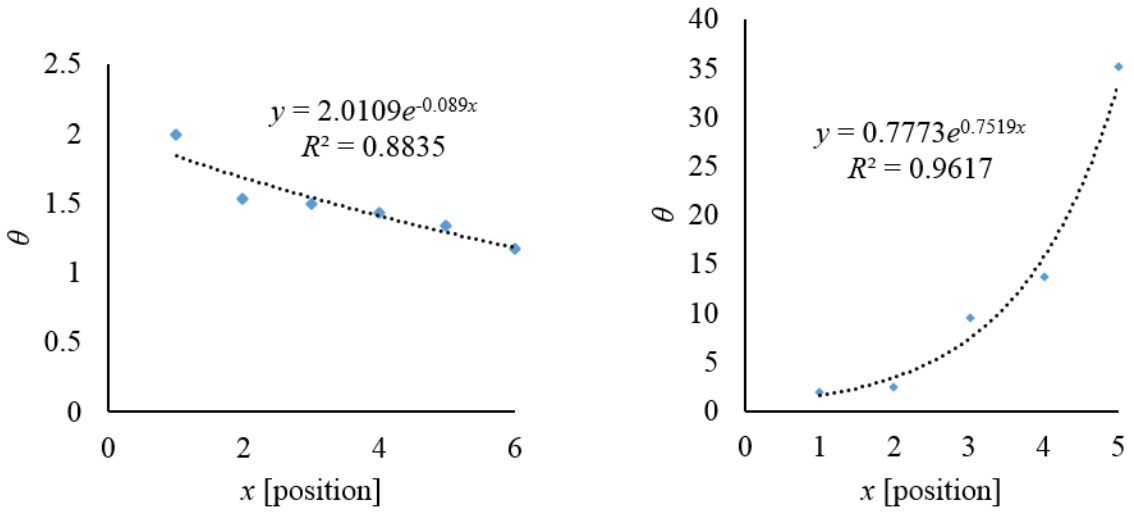

(a) (b)

Figure 5.14 Theoretical dimensionless temperature profiles across the bed. (a) Model compared to test data for melting. (b) Model compared to test data for freezing.

heating, and subsequent melting, heat flux encounters resistance to conduction in the outer spherical liquid phase-change material, as the continual addition of heat drives the frozen core to a completely melted state. During cooling, and subsequent freezing, the heat flux encounters resistance to conduction through the freezing outer spherical shell of the liquefied phase-change material as it approaches a completely frozen state (Figure 5.15). This phenomena quantifies the degree to which the velocity of phase-change waveforms is effected by the rate of change of core radius with respect to capsule radius, ω, and the time constant β. In this application, the Biot number, *Bi*, is a function of the capsule radius, *R*, and makes quantifying the convection heat transfer coefficient, *h*, possible, given that the thermal conductivity of the phase-change material, k_{pc}, is known.

$$\omega = \frac{r_{pc}}{R} \tag{5-7}$$

$$\beta = \frac{(T_\infty - T_{pc})k_{pc}}{R^2 \rho_{pc} \varepsilon \Delta u_{pc}} \tag{5-8}$$

Equations 5-9 and 5-10 imply two different time scales, one for large Biot numbers where time scales with β, and a second one for small Biot numbers that scale with βBi. For large Biot numbers, a scaled time, *t'*, is defined as

$$t' \equiv \beta t \tag{5-9}$$

For small Biot numbers, a scaled time *t**, is defined as

$$t^* \equiv Bi\beta t \tag{5-10}$$

Computation of the Biot number gives a relative measure regarding the method chosen for transient conduction heat transfer analysis. For $Bi << 1$, a lumped capacitance method may be used. For $Bi > 1$, a method that takes spatial effects into consideration, in terms of temperature gradients within the capsules, is a more suitable approach [32]. Both

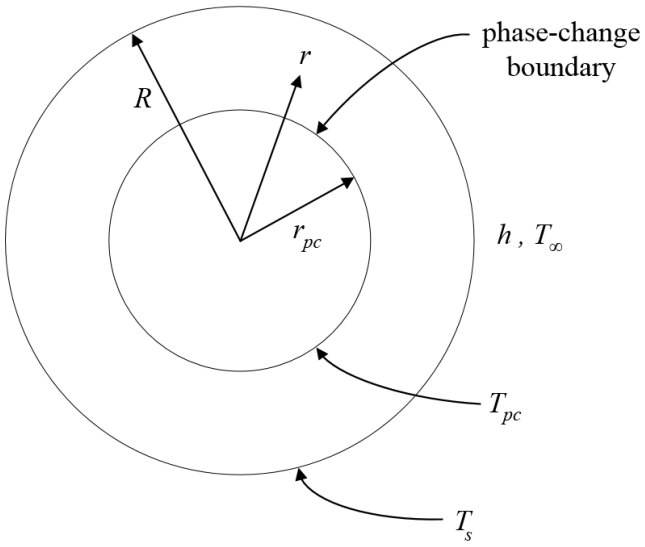

Figure 5.15 Shrinking core model for spherical domain. This model shows the change in the position of the phase-change boundary, for a spherical shell encapsulating a phase-change material, under both melting and solidification processes occurring at a constant temperature.

methods are sufficient in covering the entire phase-change process. Longer scaled times indicate a lag, or with respect to wave propagation and in turn velocity, and are more notable during the melting process, while conversely, shorter scaled times are more evident in reviewing the data for the freezing process. The effect of the shrinking core model with regard to the degree of solidification is depicted in Figures 5.16 and 5.17.

Calculations for various Biot numbers are presented in Figures 5.18 through 5.22. Figure 5.22 shows the results of the analysis in terms of ω as well as the degree of solidification λ. When $\lambda = 1$, the PCM is completely melted, whereas a value of $\lambda_o = 0.5$ indicates a state in which 50% of the volume of the PCM is frozen.

As shown in Figures 5.18 through 5.22, for low Biot numbers, the convection heat transfer coefficient, *h*, is the predominant factor effecting the rate of heating of the capsule, with scaled time converging for $Bi < 0.2$. For high Biot numbers, $Bi > 10$, the rate of heating for the capsules is most noticeably effected by the thermal conductivity of the bed. Best estimates for the convection heat transfer coefficient from the literature review are between 2 to 25 W/m^2 K based on the models cited the review.

For a capsule thermal conductivity of 0.09 W/m-K, and radius of 0.002m, the prescribed convection heat transfer coefficients produce Biot numbers between 0.21 to 0.61 for the freezing process and 0.1 to 0.79 for the melting process, producing scaled times of near 1. These values show that application of the lumped capacitance method for transient conduction analysis is an acceptable approach.

5.7 Exergy Efficiency

Packed-bed thermal energy storage devices should be designed such that physical characteristics and operating parameters minimize axial dispersion and wall heat loss

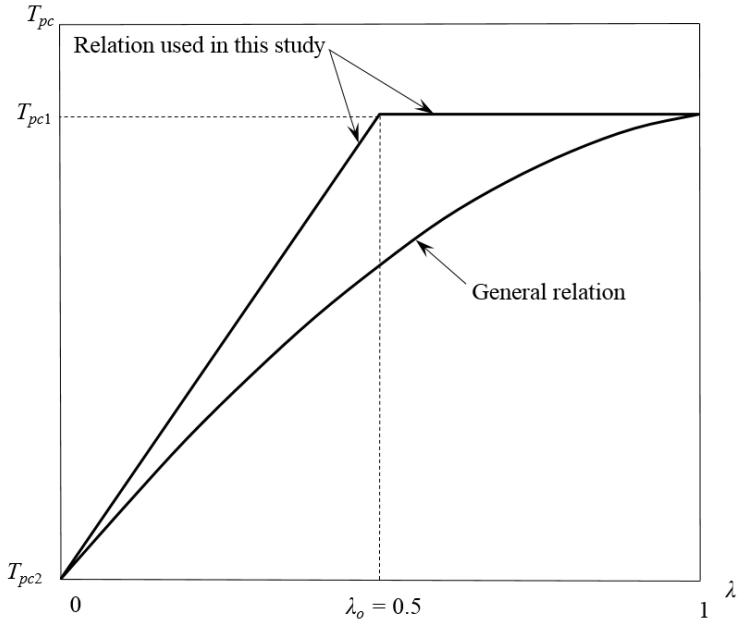

(a)

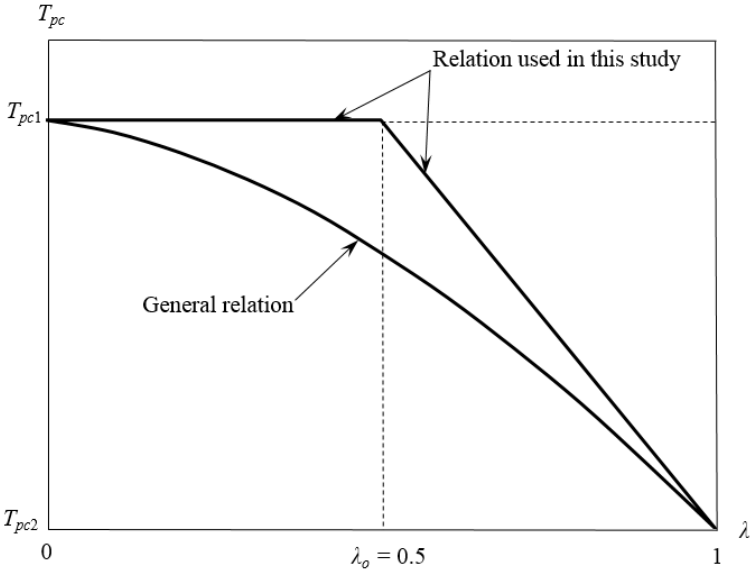

(b)

Figure 5.16 Shrinking core effect. (a) Percent solidification of axial location in packed-bed due to shrinking core phenomena for capsules during melting [11]. (b) Percent solidification of axial location in packed-bed due to shrinking core phenomena for capsules during freezing [11].

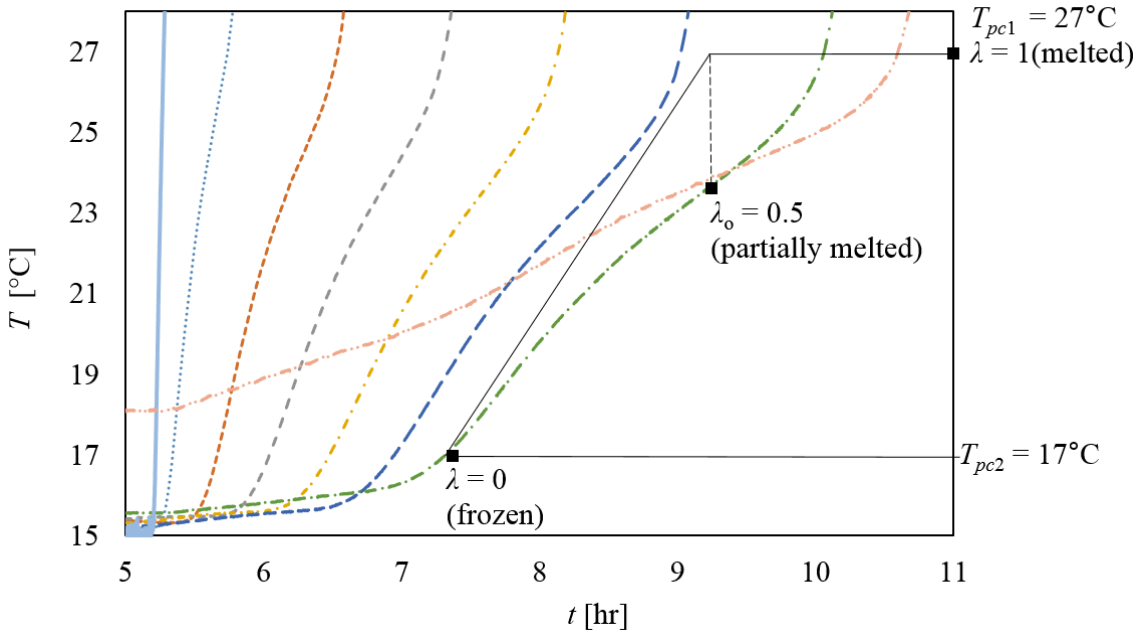

(a)

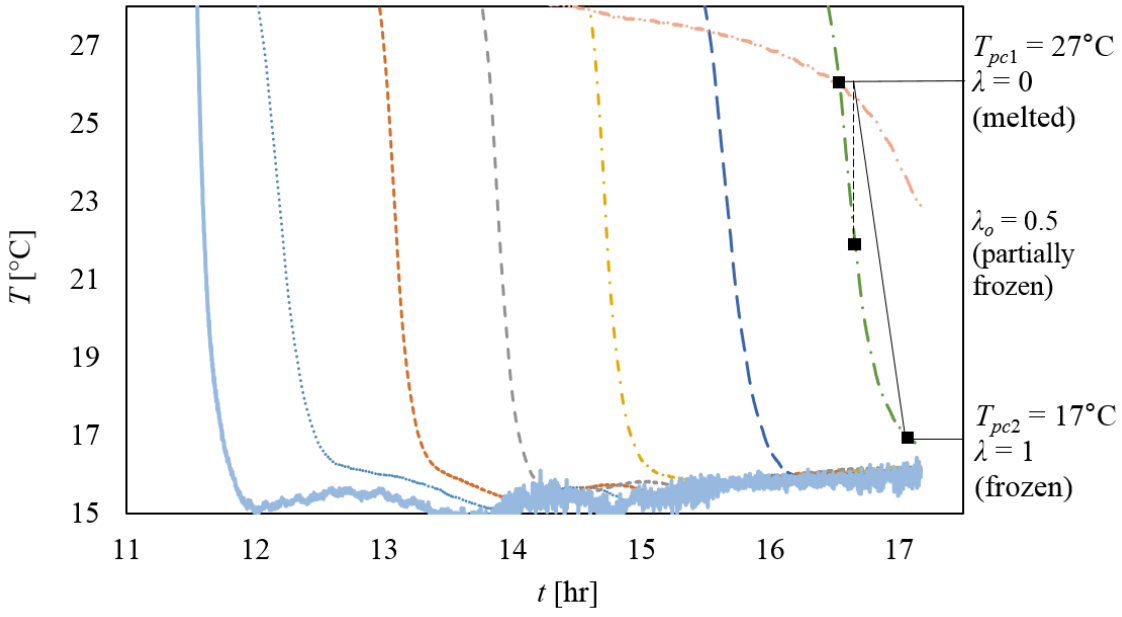

(b)

Figure 5.17 Shrinking core effect. (a) Theory compared to test data for melting. (b) Theory compared to test data for freezing.

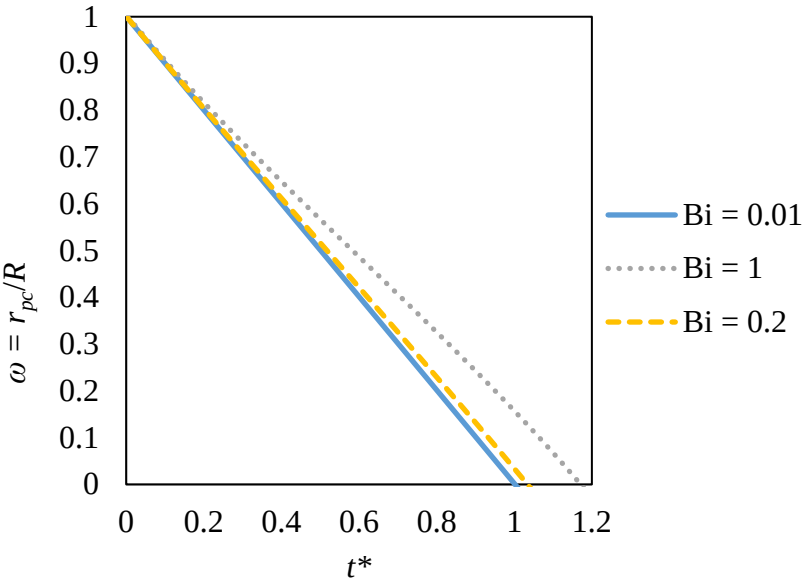

Figure 5.18 Shrinking core boundary location for low Biot numbers. The figure shows the shrinking core boundary location as a function of the ratio of the phase-change boundary location and the capsule radius, $\omega = r_{pc}/R$ for low Biot numbers.

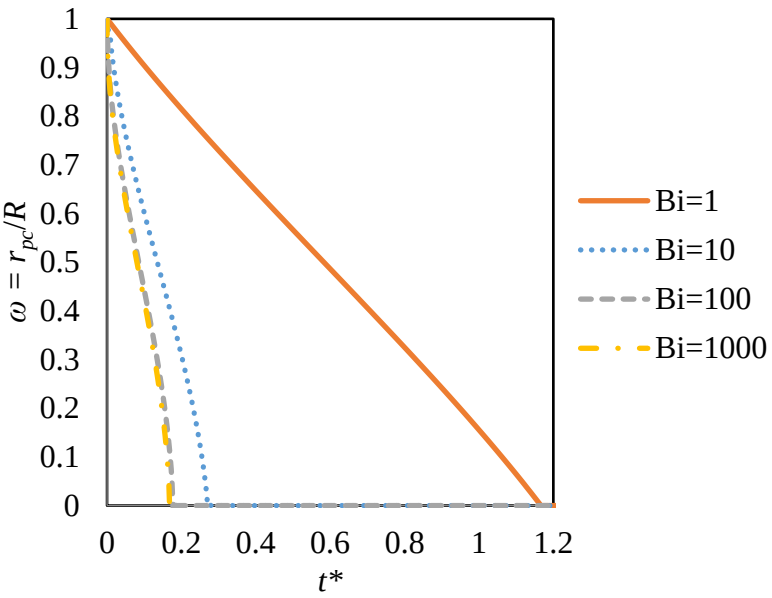

Figure 5.19 Shrinking core boundary location for high Biot numbers. The figure shows the shrinking core boundary location as a function of the ratio of the phase-change boundary location and the capsule radius, $\omega = r_{pc}/R$, for high Biot numbers.

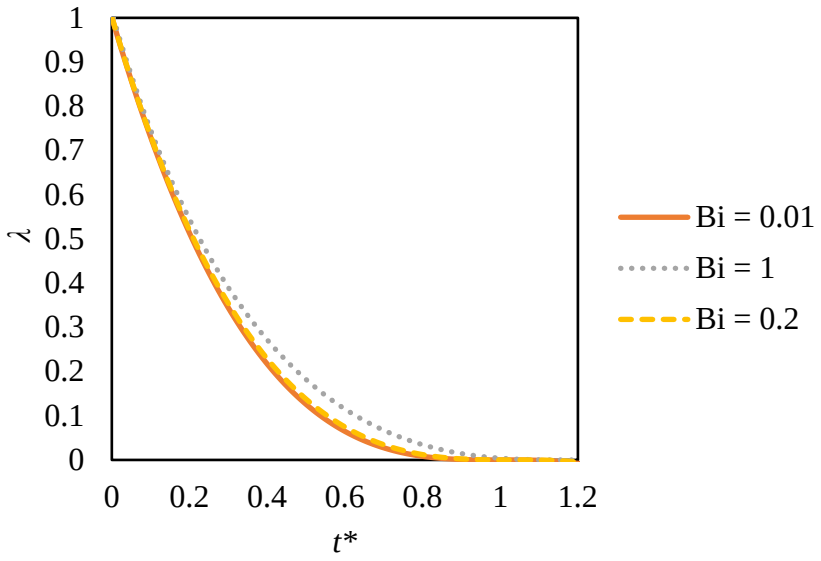

Figure 5.20 Shrinking core solidification for low Biot numbers. The figure shows the boundary location as a function of the degree of solidification, λ , for low Biot numbers.

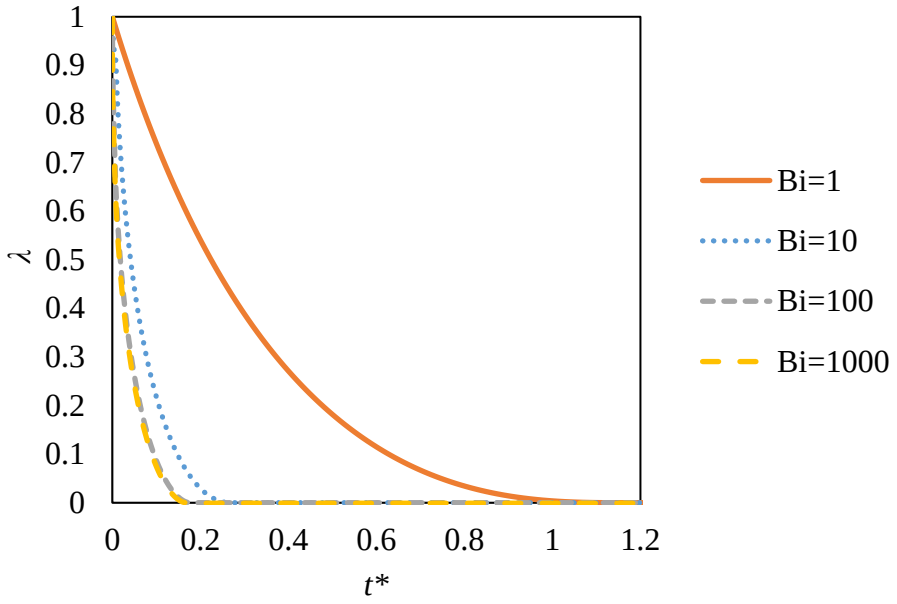

Figure 5.21 Shrinking core boundary location as a function of the degree of solidification, λ , for high Biot numbers.

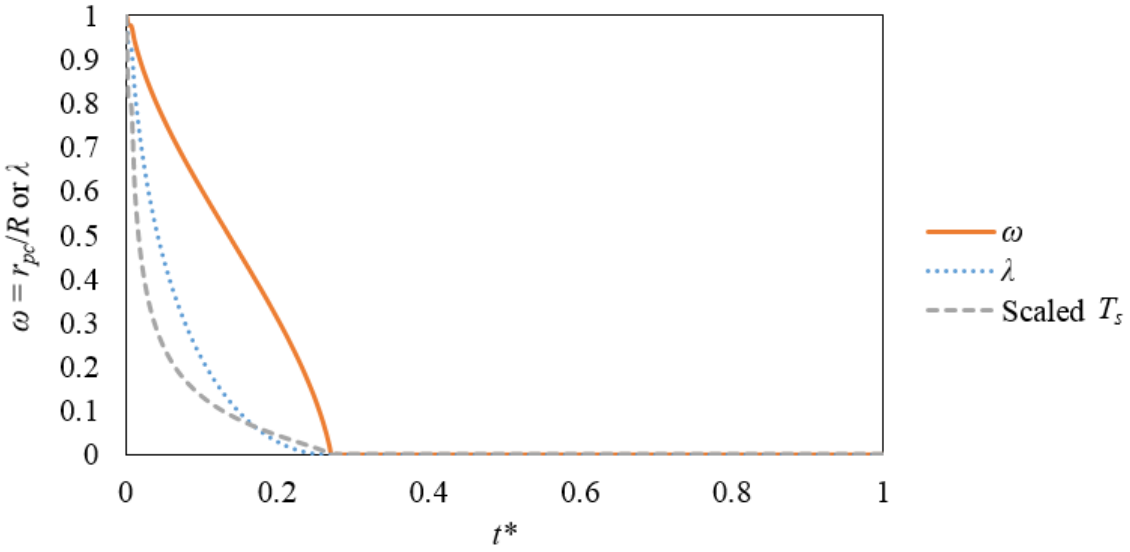

Figure 5.22 Comparison of the shrinking core boundary location. The figure shows the boundary location as a function of the ratio of the phase-change boundary location and the capsule radius, $\omega = r_{pc}/R$, the degree of solidification, λ , and the scaled capsule surface temperature, T_s.

effects in order to maximize the exergy efficiency of the system. Because axial dispersion directly effects the amount of thermal energy stored and retrieved, increased axial dispersion results in increased entropy generation or exergy destruction [9].

Table 5.2 summarizes both the exergy stored and the exergy recovered, for sensible heat transfer processes, as a result of the charging and discharging processes, respectively. Also indicated in the table are the values for the Carnot efficiency, the exergy efficiency during the charging process, and the steady-state exergy efficiency for the overall system. The exergy efficiency increases when the outlet fluid temperature is as low as possible during the charging process and as high as possible during the discharging process [11].

Packed-bed, thermal energy storage systems with large temperature gradients exhibit higher, ideal efficiencies than those containing the same amount of exergy but with more subtle thermal stratification [10].

Qualitatively, the first-law thermodynamic efficiency is simply a measure of the ratio of the thermal energy discharged to the thermal energy input to the system, and is dependent upon the flow arrangement. Parallel flow arrangements (Fig. 3.1) typically exhibit longer charging times. The second-law efficiency may be quantified by considering the duration of time for a nearly constant temperature discharge stream (Fig. 5.2 (d) and 5.3 (d)), as opposed to one that declines much faster in a linear fashion (Fig. 5.2 (b) and 5.3 (b)).

Table 5.2 Energy and exergy efficiencies.

Test	Charging (heating) [hrs]	Discharging (cooling) [hrs]	Exergy stored [J]	Exergy recovered [J]	Carnot efficiency	Exergy efficiency charging (heating)	Steady-state exergy efficiency (system)
1	4.6	1.4	745	177	0.45	0.53	0.61
2	4.6	1.4	714	144	0.42	0.53	0.60
3	4.6	1.4	575	162	0.40	0.53	0.62
4	4.6	1.4	459	128	0.36	0.53	0.64

CHAPTER 6

DISCUSSION

6.1 Sensible and Latent Heat Transfer Processes

The cascading wave model (Figure 2.2) contributes new knowledge to the scientific community in that it covers both the latent as well as the sensible heat transfer regimes, all in one model, independent of the shrinking core model, for both the thermal velocity, v_{th}, and the phase-change velocity, v_{pc}. However, under partial solidification conditions, when shrinking core phenomena effect is present, the velocity of an isotherm, v_T, may be computed, and exhibits some effect on the thermal wave velocity, v_{th}. In other words, the velocity of an isotherm, v_T, in the phase-change region during melting, is slowed as a result of significant heat transfer to the surroundings, whereas this same type of effect is not manifest during freezing because the rate of heat transfer to the surroundings is much less than that for melting (Fig. 5.3 and 5.4).

The experiments' interstitial fluid velocity multiplied by an average particle diameter of 4 mm and divided by the air kinematic viscosity results in a Reynolds number of 3.3. Multiplying by air's Prandtl number (.707) produces a Peclet number of 2.3, which would suggest that thermal dispersion effects are present, and are indicative of longitudinal convective dispersion and gas-solid heat transfer limits. However, in observing the temperature trends of Figures 4.5 and 4.6, it appears that dispersion was not a significant factor in the heat transfer. The widening of the temperature waves in Figure 4.5, and the

rounding of the temperatures near the phase-change temperature in both Figure 4.5 and 4.6, and the length of the region of variation from the injected fluid temperature to the phase-change front temperature are indicative of diffusion limitations and dispersion. While these effects may be important in packed-beds with higher interstitial velocities and larger PCM capsule sizes, they were not found to have significant effect on these results.

Further, heat transfer limitations within the capsules during phase-change were not expected. Typical periods for the passage of a phase-change front were of the order of 5 minutes. The time for freezing and melting can be estimated from an energy balance using the heat transfer coefficient, a temperature difference between the phase-change temperature and the air temperature, and the energy that must be transferred to accommodate the phase-change energy requirement. Assuming the heat transfer coefficient and temperature differences are constant and that the sphere temperature is the phase-change temperature, the time for melting or freezing can be written as

$$t = \frac{D}{6} \frac{\rho_{pc} \Delta u_{pc} \varepsilon}{h(T_i - T_{pc})} \tag{6-1}$$

For a 4 mm capsule in air with a 10°C temperature difference and a heat transfer coefficient of 10 W/m^{2}K, the phase-change time would be about 180 seconds or 3 minutes. As this calculation is considered conservative with a high heat transfer coefficient and temperature difference, it implies that the partially frozen observation may be a result of heat transfer limitations on the capsule surface and within the capsule shell.

6.2 Shrinking Core Phenomena

In comparing the time for sensible heating to occur (approximately 5 hours) over the entire length of the bed to the time required for sensible cooling to occur (approximately

2 hours) over the same bed length, the time for heating is much longer due to significant heat transfer to the surroundings during melting and heating, resulting in delayed melting and extended time for sensible heating. A lack of insulation at the wall of the container causes slight waveform inconsistency (lagging) during melting due to heat transfer to the surroundings resulting in a loss of heat that might otherwise be absorbed by the PCM during the melting process.

Negligible heat transfer to the surroundings during cooling results in faster cooling and a somewhat more uniform distribution of waveforms as propagation occurs over time and the entire length of the bed. The same is true for freezing. The elapsed time required for either the melting or freezing process is nearly equal at an elapsed time of about 5 hours for each of the phase-change process. Phase-change for melting is slowed as compared to phase-change for freezing, due to heat loss to the surroundings during melting as a result of $T_i > T_\infty$, thus resulting in a more pronounced shrinking core effect during melting.

The low temperature waves in Figure 4.5, where temperatures are lower than the phase-change temperature, do not behave like the high temperature thermal wave in the melted zone. From Figure 5.21, the value of t^* correlated with complete melting for a Bi = 1 is about 1.1. For a high value of β = 0.0041, that results from the largest injection to phase-change temperature difference, a time of over an hour is estimated for complete melting. As shown in Figure 4.5, the time for complete melting extends past the time of the passing of the melt front, leaving additional frozen capsule core, and thus slowing the velocity of the low temperature isotherms.

As a result of the thermal energy storage system evaluated in this work being a design that is exposed to ambient conditions, all of the heat loss associated with the storage

process is lost to the surroundings if not discharged in a timely manner. The time associated with the ability of the bed to store thermal energy for long periods of time is a direct function of the effectiveness of the insulation properties of the thermal energy storage device.

6.3 Latent Heat Transfer

Temperature distributions near phase-change fronts for both melting and freezing are in good agreement with the exponential model developed in Equation 2-45, particularly for freezing. Trends shown in Figures 5.11 and 5.12 represent the average temperatures measured and the average theoretical temperatures calculated according to the model for predicting temperature distributions near the phase-change front. A common front temperature, T_f, was used in the analysis for the melting and freezing front temperature distributions. For melting, the ratio of the phase-change boundary to the capsule radius is similar to the theoretical curve for temperature distribution, while the degree of solidification is more closely related to measured temperature data. Biot numbers were calculated based on the convection coefficients yielded by the analysis. Biot numbers ranged from 0.10 to 0.79 for the melting process and 0.21 to 0.61 for the freezing process producing Biot numbers ranging from 0.2 to 1. For complete freezing, scaled times t^* from 1.03 to 1.07 are computed for complete freezing, and from 0.87 to 1 for freezing to 83% as suggested by the slower velocities of the subfreezing waves. A time constant for these conditions, Equation 2-67, based on a temperature difference of 1°C between the fluid temperature and the phase-change temperature, is 0.000735/s. For t^* ranging from 1.07 to 0.87, melting or freezing time range from 0.4 hours to 0.33 hours. This is similar to the time it takes to change the temperature from the phase-change temperature to the injection

temperature as illustrated in Figures 4.5 and 4.6. The driving temperature difference is unknown, and would vary with time from the maximum representing the difference between the injection temperature and the phase-change temperature. For these experiments, that driving temperature difference appears to be on the order of 1°C.

6.4 Sources of Variability

Possible sources of disparity between the temperatures measured at locations internal to the bed, as compared to the temperatures measured at the inlet and the outlet of the bed, are attributed to the fact that neither of the external probes are in close proximity to, or are embedded within, the encapsulated PCM that constitutes the packing. The lack of insulation, and the distance or spacing between the bed and these probes due to the inclusion of flow control diffusers (Fig. 3.3), may also have an effect on these temperature differences. Consideration of this difference between the group of temperature probes including the inlet and the six within the confines of the bed, compared to the exit temperature probe, may show significant differences in temperature as a result of being downstream from the flow diffusers. In other words, the temperature probe at the inlet to the bed during injection will be closely grouped with the other internal temperature probes due to the present thermal state of the bed and fluid flow stagnation at the inlet. Some channeling effects of the air at the sides of the container may have been present during testing, possibly resulting a nonuniform velocity profile.

As a result of significant differences in the consistency of isotherms for independent melting and freezing processes, it appears that the specific heat values between the liquid and solid phases of the media are of considerable difference, as is evident in the formation of the transient temperature profiles associated with the melting and freezing processes.

The specific heat, c_{pc} , of the PCM was not available from the manufacturer; a constant value was used in the analysis (Table 3.1). The manufacturer stated that the PCM is a mixture of octadecane and eicosane. The manufacturer of the PCM also reported a thermal conductivity, k_{pc} , of 0.09 W/m K for a similar products (MicroPCMs). The manufacturer stated that the difficulty in measuring the thermal conductivity of the material is a result of air between the capsules. This comment indicates that the reported value was for the packing, and not the capsule itself. According to the manufacturer, the average latent heat of the PCM, u_{pc} , is 140 to 150 J/g, with the most recent lot tested measuring 152 J/g. The manufacturer lists the density of the product, ρ_{pc} , at 1 g/mL.

Deviations in dimensionless temperature profiles and thermal waveforms resulting from testing, when compared to ideal models, may be attributed to the fact that temperature measurements were recorded for a composite packed-bed comprised of both the heat transfer fluid and the encapsulated phase-change material, connected through the porosity or void fraction, as opposed to separate temperature profiles for the heat transfer fluid and the solid material.

Test efforts might be considered somewhat randomized, based on the order of tests, with respect to the test plan formulated, as a function of the order of charging and discharging the bed, the location of the inlet and outlets used for charging and discharging the unit, and the degree to which the bed temperature reached the temperature of the surroundings during overnight cooling.

Some inconsistencies in the temperature profiles near the beginning of the charging process for Test 2 and Test 4 were observed. These variations may be attributed to shorter elapsed time intervals over increasing axial position with respect to the bed. It should be

noted that as time increases, the stability of the profiles generated during testing improves, when compared to those produced using mathematical models. A strong correlation also seems to be present when evaluating the temperature profiles and thermal waveforms associated with temperature probes that are nearest to the bed inlet for the discharging process, as compared to the charging process.

Minimal deviations in the temperature and pressure of the air flowing through the supply tank seem to have a negligible effect on the temperature of the bed over short intervals of time, indicating the slow response or reactivity of the bed, or in other words, the bed exhibited long charging times. As a result, the thermal energy may be recovered relatively faster than it is stored.

The charging process also resulted in substantial superheating of the phase-change material, over an extended period of time, as the entire bed approached a uniform temperature distribution.

6.5 Convection Heat Transfer Coefficients

The Colburn *j* factor is a dimensionless heat transfer coefficient that may be applied to packed-beds containing various particle shapes, sizes, and packing densities. The Reynolds number for this arrangement is a function of the diameter of the particles that make up the packed-bed, along with the upstream velocity that would exist in a channel of the same cross-sectional dimensions, but without the packing. The heat transfer fluid properties for this arrangement are evaluated at the arithmetic mean of the fluid temperatures entering and exiting the bed. For particles at a uniform surface temperature, the rate of heat transfer from the bed is a function of the convection heat transfer coefficient, the total surface area of the particles in the packed-bed, and the log mean

temperature difference for the packed-bed. The log mean temperature difference is related to the density, velocity, specific heat, and inlet and outlet temperatures of the heat transfer fluid, as well as to the surface temperature of the particles within the packed-bed, and the packed-bed channel cross-sectional area [13].

Using the model from Schmidt and Willmott [5] results in a conservative estimate for the convection heat transfer coefficient, as compared to the average coefficient values for all other models combined. Increases in the convection heat transfer coefficient results in an increased dimensionless time interval, while reducing the coefficient reduces the dimensionless time interval.

Defining parallel flow through the bed as the condition in which the bed is charged and discharged from a common inlet (i.e., charging and discharging from the bottom or the top inlet) and counter flow as the condition in which the bed is charged and discharged through opposite inlets (i.e., charging from the bottom and discharging from the top), the results shown in Figures 5.2 (b) and (d), and 5.3 (b) and (d), display longer charging times, as well as more uniform, sustained discharge temperatures, for parallel flow arrangements when compared to counter flow configurations (Fig. 3.6).

Uniform spacing between the thermal waveforms implies a lack of thermal inertia during the charging and discharging operations. This uniform spacing makes it possible to predict the time required for each section of the bed to reach its maximum temperature. The test results indicate that the slope of the thermal waveform is dramatically effected by the volumetric flow rate of the heat transfer fluid. Lower flow rates tend toward a more shallow, linearly increasing profile, while higher flow rates represent an almost infinite slope with respect to thermal waveform temperature profiles.

CHAPTER 7

CONCLUSIONS AND RECOMMENDATIONS

7.1 Observations

Mathematical models governing the temperature distributions and thermal wave front propagation under phase-change conditions, as well as sensible heat transfer temperature distributions, in packed-beds comprised of encapsulated PCMs were developed and compared to experimental data. Comparisons of temperature distributions, thermal wave front velocities, and the shrinking core model time scales with the data reveal significant features of the thermal characteristics of the bed. As a result of the hypothetical approach to this unique combination of latent and sensible heat transfer processes, new models have been developed to describe this phenomena.

A design of experiment was developed and testing conducted in an effort to acquire the data necessary to support hypotheses and mathematical models governing the exploration of temperature distributions and thermal wave front propagation under phase-change conditions, as well as sensible heat transfer temperature distributions, in packed-beds comprised of encapsulated PCMs. In addition to definitions of thermal and phase-change wave speeds, exponential temperature distributions were predicted near the phase-change fronts. Profiles described by the complimentary error function match the measured profiles very well for regions where there is no phase-change. Shrinking core models predict that complete melting may not occur for low Biot numbers and small temperature

differences in the time characteristic of the passing of the phase-change wave, resulting in lower exit temperatures at values less than those expected for complete melting during the passing of the phase-change front.

The results of both the charging and discharging processes show that thermal waveform propagation is similar to the dimensionless models in terms of heat transfer fluid and PCM temperature profiles. Isotherm velocities implied that complete freezing occurred over a range of temperatures, resulting in slower thermal wave propagation**.** Overall, the bed exhibited stable thermal reactivity with regard to thermal energy storage.

Generally speaking, the system behaved as a transient thermal energy storage device whose performance is governed by steady-state heat flow properties, and could be classified as a time-dependent heat exchanger. The results of both the charging and discharging processes show that thermal waveform propagation is similar to the dimensionless models in terms of heat transfer fluid and PCM temperature profiles. Isotherm velocities implied that complete freezing occurred over a range of temperatures, resulting in retarded thermal wave propagation**.**

While packed-bed designs involving open-ended bed configurations that rely on passive, or natural convection mechanisms for heating, and forced convection for cooling, may be feasible for waste energy capture and release, the energy densities and capacities of beds of PCMs will be much larger for similar systems with significant pressure drops across the bed. Optimal designs may be found using packed-beds of encapsulated PCMs that reduce the temperature difference between the injection temperature and the phase-change temperature, to minimize the entropy loss during charging and discharging. The size of the PCM capsules should be small enough to allow full melting or freezing in the

time period that corresponds to the passing of a freezing or melting wave, as determined by the shrinking core phase-change model presented herein.

The data show that charging times are directly related to the initial bed temperature, and that discharge times were consistent across multiple charging and discharging cycles. Charging times are effected by the ambient temperature in terms of heat rejection to the surroundings.

While the thermal energy storage system evaluated in this work is a design that is exposed to ambient conditions, all of the heat loss associated with the long-term storage process is lost to the surroundings if not discharged in a timely manner. The time associated with the ability of the bed to store thermal energy for long periods of time is a direct function of the effectiveness of the design in terms of the insulation properties of the thermal energy storage device.

7.2 Optimization

Optimal design solutions may reside in packed-beds of encapsulated PCM that reduce the temperature difference between the injection temperature and the phase-change temperature, thus minimizing sensible heat transfer that contributes to entropy generation; however, for equal charging time, a smaller temperature difference means higher flow rates that will increase entropy generation due to additional pressure drop.

Torab [27] applied a monotinicity method to packed-bed, thermal energy storage devices, with the goal being to establish the optimum combination of variables associated with thermal performance, as compared to the pressure drop across the bed. Torab's optimization procedure maximized the ratio of available energy in storage, at the termination of the charging process, to the total operational power consumption.

Alternatively, Torab suggested an optimization scheme based on the total energy provided to the system as a function of temperature constraints. Negligible differences were observed in comparing these two system optimization techniques.

The optimization of packed-bed, thermal energy storage devices is complex as a result of multiple variables. While research has led to the optimization of thermal energy storage devices, in the form of packed-beds comprised of solids, minimal work has been performed in this area for systems containing encapsulated phase-change materials. Practical optimization strategies for packed-bed, thermal energy storage devices are scarce. Further work is required to maximize the benefits of thermal energy storage, in the form of packed-beds containing encapsulated phase-change materials, while minimizing capital costs related to the production of these unique storage devices.

While some definitions have been established for both energy and exergy efficiencies, considerable uncertainty exists in terms of opinions with regard to optimal flow arrangements and conditions for charging and discharging packed-beds containing encapsulated phase-change materials. Exergy losses, in some instances, are identified as heat loss at the boundary of the thermal energy storage device, internal diffusion, and mixing of the fluid within the packing. As it is difficult to weight the impact of these effects, further research needs to be conducted to quantify the contributions of these factors.

Variables that most notably effect the capacity for packed-bed, thermal energy storage can be categorized into three groups, namely, bed construction materials, heat transfer fluid properties, and the time-dependent response of the bed material.

Investigation of the factors effecting the overall economic feasibility of the system designed and used for data collection to confirm the hypotheses associated with this work,

might include the application of insulation materials best suited in augmenting the long-term storage capacity of packed-bed thermal energy storage devices, heat transfer fluid distribution systems designed for specified pressure levels and flow rates, air handling equipment that is effective in minimizing heat transfer fluid losses, and thus heat energy losses, and appropriate phase-change material temperatures that are optimal for the system under consideration, and that exhibit stable thermodynamic properties, particularly under conditions of extended superheating and subcooling, in order to minimize the potential for phase-change material loss in the form or secretion beyond encapsulation, and breakdown or shrinkage of the capsules due to the effects of thermal cycling. Long-term maintenance costs would be a significant factor in justifying the design and development of such systems.

Other opportunities reside in packed-bed designs involving open-ended bed configurations that rely on passive, or natural convection mechanisms for charging, or heating the bed, and forced convection for discharging, or retrieving stored thermal energy. The practicality of such systems would be dramatically effected by the pressure drop across the bed. Minimizing the interstitial velocity is paramount in minimizing the pump work required to transport the fluid across the bed. Convection heat transfer coefficients on the order of those associated with natural convection heat transfer modes might be expected. At a Reynolds number of 1, the effects of inertia are manifest. Optimal design solutions may reside in packed-beds of a thin slab configuration in order to reduce the temperature difference between the injection temperature and the phase-change temperature, thus minimizing sensible heat transfer and pressure drop, both of which contribute to entropy generation.

7.3 Design Criteria

Some of the factors that are most dominant in terms of the optimization of thermal energy storage devices, in the form of packed-beds, are characteristics such as vessel dimensions and geometry, storage material, heat transfer fluid and the mass flow rate of the fluid, the duration over which the thermal energy is to be stored or retrieved, the length of time that the heat is to be stored, and the transient response of the unit during charging and discharging operations. It may be desirable to maximize the amount of heat stored per unit volume in the device, as compared to the overall cost of the system [2].

Packed-bed geometry is defined by the size, shape, and packing of the particles, the length of the unit, and the geometric configuration of the storage vessel. Fluid properties and the mass flow rate of the fluid, in conjunction with the bed characteristics, govern the dynamic temperature and heat transfer relationships occurring within the bed. Pressure drop in the fluid as it crosses the bed, as well as the flow field in terms of velocity, are of interest as both effect convective heat transfer.

The total heat storage is dependent upon the initial thermal state of the bed, the temperature of the inlet fluid stream, the thermal properties of the storage material, and the convection heat transfer coefficient.

The practical nature of the unit in terms of size, performance, and cost, is governed by limiting the minimum and maximum length of the bed, the minimum and maximum mass flow rate of the heat transfer fluid, the maximum pressure drop across the bed, the minimum amount of heat stored in the bed, and the maximum fluid outlet temperature [2].

7.4 Summary

A knowledge of thermal wave propagation in packed-beds comprised of encapsulated phase-change materials (PCMs) is important in thermal energy storage applications. In this study, a set of experiments were conducted in order to better understand energy exchange in packed-beds and porous media comprised of solid and solid-liquid phase capsules. Air was used as the heat transfer fluid; hot air was injected in order to drive the melting process, while cold air was injected to accomplish freezing or solidification of the PCM. Temperature data supported the mathematical models developed to predict the behavior of both the thermal as well as the phase-change fronts advancing through the bed during the melting and freezing processes. Test temperature data were used to determine the time of arrival for thermal wave fronts to estimate the front velocities. Unexpectedly low velocities of isotherms at temperatures just below the phase-change temperature led to the conclusion that a partial phase-change region exists where solidification is not complete. A model was developed to predict velocities of isotherms in that region as a function of the Darcy velocity, and the degree to which the PCM is solidified.

Phase-change materials (PCMs) are attractive components of thermal energy storage systems due to their high energy densities and the relatively small temperature differences needed for effective charging and discharging. Theory was developed to describe the temperature variations throughout the bed. Temperatures in the bed were found to vary exponentially near the phase-change fronts. For hot air injection into a packed-bed of solidified PCM capsules initially at a temperature below the phase-change temperature, the thermal waves in the cold region showed isotherm velocity reduction due

to incomplete melting. A shrinking core model of the melting or solidification of the PCM in the capsules was developed to document the internal heat transfer constraints within the capsules. The results of the study support the conclusion that slower wave velocities occur due to partial melting.

REFERENCES

[1] Schumann, T.E.W., "Heat transfer: a liquid flowing through a porous prism", *Journal of the Franklin Institute, Issue 3* **208**, 405-416 (1929).

[2] Schmidt, F.W., Willmott, A.J., 1981, *Thermal Energy Storage and Regeneration*, Hemisphere Publishing Corporation, McGraw-Hill Book Company, New York, NY.

[3] Benmansour, A., Hamdan, M.A., Bengeuddach, A., "Experimental and numerical investigation of solid particles thermal energy storage unit", *Applied Thermal Engineering* **26**, 513-518 (2006).

[4] Kousksou, T., Strub, F., Lasvignottes, C., Jamil, A., Bédécarrats, J.P., "Second law analysis of latent thermal storage for solar system", *Solar Energy Materials & Solar Cells* **91**, 1275-1281 (2007).

[5] Oró, E., Castell, A., Chiu, J., Martin, V., Cabeza, L.F., "Stratification analysis in packed-bed thermal energy storage systems", *Applied Energy* **109**, 476-487 (2013).

[6] Ananthanarayanan, V., Sahai, Y., Mobley, C.E., Rapp, R.A., "Modeling of fixed bed heat storage units utilizing PCMs", *Metallurgical and Materials Transactions: B, Process Metallurgy and Materials Processing Science* **18B,** 339-346 (1987).

[7] Lei Yang, Xiao-song Zhang, "Performance of a new packed-bed using stratified phase-change capsules", *International Journal of Low-Carbon Technologies* **7**, 208-214 (2012).

[8] Regin, F.A., Solanki, S.C., Saini, J.S., "An analysis of a packed-bed latent heat thermal energy storage system using PCM capsules: numerical investigation", *Renewable Energy* **34**, 1765-1773 (2009).

[9] Ismail, K.A.R., Henríquez, J.R., "Numerical and experimental study of spherical capsules packed-bed latent heat storage system", *Applied Thermal Engineering* **22**, 1705-1716 (2002).

[10] Bédécarrats, J.P., Castaing-Lasvignottes, J., Strub, F., Dumas, J.P., "Study of a phase-change energy storage using spherical capsules. Part II: numerical modelling", *Energy Conversion and Management* **50**, 2537-2546 (2009).

[11] Karthikeyan, S., Velraj, R., "Numerical investigation of packed-bed storage unit filled with PCM encapsulated spherical containers – A comparison between various mathematical models", *International Journal of Thermal Sciences* **60**, 153-160 (2012).

[12] Bindra, H., Bueno, P., Morris, J.F., Shinnar, R., "Thermal analysis and exergy evaluation of packed-bed thermal storage systems", *Applied Thermal Engineering* **52**, 255-263 (2013).

[13] Haller, M.Y., Cruickshank, C.A., Streicher, W., Harrison, S.J., Anderson, E., Furbo, S., "Methods to determine stratification efficiency of thermal energy storage processes – Review and theoretical comparison", *Solar Energy* **83**, 1847–1860 (2009).

[14] Dincer, I, Dost, S., "A perspective on thermal energy storage systems for solar energy applications", *International Journal of Energy Research* **20**, 547-557 (1996).

[15] Atul, S., Tyagi, V.V., Chen, C.R., Buddhi, D., "Review on thermal energy storage with phase-change materials and applications", *Renewable and Sustainable Energy Reviews* **13**, 318–345 (2009).

[16] Bédécarrats, J.P., Strub, F., Falcon, B., Dumas, J.P., "Phase-change thermal energy storage using spherical capsules: performance of a test plant" Intl. *Refrig.* **19**, *2*, 187-196 (1996).

[17] Bédécarrats, J.P., Castaing-Lasvignottes, J., Strub, F., Dumas, J.P., "Study of a phase-change energy storage using spherical capsules. Part I: experimental results", *Energy Conversion and Management* **50**, 2527-2536 (2009).

[18] Nallusamya, N., Sampatha, S., Velrajb, R., "Experimental investigation on a combined sensible and latent heat storage system integrated with constant/varying (solar) heat sources", *Renewable Energy* **32**, 1206–1227 (2007).

[19] Mertens, N., Alobaid, F., Frigge, L., Epple, B., "Dynamic simulation of integrated rock-bed thermocline storage for concentrated solar power" *Solar Energy* **110**, 830–842 (2014).

[20] Regin, F.A., Solanki, S.C., Saini, J.S., "Heat transfer characteristics of thermal energy storage system using PCM capsules: a review", *Renewable and Sustainable Energy Reviews* **12**, 2438–2458 (2008).

[21] Nagano, K., Takeda, S., Mochida T., Shimakura, K., "Thermal characteristics of a direct heat exchange system between granules with phase-change material and air", *Applied Thermal Engineering* **24**, 2131–2144 (2004).

[22] Nithyanandam, K., Pitchumani, R., Mathur, A., "Analysis of a latent thermocline storage system with encapsulated phase-change materials for concentrating solar power", *Applied Energy* **113,** 1446–1460 (2014).

[23] Dreißigacker, V., Zunft, S., Müller-Steinhagen, H., "A thermo-mechanical model of packed-bed storage and experimental validation", *Applied Energy* **111**, 1120–1125 (2013).

[24] Zanganeh, G., Pedretti, A., Zavattoni, S., Barbato, M., Steinfeld, A., "Packed-bed thermal storage for concentrated solar power – Pilot-scale demonstration and industrial-scale design", *Solar Energy* **86**, 3084–3098 (2012).

[25] Bouadila, S., Kooli, S., Lazaar, M., Skouri, S., Farhat, A., "Performance of a new solar air heater with packed-bed latent storage energy for nocturnal use", *Applied Energy* **110** 267–275 (2013).

[26] Singh, H., Saini, R.P., Saini, J.S., "A review on packed-bed solar energy storage systems", *Renewable and Sustainable Energy Reviews* **14**, 1059–1069 (2010).

[27] Torab, H., Beasley, D.E., "Optimization of a packed-bed of encapsulated phase-change material for thermal energy storage", *Proceedings of the 21st Intersociety Energy Conversion Engineering Conference* **2**, 725-729 (1986).

[28] Sanderson, T.M., Cunningham, G.T., "Performance and efficient design of packed-bed thermal energy storage systems. Part 1", *Applied Energy* **50**, 119-132 (1995).

[29] Bouguettaia, H., Harker, J.H., "Energy storage in pack beds of spheres containing palm oil", *Journal of the Institute of Energy* **65**, *459*, 89-94 (1991).

[30] Ismail, K.A.R., Stuginsky, R. Jr., "A parametric study on possible fixed bed models for pcm and sensible heat storage", *Applied Thermal Energy* **19**, 757-788 (1999).

[31] Chen, S.L., Nakamura, H., Reistad, G.M., "A simplified analysis for cold storage in porous capsules with solidification", *Journal of Energy Resources Technology* **113**, *2*, 108-116 (1991).

[32] Incropera, F.P., DeWitt, D.P., 1990, *Introduction to Heat Transfer*, John Wiley & Sons, New York, NY.

[33] Heisler, M.P., "Temperature charts for induction and constant temperature heating", *Journal of Heat Transfer ASME*, **69**, 227-236 (1947).

[34] Karthikeyan, S., Solomon, G.R., Kumaresan, V., Velraj, R., "Parametric studies on packed-bed storage unit filled with PCM encapsulated spherical containers for low temperature solar air heating applications", *Energy and Conversion Management* **78**, 74-80 (2014).

[35] Bédécarrats, J.P., Castaing-Lasvignottes, J., Strub, F., Dumas, J.P., "Study of a phase-change energy storage using spherical capsules. Part II: numerical modelling", *Energy Conversion and Management* **50**, 2537-2546 (2009).

[36] Hernandez-Guerrero, A., Aceves, S.M., Cabrera-Ruiz, E., Romero-Mendez, R., "Effect of cell geometry on the freezing and melting process inside a thermal energy storage cell", *Journal of Energy Resources Technology* **127**, *2*, 95-102 (2005).

[37] Aceves-Saborio, S., Nakamura, H., Reistad, G.M., "Optimum efficiencies and phase-change temperatures in latent heat storage systems", *Journal of Energy Resources Technology* **116**, *1*, 79-86 (1994).

[38] Torab, H., Beasley, D.E., "Optimization of a packed-bed thermal-energy storage unit", *J. Solar Energy Engineering* **109,** 170-175 (1987).

[39] Ramana, A.S., Venkatesh, R., Aroul Raj, V.A., Velraj, R., "Experimental investigation of the LHS system and comparison of the stratification performance with the SHS system using CFD simulation", *Solar Energy* **103**, 378-389 (2014).

[40] Barton, N.G., "Simulations of air-blown thermal storage in a rock bed", *Applied Thermal Engineering* **55**, 43-50 (2013).

[41] Adebiyi, G.A., Hodge, B.K., Steele, W.G., Jalalzadeh-Aza, Nsofor, E.C., "Computer simulation of a high-temperature thermal energy storage system employing multiple families of phase-change storage materials", *Journal of Energy Resources Technology* **118**, *2*, 102-111 (1996).

[42] Beasley, D.E., Clark, J.A., Holstege, M.J., "Observations on the decay of a thermocline in a rock bed with no net fluid flow", *Journal of Solar Energy Engineering* **107**, 50-53 (1985).

[43] Arias, D.A., McMahan, A.C., Klein, S.A., "Sensitivity of long-term performance simulations of solar energy systems to the degree of stratification in the thermal storage unit", *International Journal of Energy Research* **32**, 242-254 (2008).

[44] Beyhan, B., Paksoy, H., Dasgan, Y., "Root zone temperature control with thermal energy storage in phase-change materials for soilless greenhouse applications", *Energy Conversion and Management* **74**, 446-453 (2013).

[45] http://www.littlegreenhouse.com/fan-calc.shtml

[46] http://www.slideshare.net/ChristopherLent1/clipboards/alternative-greenhouse-heating

[47] Badache, M., Eslami-Nejad, P., Ouzzane, M., Aidoun, Z., Lamarche, L., "A new

modelling approach for improved ground temperature profile determination", *Renewable Energy* **85**, 436-444 (2016).

[48] Udell, K., 2012, Professor at the University of Utah, Salt Lake City, UT, USA, private communication.

[49] Cengel, Y.A., Boles, M.A., 2011, *Thermodynamics: An Engineering Approach*, McGraw-Hill, New York, NY.

[50] Fang, G., Xu Liu, S.W., "Experimental study on cool storage air-conditioning system with spherical capsules packed-bed", *Energy and Buildings* **42**, 1056-1062 (2010).

[51] Harris, N.C., 1990, *Modern Air Conditioning Practice*, GLENCOE Macmillan/McGraw-Hill, New York, NY.

[52] Repshas, J., 2012, Project Development Manager at Dresser-Rand, Los Angeles, CA, USA, private communication.

[53] Dresser-Rand, West8 Tower, Suite 1000, 10205 Westminster Road, Houston, TX, USA, from url http://www.dresser-rand.com

[54] Udell, K.S., 2016, Professor in the Department of Mechanical Engineering at the University of Utah, Salt Lake City, UT, USA, private communication.

[55] Smith, Amanda D., Mago, Pedro J., Fumo, N., "Benefits of thermal energy storage option combined with CHP system for different commercial building types", *Sustainable Energy Technologies and Assessments* **1**, 3-12 (2013).

[56] West, G.O., Udell, K.S., "Heat transfer during heating and cooling of a packed-bed comprised of encapsulated phase-change material", *Journal of Energy Resources Technology*, in press, (2017).

[57] West, G.O., Udell, K.S., "Thermal wave propagation in packed-beds of encapsulated phase-change materials", *ASME 2017 Summer Heat Transfer Conference*, in press, (2017).

[58] Incropera, F.P., DeWitt, D.P., Bergman, T.L., LaVine, A.S., 2003, *Principles of Heat and Mass Transfer*, John Wiley & Sons, New York, NY.